
DELEGACIÓN SUR SURESTE

San Francisco de Campeche, Camp., a 31 de octubre de 2022

ASUNTO: Invitación

*Dr. Álvaro Raúl Lara Rodríguez*

Universidad Autónoma Metropolitana-Cuajimalpa

PRESENTE

Estimado colega,

En consideración a su destacada trayectoria académica en el área de la Biotecnología, tengo el agrado de invitarle a participar como **Ponente** del *Simposio IV. Medicina y diagnóstico***,** en el marco de las actividades del **XI Congreso de Biotecnología y Bioingeniería del Sur-Sureste**, a realizarse del 08 al 11 de noviembre de 2022 en modalidad híbrida. Consideramos de gran interés que usted exponga de manera concreta sus principales y más recientes avances en el área respectiva, con un enfoque de hacia donde se perfila su investigación en el futuro. Para tal efecto, le agradeceríamos que compartiera su experiencia con nuestros asistentes, a través de una disertación de aproximadamente 25 min. Su ponencia está programada para el día **10 de noviembre de 2022**, en un horario de **10:30-11:00** hrs, la cual será transmitida en forma de videoconferencia en vivo a la **Sala 2** del Centro Internacional de Convenciones y Exposiciones Campeche XXI. Le pedimos que se conecte al siguiente enlace (https://bit.ly/3ffaP25) 10 min antes de su presentación. Le pedimos por favor pueda enviar a la brevedad la siguiente información a Dra. Karla Rossanet Dzul Rosado, a la dirección karla.dzul@correo.uady.mx:

- su presentación de diapositivas
- una breve semblanza de su trayectoria
- un resumen de 1 cuartilla de su disertación

A nombre de la Sociedad Mexicana de Biotecnología y Bioingeniería Delegación Sur-Sureste, anfitriona del Congreso, le agradezco de antemano su consideración para esta importante labor y le reitero que su participación es de gran importancia para la comunidad académica que presentará sus proyectos de investigación en el mismo.

Sin más por el momento, quedo de usted.

**Dr. José Efraín Ramírez Benítez**
**Presidente del Comité Organizador**
XI Congreso de Biotecnología y Bioingeniería del Sureste

**La Sociedad Mexicana de Biotecnología y Bioingeniería**
**Delegación Sur-Sureste, el COESICYDET, El COLPOS Campus Campeche y**
**el Tecnológico Nacional de México Campus Chiná y Calkiní**

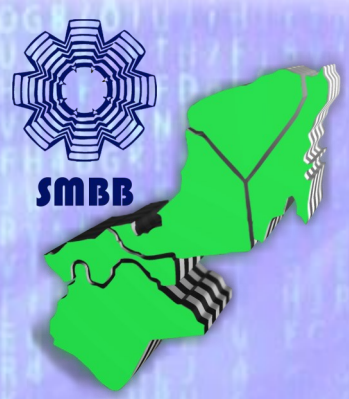


otorgan la presente

# Constancia

a:

## Dr. Álvaro Raúl Lara Rodríguez

por su participación como Ponente del **Simposio IV. Medicina y diagnóstico** con la Conferencia titulada:

*Avances y retos en la manufactura de ADN plasmídico*

presentada en el **XI Congreso de Biotecnología y Bioingeniería del Sur-Sureste** el 10 de noviembre de 2022.

San Francisco de Campeche, Camp., México, a 11 de noviembre de 2022.

**Dr. José Humberto Caamal Velázquez**
Presidente MD Sur Sureste 2020-2022

**Dr. José Efraín Ramírez Benítez**
Presidente del Comité Organizador XI CBBSS

| MPS | Journal | MSP No. | Dispatch: February 24, 2023 | CE: |
|---|---|---|---|---|
| | MLF2 | 12058 | No. of Pages: 5 | PE: Praveendra Kumar |

ORIGINAL RESEARCH

# Design of microaerobically inducible miniR1 plasmids

Fabiola Islas, Andrea Sabido, Juan-Carlos Sigala, and Alvaro R. Lara*

Edited by Yongqun He, University of Michigan Medical School, 1150 W. Medical Center Dr., Ann Arbor, MI, USA; Received November 18, 2022; Accepted February 13, 2023; Published online xxx

## Abstract

Oxygen limitation can easily occur in cultures for pDNA production, which requires innovative biological solutions. A synthetic miniR1 plasmid (pminiR1) was produced under aerobic, microaerobic, and biphasic regimes in 2L bioreactors. An inducible plasmid named pminiR1-MAInd, containing a second copy of repA under control of a microaerobic promoter, was designed and produced in biphasic cultures, where plasmid copy number per chromosome (PCN) and yields were monitored. Microaerobic regime increased the pDNA yield from biomass (YpDNA/X) by 20%, and the PCN 3.8-fold, compared to the aerobic regime. The PCN increased from 22 ± 14 to 85 ± 7 copies/chromosome, and YpDNA/X increased by 70% after the shift from aerobic to microaerobic conditions. Moreover, the final pDNA concentration in biphasic cultures was 47% higher than for aerobic cultures. Expression levels of the genes related to replication control, repA (positive regulator) and copA (negative regulator), were measured. The ratio of expression repA/copA increased by 30% in the microaerobic cultures, compared with the aerobic ones, and was 2.2-fold greater in the microaerobic phase than in the aerobic phase. Using pminiR1-MAInd, the repA/copA expression ratio and YpDNA/X increased 6.6- and 3.7-fold, respectively, upon the change of the regime. Moreover, the PCN reached 270 ± 58 copies/chromosome. The presented results indicate that increasing the repA/copA expression ratio is useful to increase the microaerobic production of miniR1 minimal plasmids.

**Keywords:** biodesign; DNA vaccines; microaerobic; plasmid DNA; synthetic miniR1 plasmid

**Impact statement**

Plasmid DNA manufacture is an essential step to produce gene therapy agents and next-generation vaccines. However, little attention has been paid toward developing alternative replicons that can be coupled with large-scale production conditions. Our results demonstrate that the miniR1 replicon can be efficiently induced by oxygen limitation when a copy of the regulatory protein RepA under control of a microaerobic promoter is used. These results are potentially attractive for industrial applications.

## INTRODUCTION

The importance of plasmids for biopharmaceuticals production keeps raising. Plasmid DNA (pDNA) is the active pharmaceutical ingredient in the so-called DNA vaccines[1] and in gene therapy products. The first pDNA vaccine for use in humans, which has shown high protection against SARS-CoV-2, was recently approved in India[2]. Furthermore, pDNA is often used as a template for in vitro transcription to produce mRNA vaccines[3]. Therefore, current and future demands of pDNA will require efficient production processes that can be implemented on a large scale, particularly considering the physical constraints in large-scale bioreactors, like imperfect mixing and mass transfer limitations. The oxygen demanded by *Escherichia coli* cells (the preferred host for pDNA production) in cultures can be difficult to meet, leading to local or global oxygen limitation. Although oxygen limitation causes undesired metabolic deviations, it can also result in increased pDNA yields ($Y_{pDNA/X}$)[3,4]. Therefore, large scale-related conditions could be used to improve pDNA production. The majority of the plasmids used for DNA vaccines contain pMB1-derived replicons, particularly pUC[1]. High pDNA yields can be obtained with pUC plasmids if the culture temperature is increased to 40–45°C, which triggers runaway replication[5]. However, this temperature increase also triggers overflow metabolism and markedly reduces the viability of cells[6]. Moreover, the pUC origin or replication contains a cruciform sequence that is sensitive to

Departamento de Procesos y Tecnología, Universidad Autónoma Metropolitana, Ciudad de Mexico, México.

* **Correspondence:** Alvaro R. Lara, alara@cua.uam.mx

DOI: 10.1002/mlf2.12058

endonuclease activity[7], which may reduce the stability of pUC vectors. Only a few options have been proposed in addition to pUC replicons for high-yield pDNA production. Namely, the pCOR plasmids contain the R6K replicon, and were modified to yield relatively high plasmid copy numbers per chromosome (PCN)[8]. More recently, the R1 replicon was used to construct vectors that yielded PCN of several hundreds upon thermal induction[9]. In a different report, a plasmid named pminiR1 was assembled. pminiR1 contains a synthetic R1 replicon, in which some of the natural R1 sequences were eliminated[3]. It was shown that the $Y_{pDNA/X}$ obtained with pminiR1 were similar to those of the high PCN plasmid pUC57kan. In the present study, pminiR1 was produced in aerobic, microaerobic, and biphasic cultures with a regime change from aerobic to microaerobic conditions. pminiR1 was modified to create a microaerobically inducible version by overexpressing the positive replication control element (the protein RepA) upon oxygen limitation.

Plasmid pminiR1 contains a minimal set of sequences to allow its replication and selection (Figure 1A). For instance, the sequence of *copB*, which is a negative regulator, is also not included. Moreover, the *parB* locus originally present in plasmid R1 is not included in pminiR1. The *parB* locus contains the genes *hok* (coding for a very stable killing protein) and *sok* (coding for unstable antisense mRNA that regulates *hok* expression). The *parB* locus, additional to antibiotic resistance is an additional mechanism to stabilize plasmid R1, known as the "postsegregational killing" of plasmid free

(A)

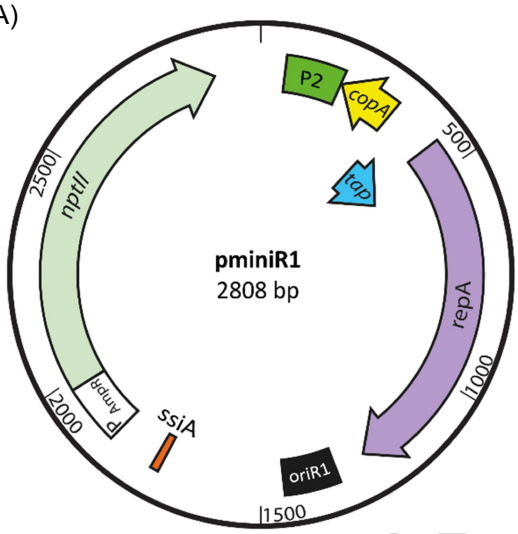


(B)

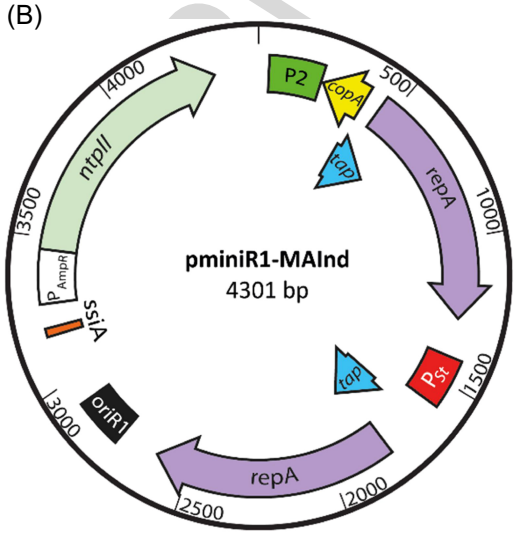


(C)

| Plasmid (condition) | $\frac{(repA/copA)_{microaerobic}}{(repA/copA)_{aerobic}}$ | Plasmid copy number | $\frac{PCN_{microaerobic}}{PCN_{aerobic}}$ | $\frac{(Y_{pDNA/X})_{microaerobic}}{(Y_{pDNA/X})_{aerobic}}$ |
|---|---|---|---|---|
| miniR1 (constant regime) | 1.31 | 22 ± 14 (aerobic)[a]<br>85 ± 7 (microaerobic)[b] | 3.8 | 1.7 ± 0.2 |
| miniR1 (biphasic regime) | 1.51 | 23 ± 2 (aerobic)[c]<br>81 ± 23 (microaerobic)[d] | 3.5 | 2.2 ± 0.1 |
| miniR1-MAInd (biphasic regime) | 6.63 | 18 ± 4 (aerobic)[c]<br>270 ± 58 (microaerobic)[d] | 14.6 | 3.7 ± 0.6 |

**Figure 1.** Design of the miniR1 plasmids and the main results of plasmid copy numbers and *repA* expression ratios in aerobic and microaerobic cultures. (A) Scheme of the plasmid pminiR1, containing the minimized R1 replicon. (B) Scheme of the plasmid pminiR1-MAInd, containing an extra copy of *repA* under control of the microaerobic promoter $P_{St}$. *copA*, gene coding for antisense RNA that lowers the transcription rate; *ntpII*, neomycin phosphotransferase gene; *oriR1*, origin of replication or R1 replicon; $P_2$, *repA* promoter; $P_{AmpR}$, promoter of the ampicillin resistance gene; $P_{St}$, promoter of a globin from *Salmonella typhi*; *repA*, replication initiation protein gene; *ssiA*, single-strand initiator; *tap*, translational activator peptide required for RepA synthesis. (primosome assembly site). (C) Main results of *repA* and *copB* expression levels, $Y_{pDNA/X}$, and plasmid copy number per chromosome (PCN) under the different conditions studied. Samples correspond to the following hours of culture: [a]10, [b]12, [c]3, and [d]11. Time profiles of the cultures are shown in the supplementary file.

cells[10]. Therefore, the stability of pminiR1 is expected to be controlled only by antibiotic resistance.

Production of plasmid pminiR1 was first characterized under aerobic or microaerobic batch cultures of *E. coli* W12, which constitutively expresses the *Vitreoscilla* hemoglobin (VHb). Expression of VHb improves the growth and metabolic performance of *E. coli* under both aerobic and oxygen-limited conditions[6]. The growth profiles of aerobic and microaerobic cultures for pminiR1 production are shown in Supporting Information: Figure S1. Under aerobic conditions, exponential growth was observed only during the first 4–6 h. Later on, growth was approximately linear (Supporting Information: Figure S1A). Linear growth was also reported in previous studies in the production of pDNA containing the R1 replicon[3,9]. Interestingly, the pDNA yield from biomass ($Y_{pDNA/X}$) increased markedly when the cell growth was linear (Supporting Information: Figure S1A). The cell growth under microaerobic conditions was very slow and both pDNA concentration and $Y_{pDNA/X}$ increased steadily during the first 10 h of culture (Supporting Information: Figure S1B). The $Y_{pDNA/X}$ at the end of the aerobic cultures was 6.4 ± 0.7 mg/g, while under the microaerobic regime, it reached 8.2 ± 0.4 mg/g. A previous study also reported an increase of $Y_{pDNA/X}$ due to oxygen limitation; however, the values shown in Supporting Information: Figure S1 are higher than those of the aforementioned report[3]. Possible causes for this are the different media and temperature used, as well as pH control in the present study. The final $Y_{pDNA/X}$ in microaerobic cultures was also higher than those reported by Bower and Prather[9], in which a plasmid containing the R1 replicon was produced in aerobic cultures at 30°C and shifted to 42°C.

To further increase $Y_{pDNA/X}$ upon oxygen depletion, microaerobically inducible pUC replicons that substantially improve pDNA production under oxygen-limited regimes have been designed[11]. In the present study, a similar design principle was applied: a second copy of the positive replication control gene (*repA*), placed under the transcriptional control of a microaerobic promoter ($P_{St}$)[12], was inserted in pminiR1 (Figure 1B). The microaerobically inducible plasmid was named pminiR1-MAInd. The initial assumption was made that increased abundance of RepA would increase plasmid replication, provided that the amount of CopA does not increase in the same proportion, in agreement with previous simulations using mathematical models[13]. The *copA* promoter strength is 12.5 transcripts/min[14], while for *repA*, it is around 1.4 transcripts/min[15], which is nearly nine times lower. Consequently, it has been established that the synthesis of the RepA protein is a rate-limiting factor for replication initiation[16]. Therefore, it is expected that increased *repA* expression may lead to higher PCN.

The production of pminiR1 and pminiR1-MAInd was evaluated under biphasic conditions, as described in Section Materials and methods (Supplementary File). Supporting Information: Figure S2 shows the growth profile of the biphasic culture of pminiR1 and pminiR1-MAInd. The $Y_{pDNA/X}$ increased for both plasmids after change in the regime to microaerobic conditions, reaching values higher than those achieved under constant regimes. This is advantageous for large-scale cultures, where a gradual transition to microaerobic conditions would occur. The maximum $Y_{pDNA/X}$ was obtained at 13 h of culture for both plasmids, reaching 9 ± 1 mg/g for pminiR1 and 12 ± 1 mg/g for pminiR1-MAInd (Supporting Information: Figure S2). This means increases of 33% and 84% over the original plasmid in biphasic and in fully aerobic cultures, respectively.

To confirm the relation between the increased $Y_{pDNA/X}$ and *repA* expression, the PCN and the ratio of *repA* copies to *copA* copies per cell were measured and are reported in Figure 1C. In cultures at constant regimes, the *repA*/*copA* expression ratio increased 31% in the microaerobic regime, compared to the aerobic regime, which led to a 3.8-fold increase of PCN. The absolute PCNs are lower than those reported by Bower and Prather[9]. However, those authors performed cultures at 30°C, which improves the stability of low-copy-number plasmids in *E. coli*. The PCN increase in the constant microaerobic regime compared to the aerobic regime was 70% greater than the change of $Y_{pDNA/X}$. Microaerobic conditions were also used for the production of the pUC plasmid (pVAX1) in batch mode. The authors reported a 61% increase of $Y_{pDNA/X}$, compared to aerobic conditions[6], which is similar to the results shown in Figure 1C. Microaerobic cultures at a very low oxygen transfer rate (10 mmol/L h) resulted in five times higher $Y_{pDNA/X}$ values for pVAX1, compared to aerobic cultures at $OTR_{max}$ of 110 mmol/L h[6]. Therefore, it may be possible to improve the results shown in Figure 1C by decreasing the $OTR_{max}$ of the culture.

The biphasic regime resulted in increased *repA*/*copA* expression ratios, compared to constant regime cultures. Notwithstanding the increase of $Y_{pDNA/X}$ of pminiR1 observed in biphasic cultures compared to constant regimes, the PCN increase was almost unchanged (Figure 1C), meaning that there was no direct equivalence between PCN and $Y_{pDNA/X}$. This was also observed by Bower and Prather[9] and contrasts with pUC plasmids.[11] The *repA*/*copA* expression ratios in cells bearing pminiR1-MAInd were more than 4-fold higher than that for pminiR1, in agreement with substantial increases of PCN and $Y_{pDNA/X}$ (Figure 1C). The PCN values obtained by the end of biphasic cultures of cells bearing pminiR1-MAInd were 3- and 12-fold higher than those attained in a constant microaerobic and aerobic regime, respectively, using pminiR1. This change is substantially higher than that reported for a microaerobically inducible pUC plasmid. In this report, the PCN was 2.3-fold greater during the microaerobic phase, compared to the aerobic phase of a fed-batch culture[11]. This could be related to the fact that the positive control molecule for miniR1 is a protein, contrary to the case of pUC plasmids, in which the PCN is controlled by RNA. The half-life of the majority of RNA molecules in *E. coli* is between 3 and 8 min[17], while the half-life for proteins (excluding abnormal or unstable proteins) is several hours[18]. Therefore, the additional expression of RepA under microaerobic conditions could lead to more stable effects than the expression of RNA.

Plasmid topology is a quality attribute when used as an active pharmaceutical ingredient[1]. It is generally recommended that at

least 80% of the pDNA is present in the supercoiled isoform (sc-pDNA)[1]. We analyzed the supercoiled content of both plasmids obtained from the different regimes. Supporting Information: Figure S3 shows the agarose gel pictures. Under both aerobic and microaerobic regimes, the sc-pDNA fraction of pminiR1 was 80%. In biphasic cultures, the sc-pDNA fraction during the aerobic phase of the sc-pDNA was 80%, while in the microaerobic phase, it increased to 90%. Similar results were obtained for pminiR1-MAInd.

Here, we present an alternative to deal with microaerobic conditions that can easily occur during the production of pDNA at virtually any culture scale. The R1 replicon can be an alternative to traditional pUC replicons. Therefore, a minimal R1 plasmid was modified to induce replication upon transition to microaerobic conditions. In the experiments presented here, it is considered that microaerobic conditions are present when dissolved oxygen tension (DOT) is below 10%. The modified miniR1 contains an extra copy of the gene *repA* under control of the microaerobic promoter $P_{St}$. Although the DOT for optimal induction of $P_{St}$ has not been reported, it has been demonstrated that the promoter from the *Vitreoscilla* hemoglobin is maximally induced at DOT below 5%[19]. Since both promoters control the expression of microbial globins, we chose DOT = 2% for induction of *repA* as an initial approximation. While precise control at such a low DOT in industrial bioreactors is difficult, our experiments show the differences between two contrasting conditions: fully aerobic and microaerobic conditions.

The presented results demonstrate that the transition to microaerobic conditions is better than constant microaerobicity to increase the production of plasmids containing the minimal R1 replicon. Furthermore, our biodesign proved that overexpression of the gene *repA* is an efficient way to increase pDNA yields and PCN upon transition to oxygen limitation. The global productivity in biphasic cultures was 1.61 ± 0.12 mg/L h for pminiR1 and 1.71 ± 0.15 for pminiR1-MAInd, which is an increase of only 6.5%. However, the SCF increased from ~80% to ~90%. Therefore, the increased pDNA yields and SCF of pminiR1-MAInd make it advantageous for downstream operations. Overall, we showed that the minimized R1 replicon could be an interesting option to the traditional pUC plasmids. Microaerobic conditions can increase the PCN of pminiR1. The designed inducible plasmid is therefore an alternative for oxygen transfer issues, and therefore, can help to efficiently scale up pDNA production processes.

## ACKNOWLEDGMENTS

Financial support from the Comisión Intersecretarial de Bioseguridad de los Organismos Genéticamente Modificados (CIBIOGEM) Grant 264460 is acknowledged. Fabiola Islas was a Postdoctoral Fellow from the Universidad Autónoma Metropolitana during the execution of the experimental work.

## AUTHORS CONTRIBUTIONS

All authors contributed to the study conception and design. Material preparation, data collection, and analysis were performed by Fabiola Islas. RT-qPCR analyses were performed by Fabiola Islas and Andrea Sabido, and supervised by Juan-Carlos Sigala. The first draft of the manuscript was written by Fabiola Islas and Alvaro R. Lara, and all authors commented on previous versions of the manuscript. All authors read and approved the final manuscript.

## ETHICS STATEMENT

This article does not contain any studies with human participants or animals performed by any of the authors.

## CONFLICT OF INTERESTS STATEMENT

The authors declare no conflict of interests.

## DATA AVAILABILITY

The data that support the findings of this study are available from the corresponding author upon reasonable request.

## SUPPORTING INFORMATION

Additional Supporting Information for this article can be found online at https://doi.org/10.1002/mlf2.12058.

## REFERENCES

1 Mairhofer J, Lara AR. Advances in strains and vector development for plasmid DNA vaccines production. *Cancer Vacc Methods Protocols Meth Mol Biol*. 2014;1139:505–42.

2 Mallapaty S. India's DNA COVID vaccine is a world first—more are coming. *Nature*. 2021;597:161–2.

3 Lara AR, Velázquez D, Penella I, Islas F, González-De la Rosa CH, Sigala JC. Design of a synthetic miniR1 plasmid and its production by engineered *Escherichia coli*. *Bioprocess Biosyst Eng*. 2019;42:1391–7.

4 Passarinha LA, Diogo MM, Queiroz JA, Monteiro GA, Fonseca LP, Prazeres DMF. Production of ColE1 type plasmid by *Escherichia coli* DH5α cultured under nonselective conditions. *J Microbiol Biotechnol*. 2006;16:20–4.

5 Williams JA, Luke J, Langtry S, Anderson S, Hodgson CP, Carnes AE. Generic plasmid DNA production platform incorporating low metabolic burden seed-stock and fed-batch fermentation processes. *Biotechnol Bioeng*. 2009;103:1129–43.

6 Jaén KE, Lara AR, Ramírez OT. Effect of heating rate on pDNA production by *E. coli*. *Biochem Eng J*. 2013;79:230–8.

7 Williams JA, Carnes AE, Hodgson CP. Plasmid DNA vaccine vector design: impact on efficacy, safety and upstream production. *Biotech Adv*. 2009;27:353–70.

8 Soubrier F, Laborderie B, Cameron B. Improvement of pCOR plasmid copy number for pharmaceutical applications. *Appl Microbiol Biotechnol*. 2005;66:683–8.

9 Bower DM, Prather KL. Development of new plasmid DNA vaccine vectors with R1-based replicons. *Microb Cell Fact*. 2012;11:107.

10 Gerdes K. The *parB* (*hok/sok*) locus of Plasmid R1: a general purpose plasmid stabilization system. *Nat Biotechnol*. 1988;6:1402–5.

11 Jaén KE, Velázquez D, Sigala JC, Lara AR. Design of a microaerobically inducible replicon for high-yield plasmid DNA production. *Biotechnol Bioeng*. 2019;116:2514–25.

12 Lara AR, Jaén KE, Sigala JC, Regestein L, Büchs J. Evaluation of microbial globin promoters for oxygen-limited processes using *Escherichia coli*. *J Biol Eng*. 2017;11:39.

13 Rosenfeld R, Grover NB. Control of miniR1 plasmid replication: a computer simulation. *Plasmid*. 1993;29:94–116.

14 Womble DD, Sampathkumar P, Easton AM, Luckow VA, Rownd RH. Transcription of the replication control region of the IncFII R-plasmid NR1 *in vitro* and *in vivo*. *J Mol Biol*. 1985;181:395–410.

15 Light J, Riise E, Molin S. Transcription and its regulation in the basic replicon region of plasmid R1. *Molecul General Genet*. 1985;198:503–8.

16 Blomberg P, Nordström K, Wagner EG. Replication control of plasmid R1: RepA synthesis is regulated by CopA RNA through inhibition of leader peptide translation. *EMBO J*. 1992;11:2675–83.

17 Bernstein JA, Khodursky AB, Lin PH, Lin-Chao S, Cohen SN. Global analysis of mRNA decay and abundance in *Escherichia coli* at single-gene resolution using two-color fluorescent DNA microarrays. *Proc Natl Acad Sci USA*. 2002;99:9697–702.

18 Maurizi MR. Proteases and protein degradation in *Escherichia coli*. *Experientia*. 1992;48:178–201.

19 Khosla C, Bailey JE. Characterization of the oxygen-dependent promoter of the *Vitreoscilla* hemoglobin gene in *Escherichia coli*. *J Bacteriol*. 1989;171:5995–6004.

20 Rosa SS, Prazeres DMF, Azevedo AM, Marques MPC. mRNA vaccines manufacturing: challenges and bottlenecks. *Vaccine*. 2021;39:2190–200.

**How to cite this article:** Islas F, Sabido A, Sigala J-C, Lara AR. Design of microaerobically inducible miniR1 plasmids. *mLife*. 2023; https://doi.org/10.1002/mlf2.12058

*microorganisms*

MDPI

*Review*

# *Vitreoscilla* Haemoglobin: A Tool to Reduce Overflow Metabolism

**Hilal Taymaz-Nikerel [1] and Alvaro R. Lara [2,*]**

[1] Department of Genetics and Bioengineering, Istanbul Bilgi University, Istanbul 34060, Turkey; hilal.nikerel@bilgi.edu.tr
[2] Departamento de Procesos y Tecnología, Universidad Autónoma Metropolitana, Mexico City 05348, Mexico
* Correspondence: alara@cua.uam.mx

**Abstract:** Overflow metabolism is a phenomenon extended in nature, ranging from microbial to cancer cells. Accumulation of overflow metabolites pose a challenge for large-scale bioprocesses. Yet, the causes of overflow metabolism are not fully clarified. In this work, the underlying mechanisms, reasons and consequences of overflow metabolism in different organisms have been summarized. The reported effect of aerobic expression of *Vitreoscilla* haemoglobin (VHb) in different organisms are revised. The use of VHb to reduce overflow metabolism is proposed and studied through flux balance analysis in *E. coli* at a fixed maximum substrate and oxygen uptake rates. Simulations showed that the presence of VHb increases the growth rate, while decreasing acetate production, in line with the experimental measurements. Therefore, aerobic VHb expression is considered a potential tool to reduce overflow metabolism in cells.

**Keywords:** overflow metabolism; P/O ratio; *Vitreoscilla* haemoglobin; flux balance analysis



**Citation:** Taymaz-Nikerel, H.; Lara, A.R. *Vitreoscilla* Haemoglobin: A Tool to Reduce Overflow Metabolism. *Microorganisms* **2022**, *10*, 43. https://doi.org/10.3390/microorganisms10010043

Academic Editor: Benjamin C. Stark

Received: 18 November 2021
Accepted: 20 December 2021
Published: 26 December 2021

**Publisher's Note:** MDPI stays neutral with regard to jurisdictional claims in published maps and institutional affiliations.



## 1. Overflow Metabolism and Bioprocessing

Fast growing cells often display incomplete oxidation of the carbon source, even if oxygen is present in non-limiting amounts. As a result, partially oxidized molecules, rather than $CO_2$, are excreted to the environment. This phenomenon was already observed for yeasts by Louis Pasteur in 1861 [1] and later on in muscle cells [2], carcinoma cells [3] and normal tissues after viral infection [4]. Traditionally referred to as the "Pasteur", "Warburg" and "Crabtree" effect, such a metabolic state is collectively known as overflow metabolism [5].

The biotechnological production of molecules requires the transformation of a substrate (most commonly glucose) into the desired molecule. Because these are autocatalytic processes, the amount of product that can be synthesized depends on the amount of cells in the culture. Therefore, a standard procedure to maximize the amount of synthesized product is to attain an elevated amount of cells in the culture. These so-called high cell-density cultures require elevated amounts of carbon source that lead to overflow metabolism.

Examples of overflow metabolites excreted by organisms of biotechnological relevance are shown in Table 1. The accumulation of such by-products lowers the pH of the broth, affecting the cellular physiology. The continuous addition of alkali to control pH can result in the accumulation of ions and osmolality increase that can negatively affect the cells. Moreover, the formation of overflow metabolites can be seen as a waste of carbon that otherwise could have been incorporated to biomass and/or product. For instance, the amount of acetate produced as overflow metabolite can be as high as 15% (*w*/*w*) of the carbon source (glucose) consumed [6].

Diverse strategies have been applied to reduce overflow metabolism in different organisms, including genetic interventions [7] and the slow addition of the carbon source (fed-batch cultures) [8]. Nevertheless, all the proposed solutions also imply disadvantages. Furthermore, despite the relevance of overflow metabolism from a physiological and biotechnological standpoint, its causes are not clearly understood. Some possible explanations are briefly presented below.

**Table 1.** Overflow metabolites in several organisms of industrial relevance.

| Organism | Main Overflow Metabolites |
|---|---|
| *Bacillus subtilis* | Acetoin, acetate [9] |
| CHO cells | Lactate [10] |
| *Clostridium thermocellum* | Lactate, acetate, ethanol [11] |
| *Corynebacterium glutamicum* | Dihydroxyacetone, acetate [12] |
| *Escherichia coli* | Acetate [13] |
| *Lachance kluyveri* | Ethylacetate [14] |
| *Saccharomyces cerevisiae* | Ethanol [13] |
| *Penicillium chrysogenum* | Gluconate [15] |
| *Pichia pastoris* | Ethanol, acetate [16] |

### *1.1. Causes of Overflow Metabolism*

#### 1.1.1. Metabolic Imbalance

A relatively straightforward explanation of overflow metabolism considers that a metabolic imbalance between catabolism and anabolism occurs at high glucose uptake rates ($q_S$) [17]. At low $q_S$, the substrate can be fully oxidized via the tricarboxylic acid cycle (TCA) and NADH regenerated by the electron transport chain (Figure 1). Increasing $q_S$ is accompanied by an increased oxygen consumption rate ($q_{O2}$). After a certain threshold value of glucose uptake ($q_{s,crit}$), overflow metabolites start to accumulate. This coincides with a maximum rate of oxygen consumption ($q_{O2,\,max}$). Above this respiratory capacity, $q_S$ can continue to increase, with the concomitant synthesis of overflow metabolites (for example, for *E. coli* cultures, see [18]). NADH regeneration rate could not be reached by the electron transport chain only, and therefore, fermentative pathways are activated. TCA activity can also be lowered [19]. Enzyme capacity constraints combined with flux balance analysis using a genome-scale model predicted the lactate shift in CHO cells coincident with a plateau in the oxidative phosphorylation flux and specific $CO_2$ formation rate ($q_{CO2}$) patterns in relation to $q_S$ [20].

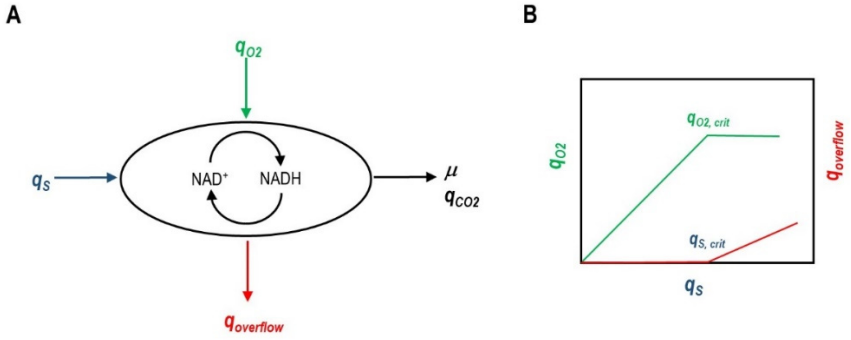


**Figure 1.** Overview of Overflow Metabolism as Originated from a Metabolic Imbalance. (**A**): NADH regeneration rate can be insufficient for given substrate and oxygen uptake rates ($q_S$ and $q_{O2}$, respectively) to fully oxidize the carbon source to $CO_2$ ($q_{CO2}$). Therefore, overflow metabolites are produced ($q_{overflow}$) to contribute to NADH regeneration. (**B**): Initially $q_{O2}$ displays a linear correlation with $q_S$. However, at some point $q_{O2}$ reaches a maximum ($q_{O2,\,crit}$) and $q_S$ continues increasing, with the concomitant production of overflow metabolites.

Maintaining the cells growing at $q_S < q_{S,crit}$ in fed-batch cultures avoids overflow metabolism and allows attaining high cell-densities. This principle has been successfully applied to a variety of microbial and animal cells [21]. Decreasing $q_S$ by genetic manipulation has also been a successful strategy to reduce overflow metabolism in *E. coli* [22–25] and CHO cells [26]. Although overflow metabolism can be completely suppressed by this approach, growth rate ($\mu$) is also affected. The activity of the tricarboxylic acid cycle (TCA) in *E. coli* was increased to better cope with the high glycolytic flux at elevated $q_S$, which

decreased acetate formation [27]. Another approach to overcome overflow metabolism considering a metabolic imbalance was to increase the $NAD^+$ regeneration rate. For instance, Vemuri and co-workers expressed a water-forming heterologous dehydrogenase in *E. coli* and *S. cerevisiae* [19,28]. Despite the strong reduction of overflow metabolism, a decrease on biomass yield was observed, which is probably linked to the waste of reductive power to form water instead of contributing to a proton gradient. The metabolic causes of overflow metabolism in mammalian cells can be more complex. For instance, Bulté and co-workers [29] proposed that pyruvate transport to the mitochondria could be a limiting factor for its complete oxidation, leading to lactate synthesis in the cytoplasm. The researchers enhanced pyruvate transport by overexpressing a mitochondrial pyruvate carrier in CHO cells, which resulted in up to 50% decrease of aerobic lactate production.

The approach of metabolic imbalance can partially explain the causes of overflow metabolism and inspire some genetic interventions to reduce it. However, other hypotheses have been proposed from different perspectives, as explained below.

#### 1.1.2. Proteome Allocation

Peebo and co-workers [30] analysed the proteome of *E. coli* growing at different $\mu$. They found that as $\mu$ increased, the abundance of proteins related to carbohydrate transport and metabolism lowered, while those related to translation increased. In order to quantitatively describe the effects on the proteome, the authors defined the investment of translational capacity as the "protein expression cost" (defined as the product of the protein concentration multiplied by its length in amino acids). The expression cost of the ATP synthase and NADH dehydrogenase I relative to the total proteome increased proportionally to $\mu$ and reached a plateau coincident with the shift to overflow metabolism. Although the authors did not clearly link these results with the control of overflow metabolism, they suggested that *E. coli* shifts to a more economic protein usage. Due to the high demand of protein resource for the respiratory chain (ATP synthase requiring up to 2.5% of the total translational capacity), different mechanisms for energy production are preferred. This hypothesis was analysed in detail by Basan and co-workers using *E. coli* as a model organism [31]. The authors described that, although respiration is more efficient to generate energy than fermentation, the proteome cost of the former is much higher than for the latter. For glycolytic carbon sources, the authors calculated that the proteome efficiency of energy biogenesis is approx. 750 mM ATP/$A_{600nm}$/h for fermentation, while for respiration it was approx. 390 mM ATP/$A_{600nm}$/h. Therefore, the authors proposed that overflow metabolism is a programmed global response of the cells to cope with the proteome demands for energy generation. Further modelling and flux balance analysis have been applied to predict overflow metabolism in *E. coli* [32]. Chen and Nielsen [33] also modelled the energy metabolism of *E. coli* and *S. cerevisiae* coupled to proteomic analysis to successfully predict the start of overflow metabolism in relation to $\mu$, $q_S$, or ATP rate. Interestingly, they found that the differences between energy yields of respiration and fermentation were much larger for *E. coli* than for *S. cerevisiae*. Proteome allocation coupled with dynamic flux balance analysis and adjustable maintenance energy level allowed good prediction of growth overflow metabolism and recombinant protein production of engineered *E. coli* strains [34].

The hypothesis of proteome allocation as the origin of overflow metabolism has also been evaluated for *Lactococcus lactis* [35] and *Clostridium ljungdahlii* [36]. Proteome reduction to develop minimal cells has been reported for *E. coli* [37]. Proteome-reduced *E. coli* strains have a superior performance for plasmid DNA vaccines production in batch and fed-batch mode [38]. However, overflow metabolism in proteome-reduced cells has not yet been thoroughly tested.

#### 1.1.3. Molecular Crowding

It has been suggested that cells have evolved to maintain the enzyme-protein levels at the minimum level compatible with function. The volume occupied by proteins in the cell is

20–30% of the cell volume (determined for bacterial, yeast and mammalian cells). This large proportion may limit the diffusion and solubility of molecules in the cell due to the viscosity of the remaining unbound water [39]. Therefore, it is possible that not only the efficiency to produce ATP, but also the amount of proteins (and the volume) needed for a given pathway may be key for the cell to choose a particular energy-generation mechanism [40]. This hypothesis has been tested using modelling and experimental measurements. A flux balance model of the metabolism of *E. coli* including the constraint for the concentration of enzymes, named "FBA with Molecular Crowding" (FBAwMC) was introduced by Beg and co-workers [41]. This model could predict the sequence of utilization of carbon sources in mixtures, as well as $\mu$. Although overflow metabolism was also predicted, the model estimated a lesser excretion of acetate than the experimentally determined. FBAwMC was refined and combined with enzyme activity measurements to analyze metabolic shifts from low to high $\mu$ in *E. coli* [42]. Vazquez et al. [43] applied FbwMC to simulate the overflow metabolism of murine LS and hybridoma cells. The shift to lactate production and the threshold $q_S$ values were estimated with good accuracy. According to their calculations, the mitochondria contribute 5 times more to molecular crowding than glycolytic enzymes and 50 times more than lactate dehydrogenase. Van Hoek and co-workers used FBAwMC to study the metabolism of *L. lactis* and S. cerevisiae yielding interesting results [44]. In agreement with previous independent reports, the authors concluded that the shift to lactate production is determined by the existence of a limited cytoplasmic solvent capacity for allocating the components of the ATP generation pathways.

Important elements of the energy production cellular machinery are located in the membranes. Therefore, molecular crowding of the membrane can be a limiting factor to shift from purely aerobic to aerobic-fermentative energy production. For example, crowding of the cytochromes in the membrane of *E. coli* was introduced as an additional constraint in FBA [45]. The well-known differential use of cytochromes depending on $q_S$ and oxygen availability was well simulated. However, the $q_{S,crit}$ obtained did not agree with the experimental data. This could be probably due to the fact that other important molecules, such as ATPase were not considered. In a more comprehensive study, Szenk et al. [46] integrated the $\mu$-dependent surface-to-volume ratio, as well as the physical size and of the proteins involved in respiration and fermentation, to evaluate whether pure respiration could be limited by membrane crowding at fast $\mu$. According to their calculation, the surface efficiency (given in ATP/s/nm$^2$) for aerobic respiration is three, while it reaches a value of 15 for acetate fermentation. Furthermore, they found that the percentage of the membrane occupied by the electron transport chain component increases with the growth rate, and plateau at a value of ca. 8%, coincident with the onset of overflow metabolism. Moreover, the authors linked the surface efficiency with the phosphate/oxygen (P/O, depending on the molecules of ATP produced per NADH equivalent) ratio. P/O ratio decreases when the surface efficiency increases (fermentation), and the growth rates at which overflow metabolism triggers are higher at lower P/O ratios.

## 2. *Vitreoscilla* Haemoglobin as a Tool to Reduce Overflow Metabolism

### *2.1. Aerobic Expression of Vitreoscilla Hemoglobin*

The haemoglobin of the aerobic bacteria *Vitreoscilla stercoraria* (VHb) is a single domain haemoglobin that exists as a dimeric protein of two identical subunits with a mass of 15.7 Da each [47]. Initially identified as a cytochrome, evidence was provided showing that VHb can pump $Na^+$ transmembranally, instead of protons [48]. VHb displays a remarkably high capacity for oxygen delivery to terminal oxidases (high dissociation rate $k_{off} = 78$ mM$^{-1}$ s$^{-1}$) [47]. In consequence, VHb has been used as a strategy to improve cellular performance, particularly under oxygen-limited environments, enhancing the $q_{O2}$ and $\mu$ and biomass formation (for reviews see [47,49–52]). The impact of VHb expression is ample and some features depend on the host. The effect of VHb has been mostly characterized in *E. coli* cells. In *E. coli*, VHb expression restored the oxygen consumption in a strain lacking both cytochromes (Cyo and Cyd), reaching 70% of the respiration rate of the wild type strain [53], and is physiologically active in

the oxygen-carrying form during aerobic respiration [54]. The $H^+$/O ratio, the transmembrane ΔpH, and the ATP content of VHb-expressing *E. coli* cells were 1.5, 1.6 and 2 times greater, respectively, than the corresponding values in non-expressing cells [55]. VHb-expressing *E. coli* cells displayed higher oxidative activity than non-expressing cells, as indicated by the Redox Sensor Green fluorescence [56].

Cellular localization of VHb has also been investigated, due to its relationship with the respiration proteins. Khosla and Bailey [57], using fractionation and proteinase K accessibility techniques, determined that nearly 40% of VHb is in the periplasmic space in *E. coli*. In contrast, Ramandeep and co-workers [58], using immunogold labelling reported that more than 90% of the VHb was located in the periplasm of *E. coli*, and that 57% of the VHb was localized within 0.1 μm of the inner membrane. Using immunofluorescence microscopy, Juarez and co-workers found that VHb is distributed in the cytoplasm and the membranes of organelles in CHO cells [59]. Because periplasmic localization of VHb would enhance the effect of VHb on the electron transport chain, VHb was fused to OmpA and expressed in *E. coli* [58]. Approximately 50% of the OmpA-VHb was located in the periplasmic space. However, no improvement of the growth characteristics or oxygen consumption, compared to the unfused VHb expression, were observed. The authors speculated that cytoplasmic location of VHb may provide an oxygen buffer to facilitate oxygen delivery to the terminal oxidase that are oriented toward the cytoplasm. The authors also mentioned that non-functional apoprotein could have accumulated in the periplasmic space, explaining the lack of effects observed. More recently, the twin-arginine translocase pathway was used to export active VHb into the periplasmic space of *Halomonas bluephagenesis*. This improved cell formation and poly (3-hydroxybutyrate) production under oxygen limitation [60]. Moreover, the authors shown that the intracellular and periplasmic VHb expression increased the amount of proteins related to aerobic respiration in *H. bluephagenesis*, particularly cytochromes and beta subunit of the ATP synthase. Therefore, the presence of VHb affects respiratory efficiency not only by increasing oxygen transport, but also by increasing a higher amount of enzymes of the respiratory chain. This contributes to a better understanding of the enhanced respiratory capacity of cells expressing VHb.

In comparison with the relatively abundant information on the use of VHb for improving bioprocesses under oxygen limitation, the application of VHb for aerobic cultures is scarce. Table 2 shows examples of VHb expression under fully aerobic conditions and the reported effects. Particular physiological responses depend on the host organism and even on the strain used. However, a common factor of the different reports is that higher oxygen uptake and ATP generation can benefit the culture performance. A key aspect to be addressed is the impact of VHb on the overflow metabolism of cells. There are few but relevant reports showing that aerobic VHb expression, in fact, reduces overflow metabolism (for instance in *E. coli* and CHO cells, Table 2). Therefore, VHb expression could be an efficient and simple strategy to overcome overflow metabolism. Potential metabolic reasons for this are discussed below.

**Table 2.** Reported Effects of *Vitreoscilla* Haemoglobin in Aerobic Cultures.

| Organism | Reported Effect |
| --- | --- |
| *Aurantiochytrium* sp. | 44% higher total fatty acid and 9-fold higher astaxanthin contents [61] |
| CHO cells | 40–100% increase of tissue plasminogen activator production [62] |
| | $\mu$ and biomass yields increase, lactate production per cell decreased by 40% [62] |
| | $NAD^+$/NADH ratio and ATP cell content decreased, $NADP^+$/NADPH ratio increased [59] |
| *Corynebacterium glutamicum* | Synthesis of biomass increased 10% and L-glutamate production increased 30% [63] |

**Table 2.** *Cont.*

| Organism | Reported Effect |
| --- | --- |
| *Escherichia coli* | Increased $q_{O2}$, $\mu$ and L-phenylalanine production [64]<br>60% decrease of acetate accumulation when VHb was expressed from a plasmid. Two-fold increase of plasmid DNA yield from biomass in strain W3110 [65]<br>37% and 50% reduction in acetate production rate in strains W3110 and BL21, respectively, when VHb was expressed from the chromosome. Different impact on the expression of genes from the TCA cycle and cytochromes, depending on the strain (W3110 or BL21) [66] |
| *Gluconobacter oxydans* | 8% increase of volumetric oxidation activity of N-2-hydroxyethyl glucamine [67] |
| *Mortierella alpina* | Increased $\mu$ and 1.6-fold higher arachidonic acid production [68] |
| *Schwanniomyces occidentalis* | $\mu$ and alpha-amylase production increased [69] |
| *Pichia pastoris* | 4-fold higher β-galactosidase activity [70]<br>31.5% higher expression of *Y. lipolytica* LIP2 lipase [71] |
| *Yarrowia lipolytica* | 23% higher $\mu$, 2.6-fold higher biomass formation, 92% higher RNase production [72] |

### *2.2. Metabolic Consequences of Aerobic Expression of Vitreoscilla Haemoglobin*

As explained before, overflow metabolism has been associated with fast growth, since under fast growth energy is generated via fermentation instead of respiration. In addition to bacteria and fungi many other organisms—mammalian cells, plants—use respiration at low glucose uptake rates and aerobic fermentation at high glucose uptake rates [73]. It was shown that $NAD^+$/NADH ratio is key to the metabolic differences between the metabolic switches: redox balance is one of the factors leading to overflow metabolism [19,44,74]. As a consequence, cofactor redox engineering strategies have been developed for industrial applications [75].

Using a network-based approach a recent study suggested that there is an upper limit to the Gibbs energy release rate of *E. coli* and *S. cerevisiae* [76]. Due to the different reactions in fermentative pathways and oxidative phosphorylation, thermodynamic driving force in terms of Gibbs energy change is different between those. The authors suggested that this limit in thermodynamics of metabolism might explain the overflow metabolism, since they observed that flux distributions were shifted from respiratory pathways to fermentative pathways with increasing substrate uptake rates.

Through a kinetic model of *E. coli* it was suggested that overflow metabolism should be considered a reversible process and be universal including ethanol consumption by *S. cerevisiae* and lactate by mammalian cells [77]. Mori et al. [78] combined genome-scale modelling with experimental data to characterize yield-cost trade-off in *E. coli* and found that the efficiency of ATP synthesis is the key driver.

Fifteen models of overflow metabolism have been reviewed recently [79]. In addition to the above mentioned constraints of free energy dissipation [76], total proteome [31,79], membrane occupancy [45,46]; the constraints such as electron transfer capacity, oxygen uptake rate, and macromolecular density were observed to be used. Overflow metabolism was also interpreted from the perspective of the regulation of oxidative stress [80] since growth increases as a response to oxidative stress. The trade-off between glucose uptake rate and growth yield was related to the changes in P/O ratio and the flux allocation between glycolysis and pentose phosphate pathway [81]. It has been demonstrated that the presence of VHb in *E. coli* enhanced by 5-fold the content of the cytochrome *bo* and by 1.5 –fold the content of the cytochrome *bd* in cells of *E. coli* [82]. Cytochrome O works as a proton pump, mobilizing 2 protons per electron ($H^+/e^- = 2$). In contrast, an $H^+/e^-$ ratio of 1 is obtained by cytochrome *bd* [83]. Therefore, it is reasonable to expect that the presence of VHb alters the P/O ratio.

Here, to investigate the effect of P/O ratio on the overflow metabolism, flux balance analysis (FBA) was carried out using *E. coli* genome scale model [84] in COBRA toolbox [85].

Following the approach in Taymaz-Nikerel et al. [86], the P/O ratio, was varied by modifying the stoichiometry of the reactions catalysed by NADH dehydrogenase (NADH10, NADH16pp, NADH17pp, NADH18pp), FADH dehydrogenase (FDH4pp) and cytochrome oxidases (CYTBD2pp, CYTBDpp, CYTBO3_4pp). Table 3 summarizes the implemented stoichiometric coefficients.

**Table 3.** Stoichiometry of dehydrogenases and cytochrome oxidases involved in the *E. coli* metabolic network [84].

| Name of the Reaction | | Stoichiometry |
|---|---|---|
| NADH dehydrogenase | NADH16pp | (2×P/O+1) h[c] + nadh[c] + q8[c] → nad[c] + q8h2[c] +(2×P/O) h[p] |
| FADH dehydrogenase | FDH4pp | (2×P/O+1) h[c] + q8[c] + for[p] → q8h2[c] + co2[p] + (2×P/O) h[p] |
| Cytochrome oxidase bd-type | CYTBD2pp | (P/O) h[c] + 0.5 o2[c] + mql8[c] → h2o[c] + mqn8[c] + (P/O) h[p] |
| Cytochrome oxidase bd-type | CYTBDpp | (P/O) h[c] + 0.5 o2[c] + q8h2[c] → h2o[c] + q8[c] + (P/O) h[p] |
| Cytochrome oxidase bo-type | CYTBO3_4pp | (2×P/O) h[c] + 0.5 o2[c] + q8h2[c] → h2o[c] + q8[c] +(2×P/O) h[p] |

Theoretically P/O ratio in *E. coli* varies between 0.67 and 2.67 [87]. For constraints of FBA, maximum glucose uptake rate of *E. coli*, namely $q_S = -11$ mmol $g^{-1}h^{-1}$ [88] and $q_{O2} = -8$ mmol $g^{-1}h^{-1}$ values were implemented for wild type (Figure 2). For the second case addition to maximum glucose uptake rate of $q_S = -11$ mmol $g^{-1}h^{-1}$, maximum $O_2$ uptake rate of $q_{O2} = -15$ mmol $g^{-1}h^{-1}$ [89] were used (Figure 3) for the wild type. In the presence of VHb cases, addition to the same $q_S$ values, 25% higher $O_2$ uptake rates were set due to the experimental measurements [66]. The values for $q_{O2}$ was selected to cover from relatively low to maximum capacity of the cell. To see the effect of P/O ratio on overflow metabolism, runs for varying P/O were carried out. At low P/O ratio values, acetate production rate was higher, in agreement with the finding that decreased P/O ratios yielded in higher rate of acetate production [81]. In all the cases studied/simulated bd-type cytochrome oxidases replace bo-type for P/O > 1. This might be related with the observation that the fraction of ATP produced by the electron transport chain is higher at high P/O ratios [46]. When $q_{O2}$ is at its maximum value (Figure 3) in the presence of VHb, $q_{CO2}$ decreases after P/O ratio of around 2.

Figures 2 and 3 clearly show the effect of P/O ratio on the overflow metabolism as acetate production decreases by increasing P/O ratio, consistent with the work of Szenk et al. 2017 [46]. At a fixed $q_{O2}$, growth rate is maximized at stable $\mu$ below P/O ratio of 1. For P/O ratio > 1 maximum growth rate increases with increasing P/O ratio. bo-type and bd-type cytochrome oxidases replace each other for P/O ratio below 1 and above 1.

In the presence of VHb, it was observed that $q_{O2}$ was around 20% higher [66] compared to that in cells without VHb. Acetate production is lower when VHb is present, consistent with previous experimental findings [65] and even totally diminishes at higher $q_{O2}$ (Figure 3). This implies possibilities for modification of aerobic respiratory chains of organisms to change P/O ratio (different ATP yields) and thus lower the impacts of overflow metabolism, although the complex responses of the organism(s) should not be avoided. On the other hand, it has already been mentioned that the periplasmic proteome of cells can change in response to VHb expression. This may be an adaptation to a presumably crowded section of the cell in order to increase energy production.

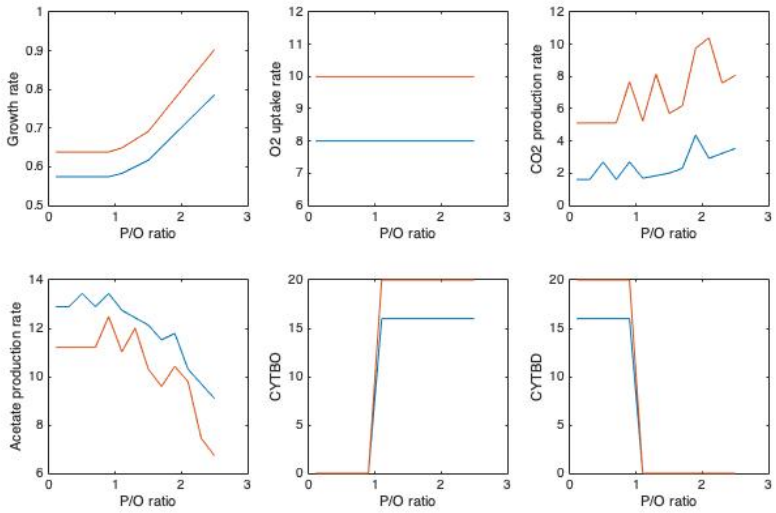


**Figure 2.** Distribution of Fluxes with Varying P/O ratio. Biomass production is Maximized, Constraints $q_S = -11$ mmol $g^{-1}h^{-1}$ [88], $q_{O2} = -8$ mmol $g^{-1}h^{-1}$ for wild type (blue) and $-8 \times 1.25$ mmol $g^{-1}$ $h^{-1}$ in the presence of VHb (red).

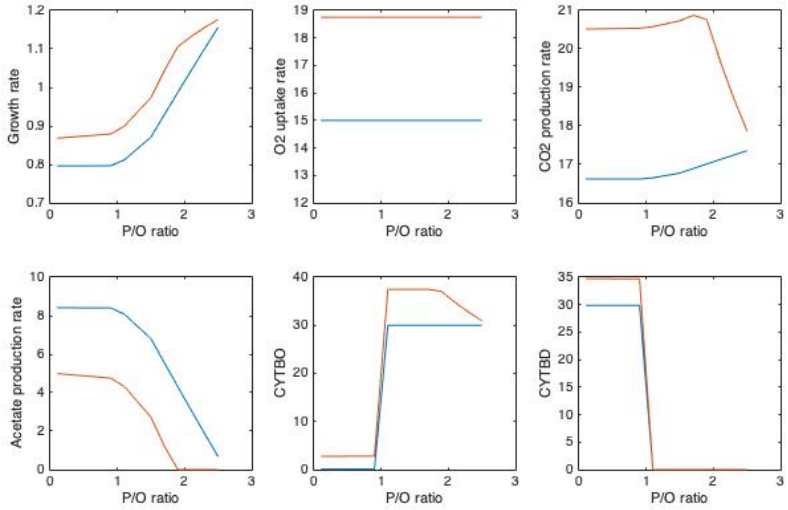


**Figure 3.** Distribution of fluxes with varying P/O ratio. Biomass production is maximized, constraints $q_S = -11$ mmol $g^{-1}h^{-1}$, $q_{O2} = -15$ mmol $g^{-1}h^{-1}$ [89] for wild type (blue) and $-15 \times 1.25$ mmol $g^{-1}h^{-1}$ in the presence of VHb (red).

These simulations may help to understand how VHb could contribute to reduce production of overflow metabolites. Considerable investigations are still needed to better understand the physiological changes caused by aerobic VHb expression. Nevertheless, the current available information point to VHb technology as a strong ally to improve aerobic bioprocesses.

**Author Contributions:** Conceptualization, A.R.L. and H.T.-N.; software, H.T.-N.; validation, H.T.-N.; investigation, A.R.L. and H.T.-N.; writing—original draft preparation, A.R.L. and H.T.-N.; writing—review and editing, A.R.L. and H.T.-N. All authors have read and agreed to the published version of the manuscript.

**Funding:** This research received no external funding.

**Conflicts of Interest:** The authors declare no conflict of interest.

## References


1. PORTER, J.R. Louis PASTEUR; achievements and disappointments, 1861. *Bacteriol. Rev.* **1961**, *25*, 389–403. [CrossRef] [PubMed]
2. Fletcher, W.M. Lactic acid in amphibian muscle. *J. Physiol.* **1907**, *35*, 247–309. [CrossRef]
3. Warburg, O.; Minami, S. Versuche an überlebendem carcinom-gewebe. *Klin. Wochenschr.* **1923**, *2*, 776–777. [CrossRef]
4. Crabtree, H.G. The carbohydrate metabolism of certain pathological overgrowths. *Biochem. J.* **1928**, *22*, 1289–1298. [CrossRef]
5. Vazquez, A. *Overflow Metabolism: From Yeast to Marathon Runners*, 1st ed.; Academic Press: London, UK, 2018.
6. Holms, W.H. The central metabolic pathways of Escherichia coli: Relationship between flux and control at a branch point, efficiency of conversion to biomass, and excretion of acetate. *Curr. Top Cell. Regul.* **1986**, *28*, 69–105. [CrossRef]
7. De Mey, M.; De Maeseneire, S.; Soetaert, W.; Vandamme, E. Minimizing acetate formation in E. coli fermentations. *J. Ind. Microbiol. Biotechnol.* **2007**, *34*, 689–700. [CrossRef] [PubMed]
8. Eiteman, M.A.; Altman, E. Overcoming acetate in Escherichia coli recombinant protein fermentations. *Trends Biotechnol.* **2006**, *24*, 530–536. [CrossRef] [PubMed]
9. Ma, W.; Liu, Y.; Lv, X.; Li, J.; Du, G.; Liu, L. Combinatorial pathway enzyme engineering and host engineering overcomes pyruvate overflow and enhances overproduction of N-acetylglucosamine in Bacillus subtilis. *Microb. Cell Fact.* **2019**, *18*, 1. [CrossRef]
10. Luo, J.; Vijayasankaran, N.; Autsen, J.; Santuray, R.; Hudson, T.; Amanullah, A.; Li, F. Comparative metabolite analysis to understand lactate metabolism shift in Chinese hamster ovary cell culture process. *Biotechnol. Bioeng.* **2012**, *109*, 146–156. [CrossRef] [PubMed]
11. Thompson, R.A.; Trinh, C.T. Overflow metabolism and growth cessation in Clostridium thermocellum DSM1313 during high cellulose loading fermentations. *Biotechnol. Bioeng.* **2017**, *114*, 2592–2604. [CrossRef]
12. Wittmann, C.; Kiefer, P.; Zelder, O. Metabolic fluxes in Corynebacterium glutamicum during lysine production with sucrose as carbon source. *Appl. Environ. Microbiol.* **2004**, *70*, 7277–7287. [CrossRef] [PubMed]
13. Paczia, N.; Nilgen, A.; Lehmann, T.; Gätgens, J.; Wiechert, W.; Noack, S. Extensive exometabolome analysis reveals extended overflow metabolism in various microorganisms. *Microb. Cell Fact.* **2012**, *11*, 122. [CrossRef]
14. Nanda, P.; Patra, P.; Das, M.; Ghosh, A. Reconstruction and analysis of genome-scale metabolic model of weak Crabtree positive yeast Lachancea kluyveri. *Sci. Rep.* **2020**, *10*, 16314. [CrossRef] [PubMed]
15. Schmitz, K.; Peter, V.; Meinert, S.; Kornfeld, G.; Hardiman, T.; Wiechert, W.; Noack, S. Simultaneous utilization of glucose and gluconate in Penicillium chrysogenum during overflow metabolism. *Biotechnol. Bioeng.* **2013**, *110*, 3235–3243. [CrossRef]
16. Nocon, J.; Steiger, M.G.; Pfeffer, M.; Sohn, S.B.; Kim, T.Y.; Maurer, M.; Rußmayer, H.; Pflügl, S.; Ask, M.; Haberhauer-Troyer, C.; et al. Model based engineering of Pichia pastoris central metabolism enhances recombinant protein production. *Metab. Eng.* **2014**, *24*, 129–138. [CrossRef] [PubMed]
17. Majewski, R.A.; Domach, M.M. Simple constrained-optimization view of acetate overflow in E. coli. *Biotechnol. Bioeng.* **1990**, *35*, 732–738. [CrossRef] [PubMed]
18. Kayser, A.; Weber, J.; Hecht, V.; Rinas, U. Metabolic flux analysis of Escherichia coli in glucose-limited continuous culture. I. Growth-rate-dependent metabolic efficiency at steady state. *Microbiology* **2005**, *151*, 693–706. [CrossRef]
19. Vemuri, G.N.; Altman, E.; Sangurdekar, D.P.; Khodursky, A.B.; Eiteman, M.A. Overflow metabolism in Escherichia coli during steady-state growth: Transcriptional regulation and effect of the redox ratio. *Appl. Environ. Microbiol.* **2006**, *72*, 3653–3661. [CrossRef]
20. Yeo, H.C.; Hong, J.; Lakshmanan, M.; Lee, D.Y. Enzyme capacity-based genome scale modelling of CHO cells. *Metab. Eng.* **2020**, *60*, 138–147. [CrossRef]
21. Shojaosadati, S.A.; Kolaei, S.M.V.; Babaeipour, V.; Farnoud, A.M. Recent advances in high cell density cultivation for production of recombinant protein. *Iran. J. Biotechnol.* **2008**, *6*, 63–84.
22. De Anda, R.; Lara, A.R.; Hernández, V.; Hernández-Montalvo, V.; Gosset, G.; Bolívar, F.; Ramírez, O.T. Replacement of the glucose phosphotransferase transport system by galactose permease reduces acetate accumulation and improves process performance of Escherichia coli for recombinant protein production without impairment of growth rate. *Metab. Eng.* **2006**, *8*, 281–290. [CrossRef]
23. Fuentes, L.G.; Lara, A.R.; Martínez, L.M.; Ramírez, O.T.; Martínez, A.; Bolívar, F.; Gosset, G. Modification of glucose import capacity in Escherichia coli: Physiologic consequences and utility for improving DNA vaccine production. *Microb. Cell Fact.* **2013**, *12*, 42. [CrossRef] [PubMed]
24. Negrete, A.; Majdalani, N.; Phue, J.N.; Shiloach, J. Reducing acetate excretion from E. coli K-12 by over-expressing the small RNA SgrS. *New Biotechnol.* **2013**, *30*, 269–273. [CrossRef]
25. Bäcklund, E.; Markland, K.; Larsson, G. Cell engineering of Escherichia coli allows high cell density accumulation without fed-batch process control. *Bioprocess Biosyst. Eng.* **2008**, *31*, 11–20. [CrossRef] [PubMed]
26. Wlaschin, K.F.; Hu, W.S. Engineering cell metabolism for high-density cell culture via manipulation of sugar transport. *J. Biotechnol.* **2007**, *131*, 168–176. [CrossRef] [PubMed]
27. Veit, A.; Polen, T.; Wendisch, V.F. Global gene expression analysis of glucose overflow metabolism in Escherichia coli and reduction of aerobic acetate formation. *Appl. Microbiol. Biotechnol.* **2007**, *74*, 406–421. [CrossRef]
28. Vemuri, G.N.; Eiteman, M.A.; McEwen, J.E.; Olsson, L.; Nielsen, J. Increasing NADH oxidation reduces overflow metabolism in Saccharomyces cerevisiae. *Proc. Natl. Acad. Sci. USA* **2007**, *104*, 2402–2407. [CrossRef]

29. Bulté, D.B.; Palomares, L.A.; Parra, C.G.; Martínez, J.A.; Contreras, M.A.; Noriega, L.G.; Ramírez, O.T. Overexpression of the mitochondrial pyruvate carrier reduces lactate production and increases recombinant protein productivity in CHO cells. *Biotechnol. Bioeng.* **2020**, *117*, 2633–2647. [CrossRef]
30. Peebo, K.; Valgepea, K.; Maser, A.; Nahku, R.; Adamberg, K.; Vilu, R. Proteome reallocation in Escherichia coli with increasing specific growth rate. *Mol. Biosyst.* **2015**, *11*, 1184–1193. [CrossRef]
31. Basan, M.; Hui, S.; Okano, H.; Zhang, Z.; Shen, Y.; Williamson, J.R.; Hwa, T. Overflow metabolism in Escherichia coli results from efficient proteome allocation. *Nature* **2015**, *528*, 99–104. [CrossRef]
32. Zeng, H.; Yang, A. Modelling overflow metabolism in Escherichia coli with flux balance analysis incorporating differential proteomic efficiencies of energy pathways. *BMC Syst. Biol.* **2019**, *13*, 3. [CrossRef] [PubMed]
33. Chen, Y.; Nielsen, J. Energy metabolism controls phenotypes by protein efficiency and allocation. *Proc. Natl. Acad. Sci. USA* **2019**, *116*, 17592–17597. [CrossRef]
34. Zeng, H.; Yang, A. Quantification of proteomic and metabolic burdens predicts growth retardation and overflow metabolism in recombinant Escherichia coli. *Biotechnol. Bioeng.* **2019**, *116*, 1484–1495. [CrossRef]
35. Chen, Y.; van Pelt-KleinJan, E.; van Olst, B.; Douwenga, S.; Boeren, S.; Bachmann, H.; Molenaar, D.; Nielsen, J.; Teusink, B. Proteome constraints reveal targets for improving microbial fitness in nutrient-rich environments. *Mol. Syst. Biol.* **2021**, *17*, e10093. [CrossRef]
36. Liu, J.K.; Lloyd, C.; Al-Bassam, M.M.; Ebrahim, A.; Kim, J.N.; Olson, C.; Aksenov, A.; Dorrestein, P.; Zengler, K. Predicting proteome allocation, overflow metabolism, and metal requirements in a model acetogen. *PLoS Comput. Biol.* **2019**, *15*, e1006848. [CrossRef] [PubMed]
37. Lastiri-Pancardo, G.; Mercado-Hernández, J.S.; Kim, J.; Jiménez, J.I.; Utrilla, J. A quantitative method for proteome reallocation using minimal regulatory interventions. *Nat. Chem. Biol.* **2020**, *16*, 1026–1033. [CrossRef]
38. de la Cruz, M.; Ramírez, E.A.; Sigala, J.C.; Utrilla, J.; Lara, A.R. Plasmid DNA Production in Proteome-Reduced. *Microorganisms* **2020**, *8*, 1444. [CrossRef]
39. Brown, G.C. Total cell protein concentration as an evolutionary constraint on the metabolic control distribution in cells. *J. Theor. Biol.* **1991**, *153*, 195–203. [CrossRef]
40. Vazquez, A.; Oltvai, Z.N. Macromolecular crowding explains overflow metabolism in cells. *Sci. Rep.* **2016**, *6*, 31007. [CrossRef]
41. Beg, Q.K.; Vazquez, A.; Ernst, J.; de Menezes, M.A.; Bar-Joseph, Z.; Barabási, A.L.; Oltvai, Z.N. Intracellular crowding defines the mode and sequence of substrate uptake by Escherichia coli and constrains its metabolic activity. *Proc. Natl. Acad. Sci. USA* **2007**, *104*, 12663–12668. [CrossRef]
42. Vazquez, A.; Beg, Q.K.; Demenezes, M.A.; Ernst, J.; Bar-Joseph, Z.; Barabási, A.L.; Boros, L.G.; Oltvai, Z.N. Impact of the solvent capacity constraint on E. coli metabolism. *BMC Syst. Biol.* **2008**, *2*, 7. [CrossRef] [PubMed]
43. Vazquez, A.; Liu, J.; Zhou, Y.; Oltvai, Z.N. Catabolic efficiency of aerobic glycolysis: The Warburg effect revisited. *BMC Syst. Biol.* **2010**, *4*, 58. [CrossRef] [PubMed]
44. van Hoek, M.J.; Merks, R.M. Redox balance is key to explaining full vs. partial switching to low-yield metabolism. *BMC Syst. Biol.* **2012**, *6*, 22. [CrossRef] [PubMed]
45. Zhuang, K.; Vemuri, G.N.; Mahadevan, R. Economics of membrane occupancy and respiro-fermentation. *Mol. Syst. Biol.* **2011**, *7*, 500. [CrossRef] [PubMed]
46. Szenk, M.; Dill, K.A.; de Graff, A.M.R. Why Do Fast-Growing Bacteria Enter Overflow Metabolism? Testing the Membrane Real Estate Hypothesis. *Cell Syst.* **2017**, *5*, 95–104. [CrossRef]
47. Stark, B.C.; Pagilla, K.R.; Dikshit, K.L. Recent applications of Vitreoscilla hemoglobin technology in bioproduct synthesis and bioremediation. *Appl. Microbiol. Biotechnol.* **2015**, *99*, 1627–1636. [CrossRef]
48. Efiok, B.J.; Webster, D.A. A cytochrome that can pump sodium ion. *Biochem. Biophys. Res. Commun.* **1990**, *173*, 370–375. [CrossRef]
49. Stark, B.C.; Dikshit, K.L.; Pagilla, K.R. The Biochemistry of Vitreoscilla hemoglobin. *Comput. Struct. Biotechnol. J.* **2012**, *3*, e201210002. [CrossRef]
50. Stark, B.C.; Dikshit, K.L.; Pagilla, K.R. Recent advances in understanding the structure, function, and biotechnological usefulness of the hemoglobin from the bacterium Vitreoscilla. *Biotechnol. Lett.* **2011**, *33*, 1705–1714. [CrossRef]
51. Yu, F.; Zhao, X.; Wang, Z.; Liu, L.; Yi, L.; Zhou, J.; Li, J.; Chen, J.; Du, G. Recent Advances in the Physicochemical Properties and Biotechnological Application of. *Microorganisms* **2021**, *9*, 1445. [CrossRef]
52. Webster, D.A.; Dikshit, K.L.; Pagilla, K.R.; Stark, B.C. The Discovery of Vitreoscilla Hemoglobin and Early Studies on Its Biochemical Functions, the Control of Its Expression, and Its Use in Practical Applications. *Microorganisms* **2021**, *9*, 1637. [CrossRef] [PubMed]
53. Dikshit, R.P.; Dikshit, K.L.; Liu, Y.X.; Webster, D.A. The bacterial hemoglobin from Vitreoscilla can support the aerobic growth of Escherichia coli lacking terminal oxidases. *Arch. Biochem. Biophys.* **1992**, *293*, 241–245. [CrossRef]
54. Dikshit, K.L.; Webster, D.A. Cloning, characterization and expression of the bacterial globin gene from Vitreoscilla in Escherichia coli. *Gene* **1988**, *70*, 377–386. [CrossRef]
55. Kallio, P.T.; Kim, D.J.; Tsai, P.S.; Bailey, J.E. Intracellular expression of Vitreoscilla hemoglobin alters Escherichia coli energy metabolism under oxygen-limited conditions. *Eur. J. Biochem.* **1994**, *219*, 201–208. [CrossRef] [PubMed]
56. Jaén, K.E.; Velazquez, D.; Delvigne, F.; Sigala, J.C.; Lara, A.R. Engineering, E. coli for improved microaerobic pDNA production. *Bioprocess Biosyst. Eng.* **2019**, *42*, 1457–1466. [CrossRef] [PubMed]

57. Khosla, C.; Bailey, J.E. Evidence for partial export of Vitreoscilla hemoglobin into the periplasmic space in Escherichia coli. Implications for protein function. *J. Mol. Biol.* **1989**, *210*, 79–89. [CrossRef]
58. Ramandeep; Hwang, K.W.; Raje, M.; Kim, K.J.; Stark, B.C.; Dikshit, K.L.; Webster, D.A. Vitreoscilla hemoglobin. Intracellular localization and binding to membranes. *J. Biol. Chem.* **2001**, *276*, 24781–24789. [CrossRef]
59. Juárez, M.; González-De la Rosa, C.H.; Sigala, J.C.; Lara, A.R. Effect of *Vitreoscilla* hemoglobin on recombinant protein expression and energy metabolism of CHO cells. *Rev. Mex. Ing. Quím.* **2021**, *20*, 281–288. [CrossRef]
60. Ouyang, P.; Wang, H.; Hajnal, I.; Wu, Q.; Guo, Y.; Chen, G.Q. Increasing oxygen availability for improving poly(3-hydroxybutyrate) production by Halomonas. *Metab. Eng.* **2018**, *45*, 20–31. [CrossRef]
61. Suen, Y.L.; Tang, H.; Huang, J.; Chen, F. Enhanced production of fatty acids and astaxanthin in Aurantiochytrium sp. by the expression of Vitreoscilla hemoglobin. *J. Agric. Food Chem.* **2014**, *62*, 12392–12398. [CrossRef]
62. Juárez, M.; González-De la Rosa, C.H.; Memún, E.; Sigala, J.C.; Lara, A.R. Aerobic expression of Vitreoscilla hemoglobin improves the growth performance of CHO-K1 cells. *Biotechnol. J.* **2017**, *12*. [CrossRef] [PubMed]
63. Liu, Q.; Zhang, J.; Wei, X.X.; Ouyang, S.P.; Wu, Q.; Chen, G.Q. Microbial production of L -glutamate and L -glutamine by recombinant Corynebacterium glutamicum harboring Vitreoscilla hemoglobin gene vgb. *Appl. Microbiol. Biotechnol.* **2008**, *77*, 1297–1304. [CrossRef] [PubMed]
64. Wu, W.B.; Guo, X.L.; Zhang, M.L.; Huang, Q.G.; Qi, F.; Huang, J.Z. Enhancement of l-phenylalanine production in Escherichia coli by heterologous expression of Vitreoscilla hemoglobin. *Biotechnol. Appl. Biochem.* **2018**, *65*, 476–483. [CrossRef] [PubMed]
65. Pablos, T.E.; Sigala, J.C.; Le Borgne, S.; Lara, A.R. Aerobic expression of Vitreoscilla hemoglobin efficiently reduces overflow metabolism in Escherichia coli. *Biotechnol. J.* **2014**, *9*, 791–799. [CrossRef]
66. Lara, A.R.; Galindo, J.; Jaén, K.E.; Juárez, M.; Sigala, J.C. Physiological Response of. *J. Microbiol. Biotechnol.* **2020**, *30*, 1592–1596. [CrossRef]
67. Liu, D.; Ke, X.; Hu, Z.C.; Zheng, Y.G. Improvement of pyrroloquinoline quinone-dependent d-sorbitol dehydrogenase activity from Gluconobacter oxydans via expression of Vitreoscilla hemoglobin and regulation of dissolved oxygen tension for the biosynthesis of 6-(N-hydroxyethyl)-amino-6-deoxy-α-l-sorbofuranose. *J. Biosci. Bioeng.* **2021**, *131*, 518–524. [CrossRef]
68. Zhang, H.; Feng, Y.; Cui, Q.; Song, X. Expression of Vitreoscilla hemoglobin enhances production of arachidonic acid and lipids in Mortierella alpina. *BMC Biotechnol.* **2017**, *17*, 68. [CrossRef]
69. Suthar, D.H.; Chattoo, B.B. Expression of Vitreoscilla hemoglobin enhances growth and levels of alpha-amylase in Schwanniomyces occidentalis. *Appl. Microbiol. Biotechnol.* **2006**, *72*, 94–102. [CrossRef]
70. Wu, J.M.; Hsu, T.A.; Lee, C.K. Expression of the gene coding for bacterial hemoglobin improves beta-galactosidase production in a recombinant Pichia pastoris. *Biotechnol. Lett.* **2003**, *25*, 1457–1462. [CrossRef]
71. Wang, X.; Sun, Y.; Shen, X.; Ke, F.; Zhao, H.; Liu, Y.; Xu, L.; Yan, Y. Intracellular expression of Vitreoscilla hemoglobin improves production of Yarrowia lipolytica lipase LIP2 in a recombinant Pichia pastoris. *Enzyme. Microb. Technol.* **2012**, *50*, 22–28. [CrossRef]
72. Bhave, S.L.; Chattoo, B.B. Expression of vitreoscilla hemoglobin improves growth and levels of extracellular enzyme in Yarrowia lipolytica. *Biotechnol. Bioeng.* **2003**, *84*, 658–666. [CrossRef]
73. Huberts, D.H.; Niebel, B.; Heinemann, M. A flux-sensing mechanism could regulate the switch between respiration and fermentation. *FEMS Yeast Res.* **2012**, *12*, 118–128. [CrossRef]
74. Pinu, F.R.; Granucci, N.; Daniell, J.; Han, T.L.; Carneiro, S.; Rocha, I.; Nielsen, J.; Villas-Boas, S.G. Metabolite secretion in microorganisms: The theory of metabolic overflow put to the test. *Metabolomics* **2018**, *14*, 43. [CrossRef]
75. Liu, J.; Li, H.; Zhao, G.; Caiyin, Q.; Qiao, J. Redox cofactor engineering in industrial microorganisms: Strategies, recent applications and future directions. *J. Ind. Microbiol. Biotechnol.* **2018**, *45*, 313–327. [CrossRef]
76. Niebel, B.; Leupold, S.; Heinemann, M. An upper limit on Gibbs energy dissipation governs cellular metabolism. *Nat. Metab.* **2019**, *1*, 125–132. [CrossRef] [PubMed]
77. Millard, P.; Enjalbert, B.; Uttenweiler-Joseph, S.; Portais, J.C.; Létisse, F. Control and regulation of acetate overflow in Escherichia coli. *Elife* **2021**, *10*, e63661. [CrossRef] [PubMed]
78. Mori, M.; Marinari, E.; De Martino, A. A yield-cost tradeoff governs Escherichia coli's decision between fermentation and respiration in carbon-limited growth. *NPJ Syst. Biol. Appl.* **2019**, *5*, 16. [CrossRef] [PubMed]
79. de Groot, D.H.; Lischke, J.; Muolo, R.; Planqué, R.; Bruggeman, F.J.; Teusink, B. The common message of constraint-based optimization approaches: Overflow metabolism is caused by two growth-limiting constraints. *Cell Mol. Life Sci.* **2020**, *77*, 441–453. [CrossRef]
80. Shimizu, K.; Matsuoka, Y. Redox rebalance against genetic perturbations and modulation of central carbon metabolism by the oxidative stress regulation. *Biotechnol. Adv.* **2019**, *37*, 107441. [CrossRef]
81. Cheng, C.; O'Brien, E.J.; McCloskey, D.; Utrilla, J.; Olson, C.; LaCroix, R.A.; Sandberg, T.E.; Feist, A.M.; Palsson, B.O.; King, Z.A. Laboratory evolution reveals a two-dimensional rate-yield tradeoff in microbial metabolism. *PLoS Comput. Biol.* **2019**, *15*, e1007066. [CrossRef]
82. Tsai, P.S.; Nägeli, M.; Bailey, J.E. Intracellular expression of Vitreoscilla hemoglobin modifies microaerobic Escherichia coli metabolism through elevated concentration and specific activity of cytochrome o. *Biotechnol. Bioeng.* **1996**, *49*, 151–160. [CrossRef]
83. Puustinen, A.; Finel, M.; Haltia, T.; Gennis, R.B.; Wikström, M. Properties of the two terminal oxidases of Escherichia coli. *Biochemistry* **1991**, *30*, 3936–3942. [CrossRef]

84. Orth, J.D.; Conrad, T.M.; Na, J.; Lerman, J.A.; Nam, H.; Feist, A.M.; Palsson, B. A comprehensive genome-scale reconstruction of Escherichia coli metabolism–2011. *Mol. Syst. Biol.* **2011**, *7*, 535. [CrossRef]
85. Schellenberger, J.; Que, R.; Fleming, R.; Thiele, I.; Orth, J.; Feist, A.; Zielinski, D.; Bordbar, A.; Lewis, N.; Rahmanian, S.; et al. Quantitative prediction of cellular metabolism with constraint-based models: The COBRA Toolbox v2.0. *Nat. Protoc.* **2011**, *6*, 1290–1307. [CrossRef] [PubMed]
86. Taymaz-Nikerel, H.; Borujeni, A.E.; Verheijen, P.J.; Heijnen, J.J.; van Gulik, W.M. Genome-derived minimal metabolic models for Escherichia coli MG1655 with estimated in vivo respiratory ATP stoichiometry. *Biotechnol. Bioeng.* **2010**, *107*, 369–381. [CrossRef] [PubMed]
87. Kalnenieks, U.; Balodite, E.; Rutkis, R. Metabolic Engineering of Bacterial Respiration: High vs. Low P/O and the Case of. *Front. Bioeng. Biotechnol.* **2019**, *7*, 327. [CrossRef]
88. Fischer, E.; Zamboni, N.; Sauer, U. High-throughput metabolic flux analysis based on gas chromatography-mass spectrometry derived 13C constraints. *Anal. Biochem.* **2004**, *325*, 308–316. [CrossRef]
89. Carlson, R.; Srienc, F. Fundamental Escherichia coli biochemical pathways for biomass and energy production: Creation of overall flux states. *Biotechnol. Bioeng.* **2004**, *86*, 149–162. [CrossRef]

Microbial Cell Factories

RESEARCH

Open Access

# Glucose consumption rate-dependent transcriptome profiling of *Escherichia coli* provides insight on performance as microbial factories

Juan Carlos Fragoso-Jiménez[1], Rosa María Gutierrez-Rios[1], Noemí Flores[1], Alfredo Martinez[1], Alvaro R. Lara[2], Frank Delvigne[3] and Guillermo Gosset[1*]

## Abstract

**Background:** The modification of glucose import capacity is an engineering strategy that has been shown to improve the characteristics of *Escherichia coli* as a microbial factory. A reduction in glucose import capacity can have a positive effect on production strain performance, however, this is not always the case. In this study, *E. coli* W3110 and a group of four isogenic derivative strains, harboring single or multiple deletions of genes encoding phosphoenolpyruvate:sugar phosphotransferase system (PTS)-dependent transporters as well as non-PTS transporters were characterized by determining their transcriptomic response to reduced glucose import capacity.

**Results:** These strains were grown in bioreactors with M9 mineral salts medium containing 20 g/L of glucose, where they displayed specific growth rates ranging from 0.67 to 0.27 $h^{-1}$, and specific glucose consumption rates (*qs*) ranging from 1.78 to 0.37 g/g h. RNA-seq analysis revealed a transcriptional response consistent with carbon source limitation among all the mutant strains, involving functions related to transport and metabolism of alternate carbon sources and characterized by a decrease in genes encoding glycolytic enzymes and an increase in gluconeogenic functions. A total of 107 and 185 genes displayed positive and negative correlations with *qs*, respectively. Functions displaying positive correlation included energy generation, amino acid biosynthesis, and sugar import.

**Conclusion:** Changes in gene expression of *E. coli* strains with impaired glucose import capacity could be correlated with *qs* values and this allowed an inference of the physiological state of each mutant. In strains with lower *qs* values, a gene expression pattern is consistent with energy limitation and entry into the stationary phase. This physiological state could explain why these strains display a lower capacity to produce recombinant protein, even when they show very low rates of acetate production. The comparison of the transcriptomes of the engineered strains employed as microbial factories is an effective approach for identifying favorable phenotypes with the potential to improve the synthesis of biotechnological products.

**Keywords:** Transcriptome, Glucose transport, Mutant, RNA-seq, Physiology

## Introduction

The bacterium *Escherichia coli* is widely used both in academia and industry. The culture media for growing this organism usually contains glucose, since this carbohydrate is relatively inexpensive, and is the preferred

*Correspondence: guillermo.gosset@ibt.unam.mx

[1] Departamento de Ingeniería Celular y Biocatálisis, Instituto de Biotecnología, Universidad Nacional Autónoma de México, Morelos, Cuernavaca, México
Full list of author information is available at the end of the article

carbon and energy source of *E. coli* [1]. When *E. coli* grows under conditions where both glucose and oxygen are non-limiting, it displays high specific glucose consumption ($qs$) and growth rates ($\mu$) with concomitant acetic acid synthesis. Acetic acid production has been a widely discussed topic by many authors. The production of acetic acid can be explained as an unbalance between the glucose uptake flux and the rate of conversion of the molecules derived from this sugar to energy and the metabolic products diverting acetyl coenzyme A (acetyl-CoA) from the tricarboxylic acid cycle (TCA) towards acetate. Acetate production is not dependent on oxygen availability, so it can occur under aerobic conditions. At low growth rates, glucose can be completely oxidized to carbon dioxide. However, when the growth rate increases, at certain threshold overflow metabolism is observed. This phenomenon coincides with the highest rate of oxygen consumption, above this value, overflow metabolism is evident. In summary, acetic acid production has been related to the saturation of TCA and respiratory chain capacity, as well as insufficient coenzymes replenishment [2–6]. Since acetate is a toxic compound, its accumulation has a negative effect on *E. coli* growth and productivity [7, 8]. Various approaches have been explored to try to reduce or eliminate acetate accumulation in cultures with *E. coli*. These include adjustments to the fermentation process, as well as strain genetic modifications. The use of various glucose feeding strategies for limiting the accumulation of acetate in the culture medium is an effective strategy to reduce overflow metabolism. Another successful approach is based on genetic modifications that eliminate acetate synthesis pathways or reduce glucose import capacity by deleting genes that encode transporter proteins. These strategies have been proven to be successful in increasing the production of chemicals, plasmid DNA vaccines, and recombinant proteins [9–12].

Glucose transport and phosphorylation in *E. coli* are dependent on the phosphoenolpyruvate:sugar phosphotransferase system (PTS) [13]. Protein $IICB^{Glc}$, encoded by gene *ptsG*, is the glucose-specific PTS component. Under glucose limitation conditions, a high-affinity glucose uptake pathway composed of the outer membrane protein LamB and the MglABC transport system is induced [14]. It is also known that the galactose:H+ symporter GalP can import glucose which is afterward phosphorylated by the glucokinase enzyme in an ATP-dependent reaction [15]. It has also been reported that PTS components, such as $IICD^{Man}$ which is normally involved in mannose import, can replace the function of $IICB^{Glc}$ for glucose import [11, 16, 17].

In *E. coli*, internal metabolic fluxes, as well as the phosphorylation state of PTS proteins, allows this organism to sense if glucose is abundant or limited in the culture medium and if other carbon sources are present. Carbon catabolite repression (CRR) can be defined as the hierarchical consumption of carbon sources that allow the highest growth rate [18–20]. As we have mentioned before, glucose is the preferred carbon and energy source of *E. coli*. This carbohydrate is simultaneously transported and phosphorylated by the glucose-specific PTS components. One of these components is the protein PTS $EIIA^{Glc}$ which transfers a high-energy phosphate group from protein HPr to the glucose-specific component $IICB^{Glc}$. Protein $EIIA^{Glc}$ is non-phosphorylated when glucose is actively transported and metabolized by the cell and in this state, it is available to bind to other non-PTS permeases inhibiting the uptake of alternate carbon sources such as lactose. On the contrary, when glucose is absent in the medium, $EIIA^{Glc}$ is mainly phosphorylated, and in this state, it is available to bind to the adenylate cyclase enzyme (CyaA), stimulating its activity, thus increasing the intracellular concentration of cyclic AMP (cAMP)[1, 18, 19]. An increased amount of cAMP and its binding to the cAMP receptor protein (CRP) leads to the expression of catabolite-repressed genes, enabling the utilization of alternative carbon sources [1, 18, 19]. In another example of cellular response to glucose availability, it has recently been reported that hydrogenase 4 subunits HyfBDF can sense two different glucose concentrations (2 or 8 g/L). Depending on the amount of glucose in the medium, hydrogenase 4 can regulate the H+/K+ fluxes to maintain proton motive force generation [21].

The physiological response of *E. coli* to nutrient limitation has been studied extensively [14, 22–25]. When glucose concentration is limiting, a hunger state is defined if it causes a reduction in the $\mu$ to a value below the maximal rate observed when this nutrient is abundant [14]. In contrast, a starvation state is defined by growth cessation because of glucose depletion. The hunger response is characterized by the expression of nutrient scavenging systems, including genes encoding proteins involved in high-affinity glucose uptake such as LamB and MglABC, that replace PTS-dependent glucose import by OmpC and $IICB^{Glc}$ [14]. Knowledge about the global transcriptional response of *E. coli* to glucose limitation has been extended by using technologies such as qPCR, microarrays, and RNA-seq. These studies have enabled a better understanding of the physiological state under specific conditions, providing insight into the roles of cellular components on cell adaptability and survival [23, 26–28]. Among key findings is the elucidation of regulatory components coordinating the response to glucose limitation. The global regulator CRP, bound to its effector cAMP, has been determined to control about one-third of the genes

responding to this condition [29]. In addition, growth rate-dependent control, including the alternative sigma factor RpoS and small untranslated RNAs is involved in the carbon source limitation response [27, 30].

Even though much is known about how *E. coli* responds to nutrient limitation conditions, there is growing interest in understanding how glucose-limitation responses would relate to the performance of this organism as a biotechnological production host. It would be useful to characterize *E. coli* strains that are improved cell factories for biotechnological products. In this regard, a set of mutant strains have been generated to display distinct glucose consumption rates, based on the deletion of PTS and non-PTS glucose importers [11, 31, 32]. These strains import glucose at fixed values that cause a growth rate below the maximum. Thus, these mutants can emulate the dilution rates of continuous culture, but without any external process control [11, 12]. When compared to wild-type *E. coli* W3110, some of these mutant strains have displayed increased production of a DNA vaccine and membrane proteins [11, 32]. A recent study compared the capacity for GFP production among a group of six isogenic strains that exhibit distinct *qs* values as a result of the deletion of glucose transporters. *E. coli* W3110 and mutant derivatives displayed *qs* ranging from 1.75 to 0.45 g/g h. It was determined that all mutant strains produced a 4 to 25 higher GFP titer when compared to W3110 [12]. These results can be explained in part by the observed reduction in acetate accumulation in the culture medium. However, the acetate titer and specific rate of production did not correlate with GFP yield or titer [12]. These data strongly suggest that a reduction in *qs* results in modifications of cell physiology that go beyond a reduction in overflow metabolism and these perturbations have an impact on recombinant protein production capacity. Thus, it is of interest to determine the physiological state of these strains to help in understanding the basis for their improved performance. To address these questions, we performed comparative transcriptome analyses.

## Material and methods

### Strains and cultivation conditions

The strains used in this work are described in Table 1 and Fig. 1. The strain *E. coli* W3110 is a derivative of K-12 [33]. Strains WG, WGM, WGMC, and WHIC are derivatives of W3110 [11]. All the strains were cultured in 5 mL Luria–Bertani medium, stored in 40% glycerol, and kept frozen at − 70 °C. These strains were grown in stirred tank bioreactors, using M9 minimum salts medium supplemented with 20 g/L of glucose, and 0.15 mL/L of trace elements solution. The M9 medium contained 6 g/L $Na_2HPO_4$, 3 g/L $KH_2PO_4$,0.5 g/L NaCl, 1 g/L $NH_4Cl$, 0.5 g/L $MgSO_4$, 0.01 g/L $CaCl_2$, 0.01 g/L thiamine hydrochloride. The trace elements solution contained the following: 1.5 g/L $Na_2EDTA \cdot 2H_2O$, 0.45 g/L $ZnSO_4 \cdot 7H_2O$, 0.03 g/L $MnCl_2 \cdot 4H_2O$, 0.1 g/L $H_3BO_3$, 0.04 g/L $Na_2MoO_4 \cdot 2H_2O$, 0.3 g/L $FeSO_4 \cdot 7H_2O$, and 0.03 g/L $CuSO_4 \cdot 5H_2O$. Glucose and salts solutions were sterilized separately at 121 °C for 20 min. The inoculum for bioreactor cultures started with a single colony placed in a tube with 5 mL of LB medium and incubated at 37 °C, 300 rpm in an orbital shaker. After 8 h, a sample of this culture was used to inoculate a 250 mL shake flask containing 50 mL of M9 medium with 20 g/L glucose starting at an OD 600 nm of 0.1 and incubated at 37 °C, 300 rpm until an OD 600 nm of 2.0 was reached. Then a sample from this culture was used to inoculate sterile bioreactors containing 750 mL of the same medium, starting at an OD 600 nm of 0.1. Batch cultures in stirred tank bioreactor were performed using 1 L autoclavable glass bioreactors (Applikon, The Netherlands). The reactors were equipped with controls for pH, temperature, agitation, and dissolved oxygen. 3% $NH_4OH$ and $H_3PO_4$ solutions were automatically added to control pH at 7.0. The temperature was maintained at 37 °C, dissolved oxygen was manually maintained above 20% by changing stirring speed, and airflow was set to 1 vvm. Samples were taken periodically for offline analyses. All cultures were performed in triplicate.

**Table 1** E. coli strains employed in this study

| Name<br>Strains | Description | Sources |
|---|---|---|
| W3110 | *E. coli* F- λ—*rph-1 IN(rrnD-rrnE)*1 | [33] |
| WG | W3110 Δ*ptsG*::FRT | [11] |
| WGM | WG, Δ*manX*::FRT | [11] |
| WGMC | WGM, Δ*mglABC*::FRT-Cm-FRT | [11] |
| WHIC | W3110 Δ*ptsHIcrr*::FRT-Cm-FRT<br>Δ*mglABC*::FRT-Cm-FRT | [11] |

### RNA extraction, purification, mRNA library construction and RNA-seq

We carried out cultures for each strain under the same conditions as described above. Cultures were started at an OD 600 nm of 0.1 and growth was monitored until each strain reached an OD 600 nm of 1.0. At this point (mid-exponential growth phase), a 50 mL sample of culture medium was taken, placed in an ice bath, immediately added 1 ml of RNA later buffer (Ambion Inc., USA) mixed it, and centrifuged 10 min at 4 °C at 5000 rpm. The pellet was immediately kept frozen at − 70 °C. To perform RNA-seq sequencing, RNA extraction was made using the RNeasy Midi Kit (Qiagen) following the

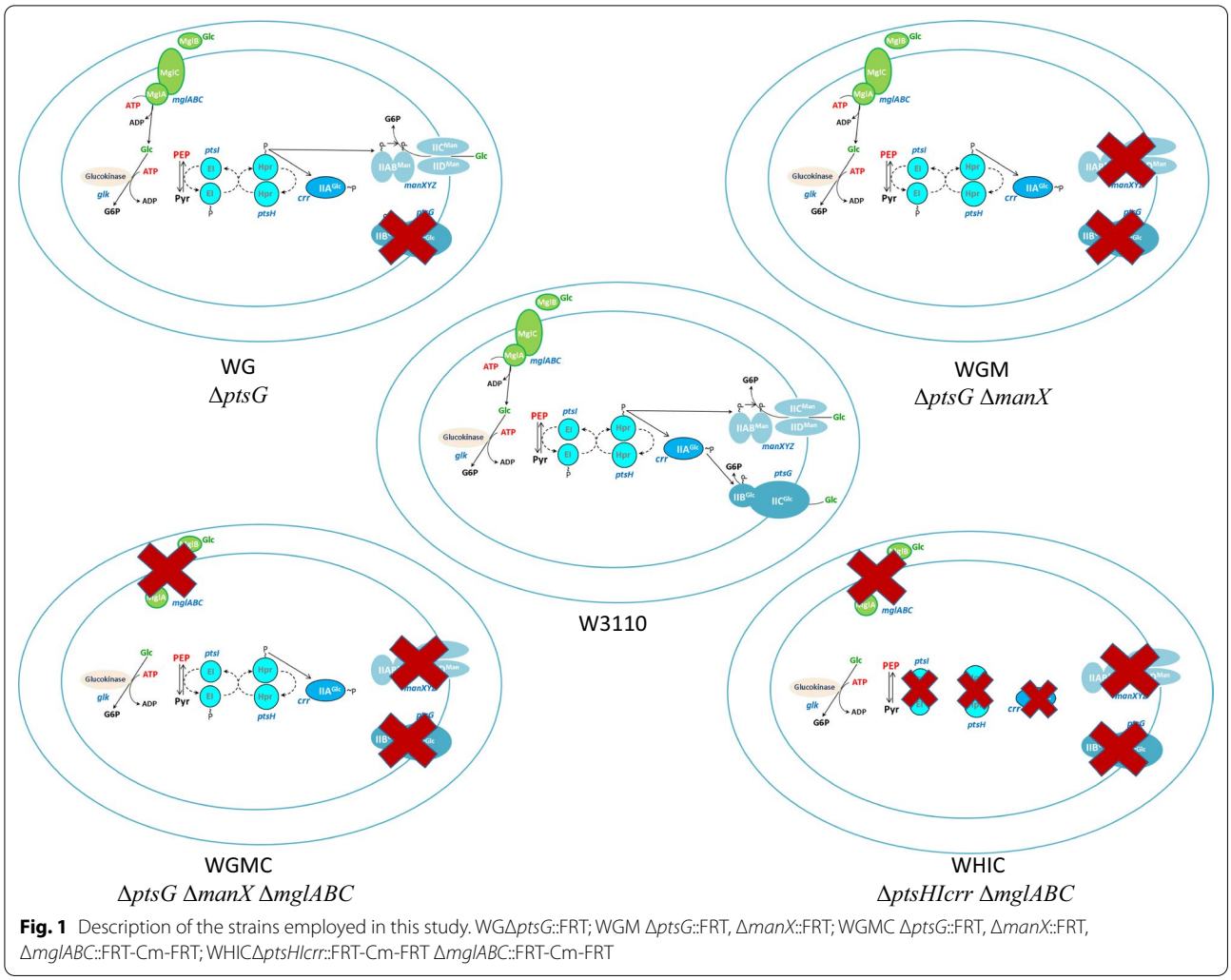


**Fig. 1** Description of the strains employed in this study. WGΔ*ptsG*::FRT; WGM Δ*ptsG*::FRT, Δ*manX*::FRT; WGMC Δ*ptsG*::FRT, Δ*manX*::FRT, Δ*mglABC*::FRT-Cm-FRT; WHICΔ*ptsHIcrr*::FRT-Cm-FRT Δ*mglABC*::FRT-Cm-FRT

manufacturer's instructions. RNA extractions and purifications were carried out from three independent cultures for each strain.

The ribosomal ribonucleic acid (rRNA) integrity was determined by the Bioanalyzer 2100 system (Agilent Technologies, Inc., Santa Clara, CA) using an Agilent RNA 6000 Nano chip, RNA Integrity Number (RIN) values were obtained for each RNA sample, and we only considered those with a value higher than 8 to elaborate RNAseq libraries. Subsequently, bacterial rRNA was depleted using Ribo-Zero rRNA Removal Kit for Bacteria (Epicentre™) following the manufacturer's instructions. RNA was analyzed using the Bioanalyzer 2100 once again. Afterward, RNAseq libraries were constructed using Illumina TruSeq Stranded mRNA sample prep kit (Illumina, Inc., San Diego, CA) from RNA obtained previously, and following instructions of the manufacturer. Briefly, RNA was chemically fragmented by divalent cations to generate 200–600 bp fragments. After that, the cDNA of each fragmented RNA sample was synthesized with retrotranscriptase enzyme using degenerated primers of 6 nucleotides. dsDNA was obtained from cDNA using a Klenow DNA polymerase. Once dsDNA was obtained, both ends of each molecule were repaired to join with Illumina adapters by employing T4 DNA polymerase and T4 DNA ligase. Later, each library was amplified by PCR with specific primers for P5 and P7 adapter of Illumina, to increase the molecule number for high-throughput sequencing. Each library was analyzed by Bioanalyzer 2100 system using a DNA High Sensitivity chip. Finally, libraries were quantified fluorometrically using a Qubit®fluorometer with Qubit dsDNA HS Assay kit (Invitrogen). Libraries were amplified clonally into a Flowcell and sequenced on Illumina NextSeq 500 employing a NextSeq 500/550 High Output v2 kit for 150 cycles. Sequencing configuration was indexed Paired-End $2 \times 76$, following the protocol described by the manufacturer.

### Differential expression analysis by pairwise comparison of strains WG-W3110, WGM-WG, WGMC-WGM, and WHIC-WGMC

RNA-seq reads were quantified by Salmon using default parameters [34], with the *E. coli* K-12 substr. W3110 genome cds file as a reference (ftp://ftp.ncbi.nlm.nih.gov/genomes/all/GCF/000/010/245/GCF_000010245.2_ASM1024v1/GCF_000010245.2_ASM1024v1_cds_from_genomic.fna.gz).

Differential expression analysis was carried out employing edgeR v 3.26.8 [35]. We used the transcript levels from the strain with the higher *qs* value as a reference among pairs. Thus, we performed the following comparisons WG-W3110, WGM-WG, WGMC-WGM, and WHIC-WGMC. In addition, we used the Benjamini-Hochberg (BH) as a *p*-value adjustment method [36]. Differentially expressed genes were those with a *p*-value < 0.01 and False Discovery Rate (FDR) < 0.01 and a fold-change ≥ 2 as the cutoff. We obtained a list of differentially expressed genes for each mutant strain against its respective partner. Afterward, we converted the RefSeq identifiers in Uniprot database (http://www.uniprot.org) using the Retrieve/ID mapping tool to obtain genes names, descriptions, and accession numbers of bnumbers and additional protein information. In addition, we calculated the Pearson correlation coefficient of the differentially expressed genes using their logarithm of fold change (logFC) and their *qs* values. Also, we calculated the slope with the parameter logFC/*qs*, similar to the method reported by Veit et al. 2007 [37].

### COG, annotation of differentially expressed genes

We performed annotation of our list of genes through Cluster of Orthologous Groups (COG's) using eggNOG-mapper (http://eggnogdb.embl.de/) with DIAMOND mapping mode, the taxonomic scope of Gamma-proteobacteria, prioritizing precision on orthologues, and prioritizing quality on gene ontology evidence. To visualize the results, we used the ggplot2 library based on R.

### RNA extraction, cDNA synthesis and RT-qPCR conditions

To confirm RNA-seq and differential expression analysis results, we performed three RNA extractions and purifications from three independent fermentations for each strain. For this purpose, 50 mL samples were taken of each different strain growing logarithmically. Those samples were collected when the biomass reached 1.0 ($OD_{600nm}$). Then, 1 mL of RNA later buffer (Ambion Inc., USA) was added to each sample, mixed, and centrifuged for 10 min at 4 °C and 5000 rpm. Conditions for total RNA extraction, cDNA synthesis, and RT-qPCR conditions were those previously reported [38], primers used are listed in Additional file 3: Table S1.

## Results

### Growth kinetics characterization

The isogenic mutant strains employed in this study are derived from W3110 and harbor deletions in genes that encode proteins related to carbohydrate import of PTS and non-PTS systems. They belong to a group of strains that displayed a wide range of *qs* values when grown in a minimal medium with glucose [11]. From this group of mutants, we selected five strains that span the full range of observed *qs* values. Strain WG lacks the gene encoding the $IICB^{Glc}$ PTS component. Strain WGM lacks both the $IICB^{Glc}$ and $IICD^{Man}$ components. Whereas strain WGMC lacks the $IICB^{Glc}$, $IICD^{Man}$ components, and the MglABC system. In strain WHIC, genes *ptsHIcrr* were deleted, causing the complete disruption of the PTS system (Fig. 1). Since the PTS phosphorelay chain is disrupted, none of the PTS components is expected to be functional. This strain also lacks the MglABC system.

The mutant strains and *E. coli* W3110 were grown in a stirred bioreactor employing minimal salts medium containing 20 g/L glucose. The kinetic and stoichiometric parameters are summarized in Table 2. These strains displayed *qs* and $\mu$ values that span from 1.52 to 0.35 g/g h and 0.67 to 0.27 $h^{-1}$, respectively (Additional file 1: Fig S1). We observed that *qs* and $\mu$ values displayed a linear correlation ($R_2 = 0.99$; Fig. 2). The final biomass

**Table 2** kinetic and stoichiometric parameter of cultures with *E. coli* W3110 and derived glucose transport mutants in stirred tank bioreactors

| Strain | $\mu(h^{-1})$ | *qs* (g/g h) | $q_{ac}$ (g/g h) | Max acetate (g/L) | Y X/S (g/g) | Max biomass (g/L) | Culture time (h) |
|---|---|---|---|---|---|---|---|
| W3110 | 0.67 ± 0.03 | 1.52 ± 0.14 | 0.433 ± 0.005 | 1.94 ± 0.04 | 0.43 ± 0.03 | 8.4 ± 1.21 | 10 |
| WG | 0.52 ± 0.02 | 1.11 ± 0.19 | 0.004 ± 0.001 | 0.13 ± 0.04 | 0.41 ± 0.01 | 8.5 ± 0.23 | 14 |
| WGM | 0.34 ± 0.01 | 0.62 ± 0.05 | ND | ND | 0.50 ± 0.02 | 9.63 ± 0.01 | 20 |
| WGMC | 0.37 ± 0.00 | 0.62 ± 0.01 | 0.015 ± 0.001 | 0.32 ± 0.02 | 0.44 ± 0.02 | 7.14 ± 0.64 | 18 |
| WHIC | 0.27 ± 0.01 | 0.35 ± 0.01 | 0.001 ± 0.001 | 0.05 ± 0.03 | 0.46 ± 0.02 | 9.23 ± 0.53 | 28 |

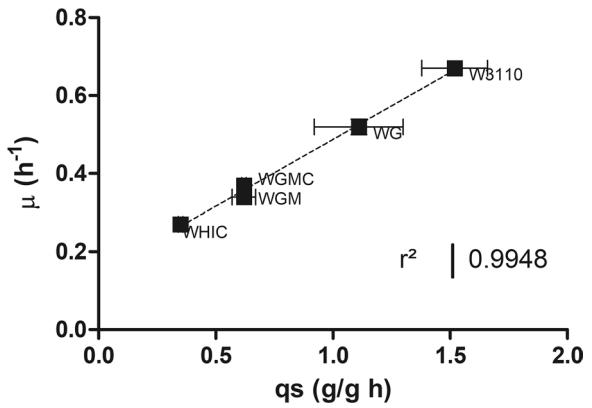


**Fig. 2** Specific growth rate as a function of specific glucose uptake rate for the *E. coli* strains characterized in this study. Specific growth rate (μ), specific glucose consumption rate (*qs*)

concentration was similar for all strains. The cultures were stopped when the stationary phase was reached at the times listed in Table 2. At these times, we did not detect residual glucose in the medium. Strains W3110, WG, WGMC, and WHIC secreted acetate, reaching the maximum concentration when glucose was depleted, afterwards, the organic acid was consumed. No acetate was detected in the culture medium of strain WGM. Strain W3110 displayed the highest specific rate of acetate production ($q_{ac}$) and acetate titer of 0.43 g/g h and 1.94 g/L, respectively. The $q_{ac}$ in W3110 was almost 28-fold higher when compared with the other strains. In these experiments, the biomass yield ($Y_{X/S}$) values differed by less than 20% among all the strains employed in this study.

### Differential expression analysis, reads abundance and mapping

RNA-seq libraries were generated from triplicate samples of WG, WGM, WGMC, WHIC, and W3110 strains. Libraries were sequenced, and 37–48 million reads were obtained from the W3110 library, 31–59, 32–53, 35–56, and 52–54, million reads for WG, WGM, WGMC, and WHIC, respectively. These results indicated that we have generated a similar amount of data among libraries of the strains. Afterward, we used the Salmon program to quantify reads against the annotated *E. coli* K-12 substr. W3110 genome. We obtained on average 3.3 ± 1.2, 2.4 ± 1.2, 3.0 ± 1.1, 4.2 ± 2.1, and 2.6 ± 0.3 million of mapped reads from W3110, WG, WGM, WGMC, and WHIC, respectively, those data are shown in Table 3. The RNA-seq data for this study have been deposited in the European Nucleotide Archive (ENA) at EMBL-EBI under accession number PRJEB32273 (https://www.ebi.ac.uk/ena/browser/view/PRJEB32273).

### The global transcriptomic response among strains with a reduced glucose uptake rate

Strains W3110, WG, WGM, WGMC, and WHIC were grown in a minimal medium containing 20 g/L glucose, and samples from these cultures were subjected to RNA-seq analysis. The transcriptomes of the mutant strains were compared to that of W3110. Figure 3 shows a comparison of the number of genes that were differentially expressed when compared to W3110, corresponding to 281, 201, 222, and 779 for strains WG, WGM, WGMC, and WHIC, respectively (Additional file 4: Table S2). It can be observed that in all mutant strains, the number of upregulated genes is higher than those downregulated. The differentially expressed genes belonged to several COGs, as will be discussed below.

To determine the effects of the change in *qs* (Δ*qs*) among strains, differential expression analysis was performed by comparing pairs of strains with progressively lower *qs* values: W3110-WG (Δ*qs* = 0.41 g/g h), WG-WGM (Δ*qs* = 0.49 g/g h), WGM-WGMC (Δ*qs* = 0 g/g h), and WGMC-WHIC (Δ*qs* = 0.27 g/g h) (Table 4). When performing this comparison, it can be observed that genes clustered in COG S (Function unknown) were the most numerous (Table 5 and Fig. 4). It cannot be discarded that the genes included in this COG have a function related to the production performance of these strains. However, since the functions of these genes are not known, they were not further considered in this study. Most of the genes with known functions belonged to COGs C, E, G, and K, related to energy production

**Table 3** Statistics of RNA-seq libraries

| Strain | Library size (million reads) | Average library size (million reads) | Mapped reads (million reads) | Average mapped reads (million reads) |
|---|---|---|---|---|
| W3110 | 48,37,42 | 43 ± 5.7 | 4.7,2.9,2.3 | 3.3 ± 1.2 |
| WG | 59,31,33 | 41 ± 15.9 | 4.2,1.4,1.7 | 2.4 ± 1.2 |
| WGM | 32,52,53 | 46 ± 11.7 | 2.2,4.2,2.5 | 3.0 ± 1.1 |
| WGMC | 51,56,35 | 47 ± 11.2 | 4.7,5.9,1.8 | 4.2 ± 2.1 |
| WHIC | 52,54,54 | 53 ± 1.5 | 2.9,2.7,2.3 | 2.6 ± 0.3 |

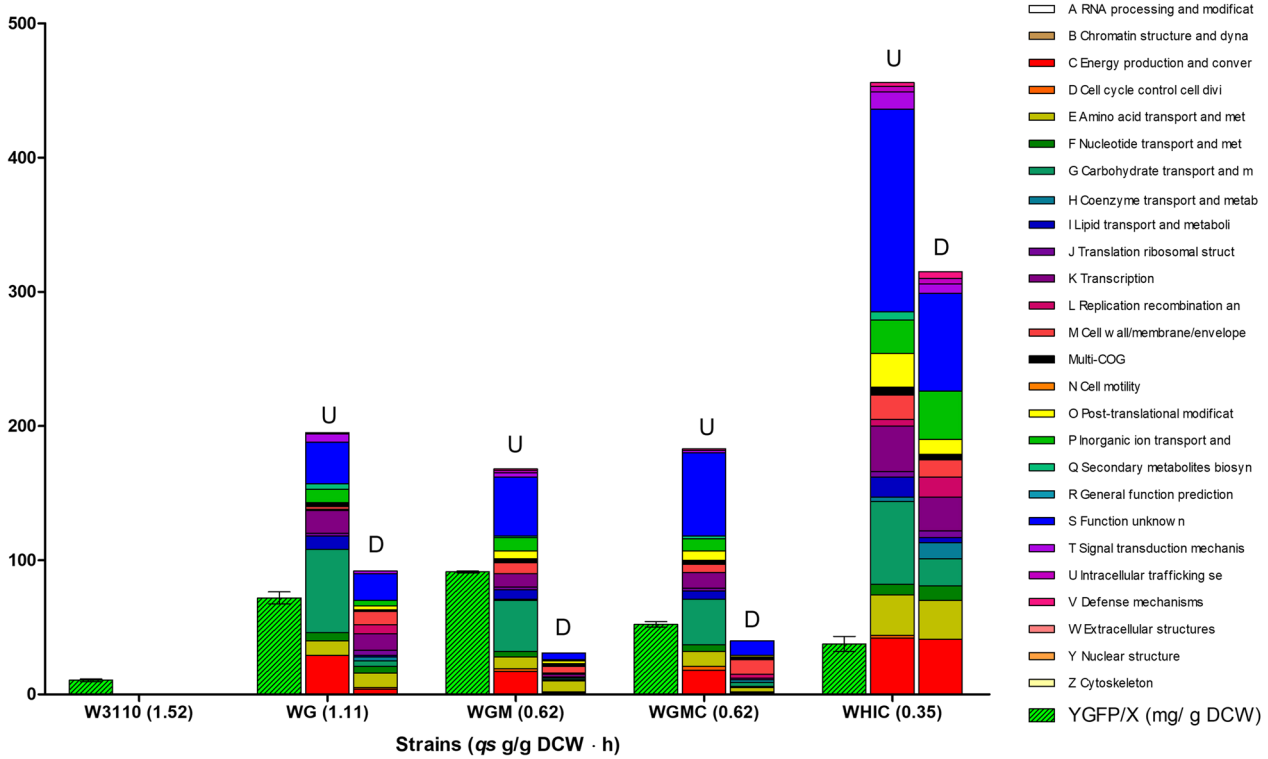


**Fig. 3** Distribution of differentially expressed genes among mutant strains in Clusters of Orthologous genes when comparing transcriptomes of W3110 with mutant strains WG, WGM, WGMC, and WHIC. The *qs* value for each strain is shown between parenthesis and it is presented as g glucose/g DCW h Values for GFP yield from biomass ($Y_{GFP/X}$) were obtained from a previous publication [11] and are expressed as mg GFP/g DCW

**Table 4** Number of differentially expressed genes in pair-wise comparisons

| Strains comparison Counts and direction | WG-W3110 | WGM-WG | WGMC-WGM | WHIC-WGMC | WGM-W3110 | WGMC-W3110 | WHIC-W3110 |
|---|---|---|---|---|---|---|---|
| Up | 194 | 116 | 1 | 218 | 170 | 182 | 459 |
| Down | 88 | 136 | 11 | 203 | 31 | 40 | 320 |
| Total | 281 | 252 | 12 | 421 | 201 | 222 | 779 |
| Δ*qs* | 0.41 | 0.49 | 0 | 0.27 | 0.9 | 0.9 | 1.17 |

and conversion, amino acid transport and metabolism, carbohydrate transport and metabolism, and transcription. Table 4 shows the number of differentially expressed genes for each pairwise comparison. It can be observed that the magnitude of this number shows a partial correlation with the Δ*qs*. An exception to this behavior stands for strains WHIC-WGMC, with a higher-than-expected number of differentially expressed genes to the observed Δ*qs*. This can be explained considering that operon *ptsHIcrr* was deleted in strain WHIC, resulting in the complete disruption of PTS activity. Inactivation of PTS not only eliminates several carbohydrate import functions but also impairs global regulatory functions [39, 40].

When comparing the transcriptomes of strains WG and W3110 (Additional file 5: Table S3, Fig. 5), we detected upregulated genes coding for PTS transport and catabolic proteins for N-acetylgalactosamine (*agaV*, 4.3-fold), fructose (*fruABK*, 9.1, 13.8, 12.4-fold), galactitol (*gatBC*, 4.2 and 4.5-fold), mannose (*manXYZ*, 4.3, 3.7, and 4.2-fold), mannitol (*mtlA*, 2.4-fold), glucitol/sorbitol (*srlABED*, 6.3, 7.8, 7.3, 5.7-fold), N-acetylglucosamine (*nagBE*, 2 and 4.2-fold), and trehalose (*treBC*, 19.9 and 18.6-fold) (Fig. 4). Upregulated genes related

**Table 5** Statistics of differentially expressed genes in Cluster of Orthologous Genes*

| Comparison | | WG-W3110 | | | WGM-WG | | | WGMC-WGM | | | WHIC-WGMC | | |
|---|---|---|---|---|---|---|---|---|---|---|---|---|---|
| COG | | U | D | T | U | D | T | U | D | T | U | D | T |
| A | RNA processing and modification | 0 | 0 | **0** | 0 | 0 | **0** | 0 | 0 | **0** | 0 | 0 | **0** |
| B | Chromatin structure and dynamics | 0 | 0 | **0** | 0 | 0 | **0** | 0 | 0 | **0** | 0 | 0 | **0** |
| C | Energy production and conversion | 29 | 4 | **33** | 8 | 28 | **36** | 0 | 0 | **0** | 24 | 35 | **59** |
| D | Cell cycle control, cell division, chromosome partitioning | 0 | 1 | **1** | 2 | 0 | **2** | 0 | 0 | **0** | 2 | 2 | **4** |
| E | Amino acid transport and metabolism | 11 | 11 | **22** | 12 | 20 | **32** | 0 | 0 | **0** | 15 | 23 | **38** |
| F | Nucleotide transport and metabolism | 6 | 5 | **11** | 3 | 4 | **7** | 0 | 0 | **0** | 4 | 10 | **14** |
| G | Carbohydrate transport and metabolism | 62 | 4 | **66** | 16 | 28 | **44** | 0 | 2 | **2** | 24 | 22 | **46** |
| H | Coenzyme transport and metabolism | 0 | 3 | **3** | 0 | 0 | **0** | 0 | 0 | **0** | 4 | 3 | **7** |
| I | Lipid transport and metabolism | 10 | 1 | **11** | 1 | 9 | **10** | 0 | 0 | **0** | 11 | 2 | **13** |
| J | Translation, ribosomal structure and biogenesis | 2 | 4 | **6** | 3 | 0 | **3** | 0 | 0 | **0** | 1 | 0 | **1** |
| K | Transcription | 17 | 8 | **25** | 13 | 14 | **27** | 1 | 1 | **2** | 15 | 25 | **40** |
| L | Replication, recombination and repair | 1 | 6 | **7** | 1 | 0 | **2** | 0 | 0 | **0** | 1 | 5 | **6** |
| M | Cell wall/membrane/envelope biogenesis | 2 | 10 | **12** | 7 | 3 | **10** | 0 | 1 | **1** | 16 | 4 | **20** |
| N | Cell motility | 0 | 0 | **0** | 0 | 0 | **0** | 0 | 0 | **0** | 0 | 0 | **0** |
| O | Post-translational modification, protein turnover, and chaperones | 0 | 3 | **3** | 3 | 1 | **4** | 0 | 0 | **0** | 9 | 6 | **15** |
| P | Inorganic ion transport and metabolism | 10 | 4 | **14** | 6 | 6 | **12** | 0 | 0 | **0** | 11 | 19 | **30** |
| Q | Secondary metabolites biosynthesis, transport, and catabolism | 4 | 0 | **4** | 1 | 1 | **2** | 0 | 0 | **0** | 2 | 0 | **2** |
| R | General function prediction only | 0 | 0 | **0** | 0 | 0 | **0** | 0 | 0 | **0** | 0 | 0 | **0** |
| S | Function unknown | 29 | 19 | **48** | 32 | 14 | **46** | 0 | 4 | **4** | 59 | 35 | **94** |
| T | Signal transduction mechanisms | 6 | 2 | **8** | 0 | 5 | **5** | 0 | 0 | **0** | 9 | 6 | **15** |
| U | Intracellular trafficking, secretion, and vesicular transport | 1 | 0 | **1** | 3 | 0 | **3** | 0 | 1 | **1** | 3 | 2 | **5** |
| V | Defense mechanisms | 0 | 1 | **1** | 2 | 0 | **2** | 0 | 0 | **0** | 3 | 1 | **4** |
| W | Extracellular structures | 0 | 0 | **0** | 0 | 0 | **0** | 0 | 0 | **0** | 0 | 0 | **0** |
| Y | Nuclear structure | 0 | 0 | **0** | 0 | 0 | **0** | 0 | 0 | **0** | 0 | 0 | **0** |
| Z | Cytoskeleton | 0 | 0 | **0** | 0 | 0 | **0** | 0 | 0 | **0** | 0 | 0 | **0** |
| [a] | Multi-COG | 3 | 1 | **4** | 3 | 3 | **6** | 0 | 2 | **2** | 5 | 3 | **8** |
| - | Without COG | 1 | 0 | **1** | 0 | 0 | **0** | 0 | 0 | **0** | 0 | 0 | **0** |

| Comparison | | WGM-W3110 | | | WGMC-W3110 | | | WHIC-W3110 | | |
|---|---|---|---|---|---|---|---|---|---|---|
| COG | | U | D | T | U | D | T | U | D | T |
| A | RNA processing and modification | 0 | 0 | **0** | 0 | 0 | **0** | 0 | 0 | **0** |
| B | Chromatin structure and dynamics | 0 | 0 | **0** | 0 | 0 | **0** | 0 | 0 | **0** |
| C | Energy production and conversion | 17 | 1 | **18** | 18 | 1 | **19** | 42 | 41 | **83** |
| D | Cell cycle control, cell division, chromosome partitioning | 2 | 1 | **3** | 3 | 1 | **4** | 2 | 0 | **2** |
| E | Amino acid transport and metabolism | 9 | 8 | **17** | 11 | 3 | **14** | 30 | 29 | **59** |
| F | Nucleotide transport and metabolism | 4 | 1 | **5** | 5 | 1 | **6** | 8 | 11 | **19** |
| G | Carbohydrate transport and metabolism | 38 | 1 | **39** | 34 | 3 | **37** | 62 | 20 | **82** |
| H | Coenzyme transport and metabolism | 1 | 1 | **2** | 0 | 2 | **2** | 3 | 12 | **15** |
| I | Lipid transport and metabolism | 7 | 0 | **7** | 6 | 0 | **6** | 15 | 4 | **19** |
| J | Translation, ribosomal structure and biogenesis | 2 | 0 | **2** | 2 | 0 | **2** | 4 | 5 | **9** |
| K | Transcription | 10 | 2 | **12** | 12 | 1 | **13** | 34 | 25 | **59** |
| L | Replication, recombination and repair | 0 | 1 | **1** | 0 | 3 | **3** | 5 | 15 | **20** |
| M | Cell wall/membrane/envelope biogenesis | 8 | 5 | **13** | 6 | 11 | **17** | 18 | 13 | **31** |
| N | Cell motility | 0 | 0 | **0** | 0 | 0 | **0** | 0 | 0 | **0** |
| O | Post-translational modification, protein turnover, and chaperones | 6 | 2 | **8** | 7 | 1 | **8** | 25 | 11 | **36** |
| P | Inorganic ion transport and metabolism | 10 | 1 | **11** | 9 | 0 | **9** | 25 | 36 | **61** |
| Q | Secondary metabolites biosynthesis, transport, and catabolism | 1 | 0 | **1** | 2 | 0 | **2** | 6 | 0 | **6** |
| R | General function prediction only | 0 | 0 | **0** | 0 | 0 | **0** | 0 | 0 | **0** |

**Table 5** (continued)

| Comparison | | WGM-W3110 | | | WGMC-W3110 | | | WHIC-W3110 | | |
|---|---|---|---|---|---|---|---|---|---|---|
| COG | | U | D | T | U | D | T | U | D | T |
| S | Function unknown | 44 | 5 | **49** | 62 | 11 | **73** | 151 | 73 | **224** |
| T | Signal transduction mechanisms | 3 | 0 | **3** | 2 | 0 | **2** | 13 | 7 | **20** |
| U | Intracellular trafficking, secretion, and vesicular transport | 2 | 0 | **2** | 0 | 0 | **0** | 4 | 4 | **8** |
| V | Defense mechanisms | 1 | 0 | **1** | 1 | 0 | **1** | 3 | 5 | **8** |
| W | Extracellular structures | 0 | 0 | **0** | 0 | 0 | **0** | 0 | 0 | **0** |
| Y | Nuclear structure | 0 | 0 | **0** | 0 | 0 | **0** | 0 | 0 | **0** |
| Z | Cytoskeleton | 0 | 0 | **0** | 0 | 0 | **0** | 0 | 0 | **0** |
| [a] | Multi-COG | 3 | 2 | **5** | 0 | 2 | **2** | 6 | 4 | **10** |
| - | Without COG | 2 | 0 | **2** | 2 | 0 | **2** | 3 | 5 | **8** |

[a] *U* upregulated, *D* downregulated, *T* total

to non-PTS carbohydrate transport and catabolic proteins were detected for maltose (*malEFG*, *malK*, and *malM*; 8.8–18.1-fold), ribose (*rbsABCK*, and *rpiB*, 13.6, 4.2, 12.7, 3.9, and 4.3-fold), galactose/glucose (*mglABC*, 7.2, 22, and 5.8-fold), arabinose (*araF*, 2.6-fold), inositol (*agp*, 3.5-fold), 2-dehydro-3-deoxygalactose (*dgoK*, 2.1-fold), fuculose (*fucA* and *fucI*, 3.3 and 3.1-fold), 5- keto-4-deoxy-D-glucarate and 2-keto-3-deoxy-D-glucarate (*garL*, 2.7-fold), tagatose (*gatYZ*, 5.4 and fourfold), maltose and maltodextrin (*malPQ, malS,* and *malZ;* 4.7, 3.9, 5.7, and twofold), N-acetilmannosamine (*nanEK*, 3.6 and 2.2-fold), 2-methylisocitrate (*prpB*, 5.1-fold), glucuronate (*uidA* and *uxaC*, 2.3 and 2.4-fold), altronate (*uxaA*, 3.1-fold), mannonate (*uxuAB*¸ 3.4 and 2.5-fold) and 5-dehydro-4-deoxy-D-glucuronate (*kduI*, 2.6-fold). It is noteworthy that none of these PTS and non-PTS carbon sources are present in the culture medium. It is also worth noting that transcriptome data detected, in most cases, the expected coordinated expression of genes when they are part of operons. Genes *acs* (17.4-fold) and *actP* (18-fold) form an operon, and they were found upregulated. The *acs-actP* operon encodes proteins of an acetate scavenging pathway, possibly contributing to lowering the accumulation of this organic acid in the culture medium. Also detected, were upregulated genes encoding transport proteins for glycerol (*glpF*, 5.6-fold), the outer porin encoded by *lamB* (14.9-fold) and the hexose-6-phosphate:phosphate antiporter (*uhpT*, 3.5-fold). Another upregulated gene was *glk* (twofold). The transport proteins encoded by the *mglABC* operon and *lamB* constitute a high-affinity pathway for glucose import that is independent of PTS activity. The induction of these genes indicates a carbon source limitation state [13]. The upregulation of *glk* encoding the enzyme glucokinase suggests its participation in the phosphorylation of glucose molecules that are not internalized and phosphorylated by PTS. In strain WG, a lower transcript level of gene *pykF* (-2.1-fold) was detected, it encodes pyruvate kinase 1 from the Embden Meyerhof-Parnas (EMP) pathway. This enzyme is involved in pyruvate formation, so the downregulation of *pykF* suggests diminished glycolytic flux in WG when compared to W3110, resulting in the observed reduced overflow metabolism. Upregulated genes also included part of the glyoxylate and TCA cycles (*aceA*, 3.1-fold; *acnB*, 2.1-fold; *fumC*, 2.3-fold; *glcB*, 4.2-fold; *gltA*, 2.6-fold; and *sdhAB*, 2.4 and 2.2-fold), as well as genes *maeB*¸(twofold) and *pckA* (2.9-fold), that are involved in gluconeogenesis. The induction of gene *pka* (threefold) that is related to the acetylation of proteins was detected in WG. It has been determined that deletion of *pka* leads to lower resistance to heat and oxidative stresses [41].

Comparison of the transcriptomes from strains WGM and WG, showed a further increase in transcript levels in the former strain for genes encoding transport and catabolic proteins for the following carbon sources: chitobiose, trehalose, maltose, and N-acetylglucosamine. The opposite response was observed for transport and catabolic genes for fructose, galactitol, glucitol, arabinose, glycerol, ribose, galactose, trehalose, altronate, and mannonate (Additional file 5: Table S3, Fig. 6). A higher transcript level in WGM was detected for genes *pykF* (2.5-fold), *talA* (2.3-fold), and *tktB* (2.2-fold), indicating a potential for higher flux in the EMP and PP pathways (Additional file 5: Table S3, Fig. 6). Compared to WG, in strain WGM downregulation was observed for genes from the TCA and glyoxylate shunt *gltA* (− 2.7-fold), *aceA* (− 2.5-fold), *acnB* (− 3.1-fold), *fumAC* (− 2.7 and − 2.5-fold), *sdhAB* (− 2.5 and − 2.2-fold), and *glcB* (− 3.1-fold). These data suggest that energy and reducing power production capacity through TCA could be lower in WGM when compared to WG. It is noteworthy that

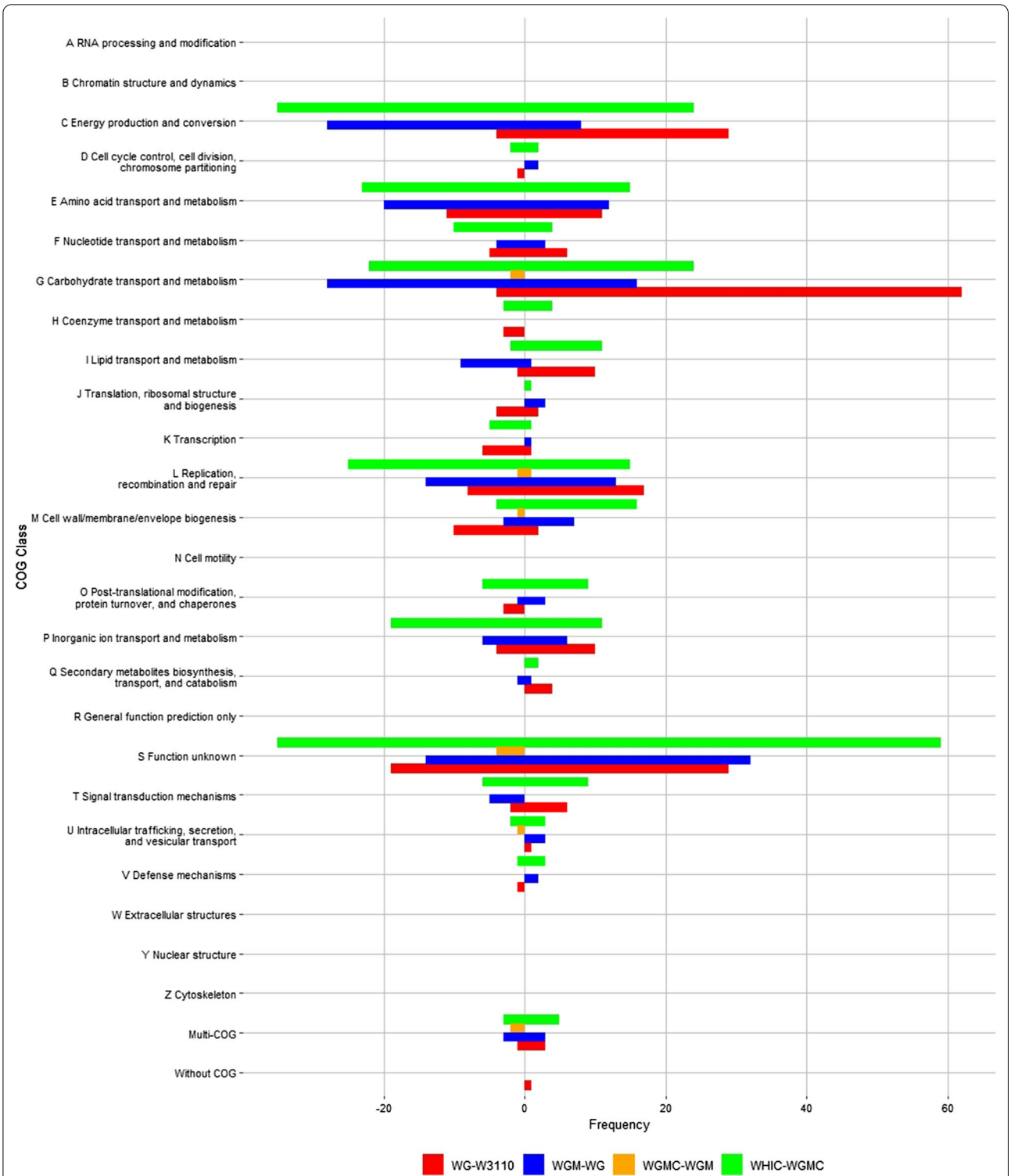


**Fig. 4** Distribution of differentially expressed genes among pairs of strains in Clusters of Orthologous genes. The number of genes upregulated (positive value) or downregulated (negative value) from each COG is indicated. Transcriptome comparisons: WG-W3110 (yellow), WGM-WG (blue), WGMC-WGM (orange) and WHIC-WGMC (red)

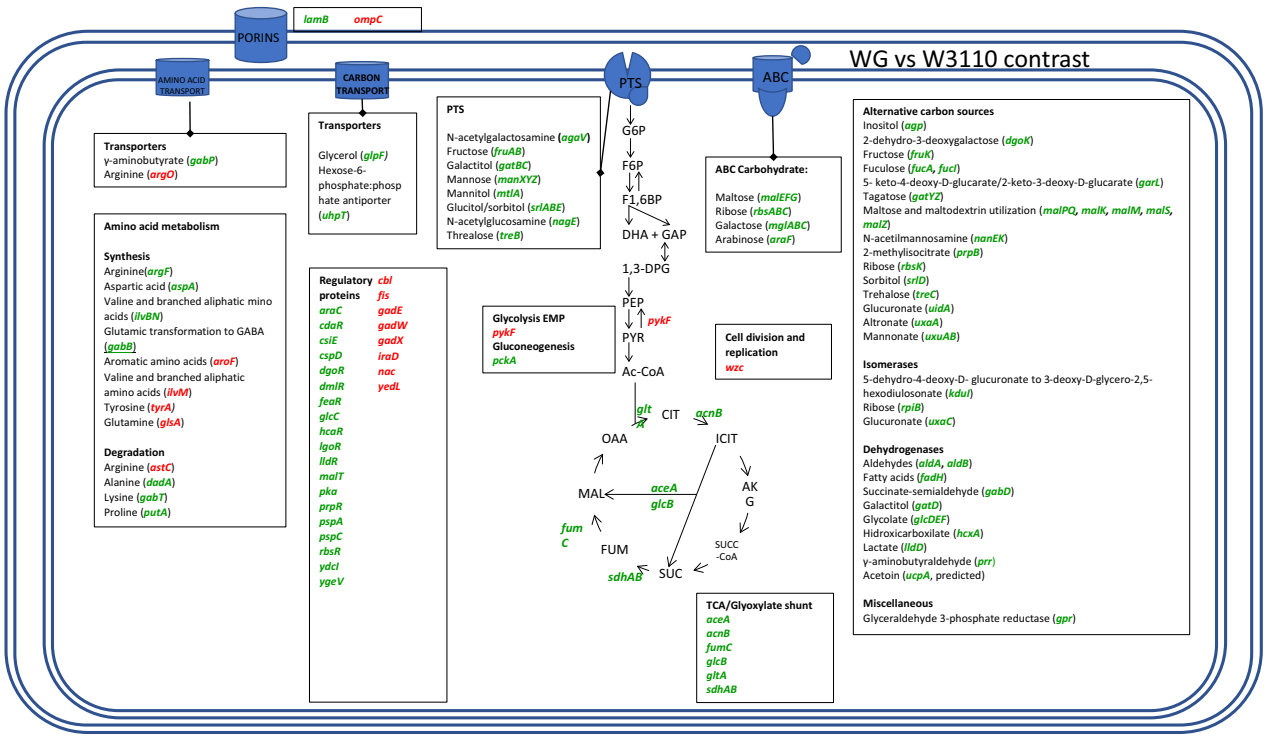


**Fig. 5** Graphical representation of genes showing differential transcript levels when comparing strains WG and W3110

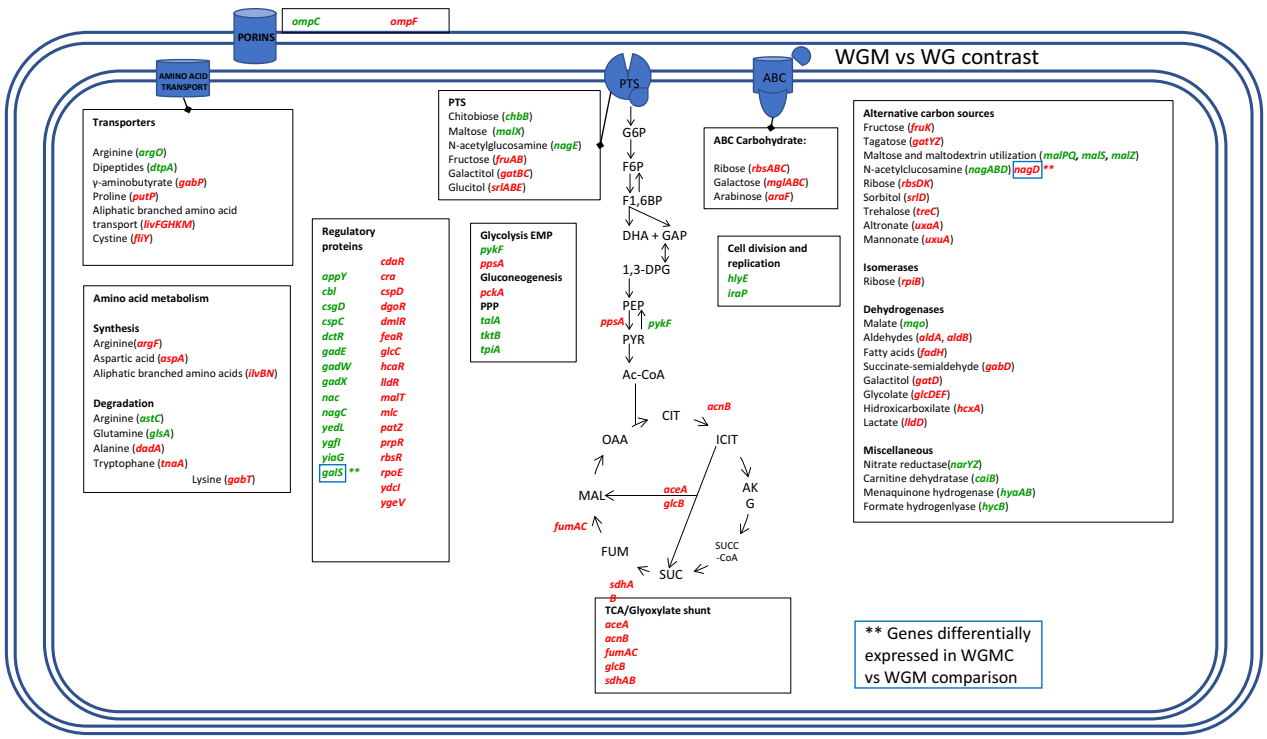


**Fig. 6** Graphical representation of genes showing differential transcript levels when comparing strains WGM and WG

genes involved in gluconeogenesis as well as the PEP/PYS metabolism *ppsA* (− 2.6-fold), *pckA* (-threefold), and the *glpK* (− 3.4-fold) gene which encodes for glycerol kinase were downregulated in this comparison but displayed the opposite response in the WG and W3110 comparison. Upregulation was detected for gene *iraP*, (2.7-fold). The gene *iraP* is required for the stabilization of σS during phosphate or nitrogen starvation and it plays a role in the stationary phase. A higher transcript level for genes *gadX* (4.8-fold) and *gadW* (5.9-fold) was detected in WG. These two genes form a complex operon and encode transcriptional regulators that control the glutamic acid decarboxylase acid resistance system. Genes belonging to this system were found induced: *gadA* (17.3), *gadB* (22.9) *gadC* (26.5), and *gadE* (22.9). It should be noted that pH was controlled and maintained at a neutral value in cultures with these strains. Therefore, the physiological role of this acid resistance system under these conditions is not clear.

Strains WGM and WGMC displayed an identical *qs* value (0.62 g/g h) under the growth conditions employed in this study. This result suggests that the MglABC high-affinity transporter is not contributing to glucose import in strain WGM or that its function was replaced by other proteins in WGMC. Strain WGMC accumulated 0.32 g/L of acetate, while this organic acid was not detected in cultures with WGM. This result indicates that deletion of *mglABC* influences metabolism by an unknown mechanism that causes an increase in acetic acid production [42–44]. The transcriptome analysis yielded 12 differentially expressed genes when comparing WGMC to WGM, most of them without a defined function (Additional file 5: Table S3). Among these genes, *galS* was found upregulated (20-fold), it encodes a transcription factor that regulates the expression of genes involved in the transport and catabolism of D-galactose. However, no increase in transcript level was detected for members of the GalS regulon. Further characterization of WGMC should be useful to determine how the deletion of *mglABC* causes the observed metabolic and transcriptional responses.

The transcriptome comparison of WHIC to WGMC yielded upregulated genes encoding transport and/or catabolic proteins for the consumption of fructose, arabinose, O-acetylserine/cysteine, α-ketoglutarate, 3-hydroxyphenylpropionate/3-hydroxycinnamate, glycerol, maltose/maltodextrin, mannose, ribose, and trehalose (Additional file 5: Table S3, Fig. 7). In contrast to the response observed in mutant strains WG and WGM, gene *lamB* (-3.1-fold) was downregulated. This result is consistent with the reported poor expression for this gene under glucose excess and glucose-starved

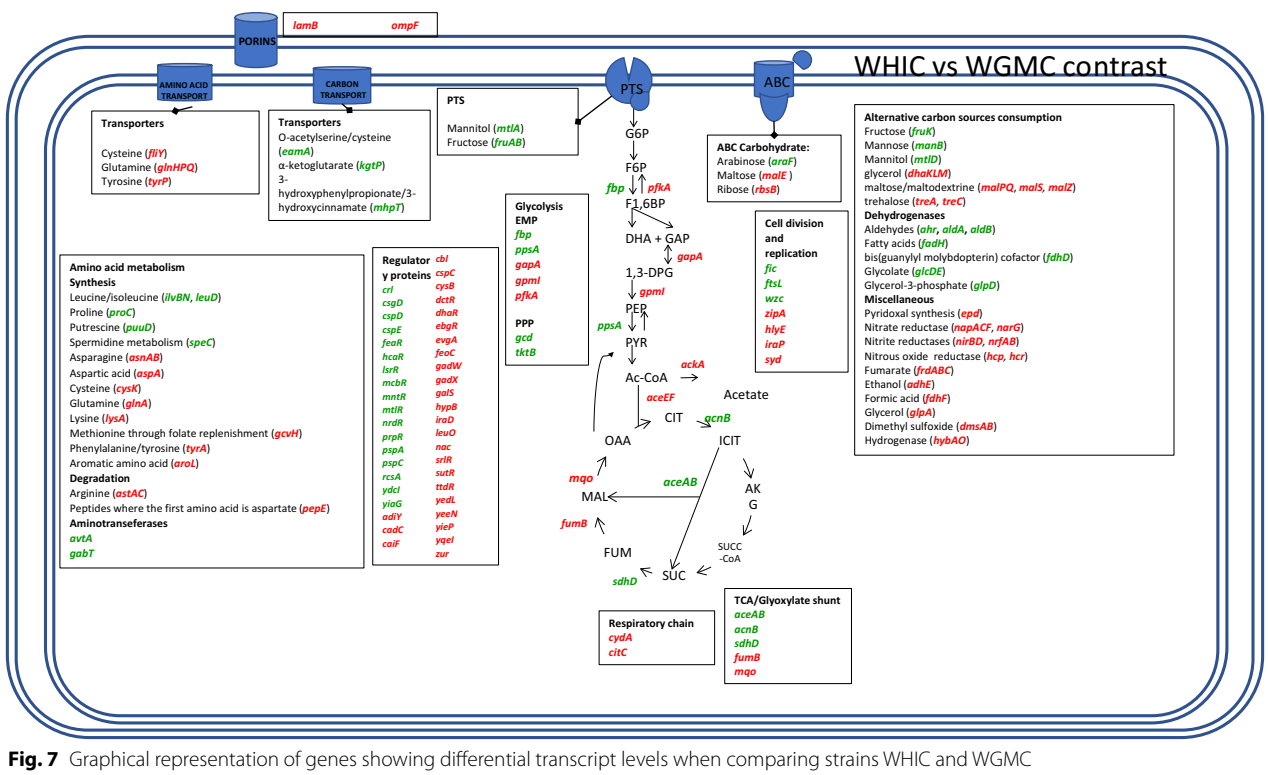


**Fig. 7** Graphical representation of genes showing differential transcript levels when comparing strains WHIC and WGMC

conditions [13]. A higher transcript level was detected for gluconeogenic genes *fbp* (2.1-fold) and *ppsA* (3.9-fold) (Additional file 5: Table S3, Fig. 7). In contrast, several genes from the EMP pathway were downregulated (*gapA*, − 2.5-fold; *gpmI*, − 3.7-fold; *pfkA*, and − 2.3-fold). Gene *cydA* (− 2.8-fold), which is related to the respiratory chain, was downregulated. Also detected were lower transcript levels of genes encoding part of the pyruvate dehydrogenase (*aceEF*, 3.2 and − 2.6-fold), and *ackA* (− 2.9-fold) related to acetic acid assimilation/production. Genes related to the synthesis of glutamine, asparagine cysteine, and lysine (*glnA* − 7.7-fold, *asnAB* − 5.6 and − 5.9-fold, *cysK* − 3.2-fold, *lysA* -two-fold) were downregulated. A lower transcript level was observed for gene *iraP* (− 2.8-fold). In this case, the response of this gene was opposite to that observed for the WG-W3110 and WGM-WG transcriptome comparisons. Genes encoding functions related to the synthesis of the extracellular polysaccharide colonic acid displayed higher transcript level in strain WHIC: *wcaA* (3.9-fold), *wcaC* (3.2-fold), *wcaD* (4.5-fold), *wcaE* (6.6-fold), *wcaF* (8.7-fold), *wcaI* (fourfold), *wcaJ* (fourfold), *wza* (7.7-fold), *wzb* (7.4-fold), and *wzc* (3.2-fold). Strain WHIC displayed the lowest *qs* among studied mutants and the observed transcriptome response is characteristic of severe carbon and energy limitation. As will be discussed below, part of the observed response can be explained considering the dual transport-regulatory role of PTS in *E. coli*.

The set of differentially expressed genes and their intersections in the WG-W3110, WGM-WG, and WHIC-WGMC pairwise comparisons are shown in Additional file 1: Fig S2 and Additional file 6: Table S4. These comparisons were tagged as A, B, and C, in the Venn diagram respectively. It is important to mention that we did not include the WGMC-WGM comparison because they displayed very similar $\mu$ and *qs* values (see Additional file 6: Table 4) and a nearly identical transcriptomic response. Comparisons A, B, and C had unique genes that appeared to be more numerous in WGMC-WHIC (C; 287), followed by WG-W3110 (A; 96) and WGM-WG (B;65).

### Validation of gene expression by qPCR

RT-qPCR experiments were performed for the following genes displaying differential expression in the RNA-seq results: *galP*, *manX*, *nagE*, *lamB*, *ompC*, *ompF*, *mglB*, *gltA*, *acs*, *poxB* and *ppsA*. (Table 6). The magnitude of the expression levels detected by qPCR was different to those observed in the RNA-seq experiments, but the general

**Table 6** qPCR and RNA-seq results of genes from carbon transport systems and central metabolism

| | Gene | RT-qPCR[a] | | | | | | | | RNA-seq | | | |
|---|---|---|---|---|---|---|---|---|---|---|---|---|---|
| | | WG | | WGM | | WGMC | | WHIC | | WG | WGM | WGMC | WHIC |
| | | AVG | SD | AVG | SD | AVG | SD | AVG | SD | | | | |
| Transport systems | *galP* | 1.19 | 0.01 | 1.63 | 0.29 | 1.48 | 0.18 | 1.59 | 0.37 | − 0.43 | 0.18 | 0.58 | 1.40 |
| | *manX* | 5.88 | 1.25 | ND | ND | ND | ND | 1.19 | 0 | 2.11 | ND | ND | 1.80 |
| | *nagE* | 4.38 | 0.54 | 43.34 | 4.43 | 53.34 | 3.83 | 30.95 | 11.49 | 2.08 | 5.10 | 5.04 | 5.96 |
| | *lamB* | 22.73 | 4.61 | 8.42 | 0.18 | 7.27 | 0.45 | 1.64 | 0.2 | 3.89 | 3.69 | 3.86 | 2.25 |
| | *ompC* | 0.25 | 0.11 | 0.73 | 0.06 | 0.91 | 0.27 | 0.96 | 0.14 | − 1.00 | 0.46 | 0.5 | 0.55 |
| | *ompF* | 2.93 | 0.07 | 0.58 | 0 | 0.56 | 0.08 | 0.14 | 0.02 | 0.97 | − 0.61 | − 0.26 | − 1.55 |
| | *mglB* | 29.11 | 10.46 | 4.55 | 0.62 | ND | ND | ND | ND | 4.46 | 1.88 | ND | ND |
| | **Gene** | **RT-qPCR** | | | | | | | | **RNA-seq** | | | |
| | | **WG** | | **WGM** | | **WGMC** | | **WHIC** | | **WG** | **WGM** | **WGMC** | **WHIC** |
| | | **AVG** | **SD** | **AVG** | **SD** | **AVG** | **SD** | **AVG** | **SD** | | | | |
| TCA | *gltA* | 3.2 | 1 | 0.65 | 0.02 | 0.93 | 0.05 | 1.39 | 0.24 | 1.35 | − 0.10 | 0.20 | 0.80 |
| | **Gene** | **RT-qPCR** | | | | | | | | **RNA-seq** | | | |
| | | **WG** | | **WGM** | | **WGMC** | | **WHIC** | | **WG** | **WGM** | **WGMC** | **WHIC** |
| | | **AVG** | **SD** | **AVG** | **SD** | **AVG** | **SD** | **AVG** | **SD** | | | | |
| Acetate | *acs* | 27.58 | 4.97 | 3.42 | 0.39 | 3.83 | 0.32 | 3.13 | 0.44 | 4.12 | 1.74 | 1.84 | 2.61 |
| | *poxB* | 0.44 | 0.02 | 1.78 | 0.23 | 1.84 | 0.37 | 1.55 | 0.2 | 0.38 | 1.16 | 1.21 | 1.98 |
| | *ppsA* | 1.82 | 0.37 | 0.41 | 0.06 | 1.89 | 0.53 | 3.72 | 0.4 | 0.98 | − 0.39 | 0.48 | 2.37 |

[a] Values represent the logarithm of fold change when comparing gene expression values from genes of each strain against *E. coli* W3110. Dispersion values are not presented from RNA-seq results but can be consulted in the supplementary files

response regarding upregulation or downregulation was conserved for most of the genes: *manX*, *nagE*, *lamB*, *ompC*, *mglB*, *gltA*, *acs*, *poxB* and *ppsA*.

#### Correlations between *qs* and expression levels

In this study, we detected genes displaying expression levels that correlated with the *qs*. This response was characterized by calculating the Pearson correlation coefficient between *qs* and the logarithm of fold change (logFC). Also, we defined that (ΔlogFC/Δqs) ratios larger than 1.5 or lower than − 1.5 were considered as differentially expressed among the full set of strains. Briefly, a negative correlation indicates that genes increase their expression values while the *qs* value is decreasing. In contrast, a positive correlation means that genes decrease their expression level while *qs* is decreasing. Lists of genes displaying positive and negative correlations with *qs* are included in Additional file 6, 7: Tables S5 and S6, respectively. The results were then organized in COG classes to facilitate their analysis. Of 292 genes having a positive or negative correlation, 47% are not classified in a COG class. The remaining 138 genes were distributed in the O, P, M, K, C, E, S, and G classes.

Inspection of COG C shows 20 genes displaying a positive correlation with *qs*, among them we found the *nuoFGHIJKLM operon* and the phosphoenolpyruvate carboxylase (*pckA*). Also, dehydrogenases for glycerol (*glpA*), sorbitol (*srlD*), galactitol (*gatD*), hydroxycarboxylate (*hcxA*), and acetoin (*ucpA*). Conversely, we detected 13 genes with negative correlation to *qs*, the pyruvate dehydrogenase (*poxB*), ubiquinol reductase (*appBC*), 2-methylcitrate synthase (*prpC*), and an alcohol/ethanol dehydrogenase (*adhP*). From this set, the response of the *nuo* genes can be explained considering that energy production requirements are lower under the reduced growth rates of the mutant strains. This assumption should be tested experimentally since *E. coli* has a second NADH dehydrogenese encoded by *ndh*. The *nuo* operon forms part of the DNA-binding transcriptional dual regulator Fis regulon, it has been demonstrated that repression by Fis, a growth-dependent regulator, occurs when this transcription factor is in high concentrations [45].

We detected 16 genes from COG E with positive and 9 with negative correlations. Among the former, there were genes related to the synthesis of arginine (*argB* and *argF*), aspartic acid (*aspA*), cysteine (*cysK*), histidine (*hysG*), serine/threonine (*sstT*), proline (*proW*), and cysteine (*fliY*). Decreased expression of genes encoding functions related to amino acid biosynthesis can be expected because of the lower growth rates of the mutant strains with the lower *qs* values. However, it is not clear why this response is selective for some amino acids. Genes displaying a negative correlation with *qs* included *gadA* and *gadBC* that encode proteins of the glutamate-dependent acid resistance system 2. Expression of these genes is increased in the mutant strains displaying the lower *qs* values. Since pH is maintained at a neutral value in these cultures, the upregulation of these genes should be dependent on another type of stress or metabolic signal. It should be noted that these genes are subject to complex regulation by transcriptional factors GadX, GadW, Fis, and CRP [46].

From COG G we found 22 and 19 genes with positive and negative correlations, respectively. Genes showing a positive correlation with *qs* encode functions related to galactitol, glucitol/sorbitol, trehalose PTS transport systems (*gatC*, *srlABC*, and *treB*), the ribose (*rbsBC*) and maltose (*malG*) ABC transporters, as well as a set of genes encoding proteins for the utilization of ribose (*rbsDK*), trehalose (*treC),* fucose (*fucA* and *fucI*), tagatose (*gatZ*), galactonate (*dgoA*), methylglyoxal (*mgsA*), and altronate (*uxaAC* and *uxaB*). These genes are likely induced as a response to carbon limitation in strain WG. Paradoxically, their expression is progressively reduced in strains with lower *qs*, possibly as a result of energy limitation or another type of metabolic perturbation. In contrast, genes encoding PTS transport proteins for chitobiose (*chbB*) and N-acetylglucosamine (*nagE*), and the non-PTS galactose symporter (*galP*) displayed a negative correlation. From these proteins, GalP has been shown to replace the PTS-dependent glucose transport function in a mutant lacking a functional PTS system [47]. Therefore, GalP may be contributing to glucose import in some of these mutants. Interestingly, some mutant strains showed increased expression of *glk*, encoding the enzyme glucokinase that can phosphorylate the glucose internalized by GalP.

Three genes from this COG J class displayed a negative correlation (*argS*, *rmf*, and *sra*). The *argS* gene encodes for the arginyl-tRNa synthetase. The *rmf* encodes for a ribosome modification factor which reversibly converts active 70S ribosomes into their 100S dimeric form during the transition from exponential growth to stationary phase [48]. Gene *sra* encodes for a protein associated to the ribosomal 30S subunit during the stationary phase [49]. The observed expression pattern for genes *sra* and *rmf* indicate that mutant strains with the lower *qs* values have a physiological state like that observed in the stationary phase. These results could indicate that strains with lower *qs* values have a physiological state that is not optimal for recombinant protein production.

## Discussion

This study aimed to characterize *E. coli* strains with impaired capacity for glucose import. We expect these data and their analysis will provide an insight into the

basis for their distinct microbial factory characteristics [12]. Transcriptome analysis was performed on *E. coli* strain W3110 and isogenic derivatives reduced glucose consumption capacity: WG, WGM, WGMC, and WHIC.

The number of differentially expressed genes when comparing WG-W3110 and WGM-WG was similar, indicating a correlation with the *qs* ratio among each pair of strains (Table 4). In contrast, strains WGMC and WGM displayed nearly identical *qs* values. The only difference between these strains is the deletion of the *mglABC* operon. In this case, 12 genes were found to be differentially expressed. Strain WGMC produced 0.32 g/L of acetic acid, while in the culture medium of WGM we did not detect this organic acid (Table 2). This phenotypic difference could explain the set of differentially expressed genes. However, further strain characterization will have to be performed to verify this assumption. When comparing strains WHIC and WGMC the Δ*qs* was about half of that detected for WG-W3110 and WGM-WG. However, the number of differentially expressed genes was about twice as expected. These results show that transcriptomic response does not have a linear relationship with changes in *qs*. It should be noted that the *qs* value for WHIC is only 23% of that determined for W3110. These data suggest that very low *qs* values cause stress that elicits a large transcriptomic response. It should also be considered that deleted glucose import proteins could have a regulatory role. This is the case for strain WHIC, the deletion of operon *ptsHIcrr* eliminates the synthesis of protein $EIIA^{Glc}$, thus disrupting the stimulation of cAMP synthesis by enzyme adenylate cyclase. Therefore, the expression of genes from the CRP regulon should be disrupted in strain WHIC. In this regard, it was found that in the WHIC-WGMC comparison there were 48 genes regulated by CRP, (33 belonging to COGs C, E, G, and K). This number is lower than that detected when comparing WG-W3110, 76 genes (53 from COGs C, E, G, and K) and WGM-WG 56 genes (39 from COGs C, E, G, and K). The transcription factor CRP-cAMP regulates several hundred genes in *E. coli*, and some of them are also transcriptional regulators [29]. The obtained data suggest that the observed transcriptomic response in WHIC is the combined effect of very low *qs*, which would induce many genes related to carbon source limitation, and the indirect disruption of the CRP regulon.

Strain WG is isogenic with W3110 except for the deletion of the gene encoding $IICB^{Glc}$ in the former. This genetic modification caused a transcriptional response consistent with a carbon limitation and hunger response characterized by a decrease in transcript level for genes encoding functions related to glycolytic activity and an increase in expression of genes from gluconeogenic metabolism. The expected reduction in overflow metabolism was observed in cultures with this strain with 6.7% of the acetate titer detected in cultures with W3110 (Table 2). As part of the hunger response, genes involved in the transport and utilization of several different carbohydrates and amino acids were upregulated. It should be noted that these compounds were not present in the culture medium, so the observed response should be a carbon source scavenging strategy. Additionally, several genes related to amino acid synthesis were downregulated, possibly caused by the 22% lower growth rate of WG when compared to W3110, resulting in lower demand for amino acids.

The deletion of *manX* in the *ptsG* background results in strain WGM that lacks two PTS components related to glucose import [11]. Strain WGM lacks gene *manX*, so PTS components $IIA^{man}$ and $IIB^{man}$ are not synthesized. This strain displays $\mu$ and *qs* values corresponding to 65 and 56% of those observed for WG (Table 2). Acetate was not detected in cultures with WGM. The transcriptome data showed that the further decrease in glucose import capacity in strain WGM, when compared to WG, caused the induction of additional genes encoding PTS and non-PTS proteins involved in the uptake and catabolism of secondary carbon sources that were not present in the culture medium. Interestingly, the observed transcriptional response included several genes from the EMP and PPP that were found upregulated. A lower level of transcripts was detected for genes from the TCA cycle. This response suggests a decrease in energy production capacity for WGM when compared to WG, likely because of the lower growth rate. Strain WGM displayed a higher transcript level for gene *iraP* (2.7-fold), encoding a small anti-adaptor protein that is required for stabilization of the alternative sigma factor $\sigma^S$. The expression of *iraP* is dependent on phosphate starvation and to a lesser extent on carbon limitation, and this response is dependent on ppGpp [50]. These data suggest an involvement of $\sigma^S$ in the observed transcriptional response in WGM. The transcriptome data is indicative of a more severe carbon limitation when comparing WGM to WG. It should be noted that no acetate accumulation was detected in cultures with strain WGM, thus, overflow metabolism was eliminated in this strain (Table 2). A derivative of strain WGM that expresses *gfp* displayed a 1.4-fold increase in the specific rate of GFP synthesis and its yield from biomass when compared to isogenic WG. Strain WGM displayed the highest GFP production capacity when compared to production strains derived from all mutants in this study [12]. This improvement in recombinant protein production capacity for WGM when compared to other strains in this study, can be attributed in part to the specific state of carbon source limitation, and the complete elimination of overflow metabolism.

The effect of eliminating the high-affinity glucose uptake system MglABC on the WGM background was studied by comparing it with strain WGMC. This modification did not alter the *qs*. However, acetate was produced to a maximum level of 0.32 g/L, whereas this organic acid was not detected in cultures with strain WGM. Among the 12 genes that showed differential expression in WGMC when compared to WGM, *nagD* was found to be downregulated (− 2.2-fold) and *galS* upregulated (20.1-fold). Gene *nagD*, also known as *umpH* is part of the N-acetylglucosamine utilization operon and encodes a ribonucleotide phosphatase [51]. It has been determined that overexpression of *nagD* results in the induction of genes related to cell envelope and heat shock stress. The co-expression of *nagD* and mammalian G protein-coupled receptors (GPCR) in *E. coli* resulted in a 3- to tenfold increase in the yield of the latter [52]. This result can be explained considering that induction of stress-related proteins provides a favourable environment to produce recombinant proteins. It remains to be determined if the lower transcript level of *nagD* in WGMC could explain in part why this strain displayed lower GFP production capacity when compared to WGM [12]. Gene *galS*, also known as *mglD* encodes the galactose isorepressor, a transcription factor that represses the transcription of genes involved in galactose catabolism [53]. It has been reported that growth under a low glucose concentration causes the synthesis of galactose as an autoinducer of the *gal* regulon [14, 54]. The *gal* regulon contains genes encoding proteins involved in the transport and metabolism of galactose. It should be noted that the transport proteins that are members of this regulon, GalP, and MglABC, can also employ glucose as substrate [11]. When comparing GFP production strains derivatives of WGM and WGMC it was determined that the latter produced about 40% less recombinant protein [12]. This result can be explained considering the increased production of acetate and possibly also the downregulation of *nagD*. However, with the available data, it is not possible to determine how the deletion of *mglABC* caused such effects. It is interesting to note the lack of correlation between the *qs* and $q_{ac}$ values when comparing strains WGM and WGMC. Elimination of MglABC may abolish the ATP-dependent high-affinity import of glucose that is dependent on ATP for phosphorylation. If MglABC has an important role in glucose import in strain WGM, the deletion of this transporter could shift glucose import to systems dependent on energy from PEP (PTS) or proton motive force (GalP). This modification could alter the energetic state of the cell and central metabolic fluxes, indirectly affecting acetate production in WGMC. These results suggest that deletion of operon *mglABC* should be carefully considered as a strategy to modify *qs* in a production strain since, as shown here, this modification causes unexpected results. Further strain characterization, including measurement of the energy state, as well as carbon flux determination in central pathways should help in understanding the consequences of this modification.

Strain WHIC displayed the lowest values for $\mu$ and *qs* among studied strains and an extremely low level of acetate production (Table 2). Strain WHIC showed the largest number of differentially transcribed genes when compared to the other strains in this study. Even when comparing transcriptome data of WHIC with the strain showing the closest *qs* value, WGMC, 421 genes were found to be expressed differentially. In this comparison, several genes encoding PTS components as well as genes encoding proteins for the transport and metabolism of alternate carbon sources were upregulated in WHIC. Downregulation of genes from the respiratory chain was detected. In the context of GFP production, this strain displayed a threefold higher titer when compared to an isogenic producer strain derived from W3110 [12]. However, WHIC showed the lowest GFP titer when compared to the other mutant strains in this study. The transcriptome profile shown by WHIC suggests the most severe level of carbon and energy limitation when compared to the other mutant strains. Overflow metabolism is reduced and nearly non-existing. However, the extreme hunger state displayed by this strain can be considered the cause for the relatively low GFP production capacity when grown in minimal salts media.

When compared to the transcriptome of wild-type strainW3110, all isogenic derivatives with reduced glucose consumption capacity displayed a relatively large number of differentially expressed genes. The ratios of upregulated to downregulated genes corresponded to 2.2, 5.5, 4.6, and 1.4 for strains WG, WGM, WGMC, and WHIC, respectively. It is noteworthy that even though these strains displayed a transcriptomic response consisting mainly of upregulated genes, all of them have shown an improved capacity for recombinant protein production when compared to W3110 [12]. The observed response suggests that a strategy for further strain optimization for recombinant protein production could be based on avoiding the upregulation of non-essential functions. This approach, also known as resource allocation engineering, has been proven to be effective in improving microbial cell factories [55]. In the case of the glucose transport mutant strains employed in this study, resource allocation engineering could be employed to determine if avoiding the induction of scavenging functions for carbon sources that are not present in the culture medium and other non-essential functions would improve performance for recombinant protein production. It should be noted that several research groups have reported the improvement of *E. coli* strains to produce recombinant proteins or chemicals by employing mutants with

reduced glucose import rates [10, 32, 56]. Those strains may be improved by applying an engineering strategy based on eliminating the non-essential induced functions identified in this study.

#### Abbreviations

AcCoA: Acetyl-coenzyme A; Ack: Acetate kinase; Spc: Spectinomycin; LB: Luria Bertani; CDW: Cell dry weight; GFP: Green fluorescent protein; Pta: Phosphotransacetylase; PEP: Phosphoenolpyruvate; LacI: Lactose repressor; PTS: Phosphoenolpyruvate:sugar phosphotransferase system; TCA: Tricarboxylic acid cycle; $q_{ac}$: Specific rate of acetate production; $q_s$: Substrate uptake rate; $q_p$: Recombinant product formation rate; SD: Standard deviation; *gfp*: Superglo GFP gene; $Y_{X/S}$: Biomass yield from glucose.

## Supplementary Information

The online version contains supplementary material available at https://doi.org/10.1186/s12934-022-01909-y.

**Additional file 1: Figure S1** Growth kinetics of strains W3110, WG, WGM, WGMC, and WHIC. Glucose concentration (triangles), biomass concentration (squares) and acetate concentration (diamonds).

**Additional file 2: Figure S2** Venn diagram representing the number of unique and overlapping genes among strain transcriptome comparisons. Comparisons WG-W3110, WGM-WG, and WHIC-WGMC were tagged as A, B, and C, respectively. The WGMC-WGM comparison was excluded from this analysis.

**Additional file 3:** Supplementary table 1 Primers used in this study.

**Additional file 4:** Supplementary table 2 List of differentially expressed genes when comparing the transcriptome of W3110 with those of the mutant strains.

**Additional file 5:** Supplementary table 3 List of differentially expressed genes when performing pair-wise comparison of transcriptomes from strain in this study.

**Additional file 6:** Supplementary table 5 List of genes displaying a positive correlation of expression with the specific rate of glucose consumption.

**Additional file 7**: Supplementary table 5 List of genes displaying a negative correlation of expression with the specific rate of glucose consumption.

#### Acknowledgements

The authors would like to thank Georgina Hernández-Chávez, Luz María Martínez, Juan Manuel Hurtado and Ricardo Ciria Merce for their technical support.

#### Author contributions

GG and JCFJ designed research, JCFJ performed microbial cultures and RNA-seq experiments, NM performed qPCR experiments, JCFJ, RMGR, ARL, FD, GG, and AM analyzed data, JCFJ, RMGR, ARL, FD, GG, and AM wrote the manuscript. All authors read and approved the final manuscript.

#### Funding

This work was supported by CONACyT grant A1-S-8646. JCFJ was supported by a fellowship from CONACyT.

#### Availability of data and materials

The datasets used and/or analyzed during the current study are available from the corresponding authors on reasonable request.

## Declarations

#### Ethics approval and consent to participate

Not applicable.

#### Consent for publication

Not applicable.

#### Competing interests

The authors declare no competing financial interest.

#### Author details

[1]Departamento de Ingeniería Celular y Biocatálisis, Instituto de Biotecnología, Universidad Nacional Autónoma de México, Morelos, Cuernavaca, México. [2]Departamento de Procesos y Tecnología, Universidad Autónoma Metropolitana, Ciudad de Mexico, México. [3]Terra Research and Teaching Centre, Microbial Processes and Interactions (MiPI) Gembloux Agro-Bio Tech, University of Liège, Gembloux, Belgium.

Received: 28 February 2022 Accepted: 27 August 2022
Published online: 14 September 2022

#### References

1. Görke B, Stülke J. Carbon catabolite repression in bacteria: many ways to make the most out of nutrients. Nat Rev Microbiol. 2008;6:613–24.
2. Ma E, Altman E. Overcoming acetate in Escherichia coli recombinant protein fermentations. Trends Biotechnol. 2006;24:530–6.
3. Valgepea K, Adamberg K, Nahku R, Lahtvee P-J, Arike L, Vilu R. Systems biology approach reveals that overflow metabolism of acetate in Escherichia coli is triggered by carbon catabolite repression of acetyl-CoA synthetase. BMC Syst Biol. 2010;4:166.
4. De M, Ae M, De Maeseneire S, Wim AE, Ae S, Vandamme E. Minimizing acetate formation in E. coli fermentations. Available from: https://academic.oup.com/jimb/article/34/11/689/5993063
5. Wolfe AJ. The Acetate Switch. Microbiol Mol Biol Rev 2005;69:12–50. Available from: https://journals.asm.org/journal/mmbr
6. Taymaz-Nikerel H, Lara AR. Vitreoscilla Haemoglobin: a tool to reduce overflow metabolism. Microorganisms. 2021;10:43.
7. Han K, Han K, Lim HC, Lim HC, Hong J, Hong J. Acetic acid formation in *Escherichia coli* fermentation. Biotechnol Bioeng. 1992;39:663–71.
8. Shiloach J, Kaufman J, Guillard aS, Fass R. Effect of glucose supply strategy on acetate accumulation, growth, and recombinant protein production by *Escherichia coli* BL21 (hDE3) and Escherichia coli JM 109. Biotechnology. 1996;49:421–8.
9. Lin C, Cheng L, Wang J, Zhang S, Fu Q, Li S, et al. Optimization of culture conditions to improve the expression level of beta1–epsilon toxin of Clostridium perfringens type B in *Escherichia coli*. Biotechnol Biotechnol Equip. 2016;30:324–31.
10. De Anda R, Lara AR, Hernández V, Hernández-Montalvo V, Gosset G, Bolívar F, et al. Replacement of the glucose phosphotransferase transport system by galactose permease reduces acetate accumulation and improves process performance of *Escherichia coli* for recombinant protein production without impairment of growth rate. Metab Eng. 2006;8:281–90.
11. Fuentes LG, Lara AR, Martínez LM, Ramírez OT, Martínez A, Bolívar F, et al. Modification of glucose import capacity in Escherichia coli: physiologic consequences and utility for improving DNA vaccine production. Microb Cell Fact. 2013;12:42.
12. Fragoso-Jiménez JC, Baert J, Nguyen TM, Liu W, Sassi H, Goormaghtigh F, et al. Growth-dependent recombinant product formation kinetics can be reproduced through engineering of glucose transport and is prone to phenotypic heterogeneity. Microb Cell Fact. 2019. https://doi.org/10.1186/s12934-019-1073-5.
13. Tchieu JH, Norris V, Edwards JS, Saier MH. The complete phosphotransferase system in *Escherichia coli*. J Mol Biotechnol. 2001;3:329–46.
14. Ferenci T. Hungry bacteria—definition and properties of a nutritional state. Enviromental Microbiol. 2006;3:605–11.
15. Death A, Ferenci T. Between feast and famine: endogenous inducer synthesis in the adaptation of *Escherichia coli* to growth with limiting carbohydrates. J Bacteriol. 1994;176:5101–7.
16. Picon A, Teixeira de Mattos MJ, Postma PW. Reducing the glucose uptake rate in Escherichia coli affects growth rate but not protein production. Biotechnol Bioeng. 2005;90:191–200. https://doi.org/10.1002/bit.20387.

17. Steinsiek S, Bettenbrock K. Glucose transport in Escherichia coli mutant strains with defects in sugar transport systems. J Bacteriol. 2012;194:5897–908.
18. Hogema BM, Arents JC, Bader R, Eijkemans K, Yoshida H, Takahashi H, et al. Inducer exclusion in Escherichia coli by non-PTS substrates: the role of the PEP to pyruvate ratio in determining the phosphorylation state of enzyme IIA(Glc). Mol Microbiol. 1998;30:487–98.
19. Gutierrez-Ríos R, Freyre-Gonzalez JA, Resendis O, Collado-Vides J, Saier M, Gosset G. Identification of regulatory network topological units coordinating the genome-wide transcriptional response to glucose in *Escherichia coli*. BMC Microbiol. 2007;7:53. https://doi.org/10.1186/1471-2180-7-53.
20. JR S, H. M. Regulation of carbon utilization. Escherichia coli Salmonella Cell Mol Biol. ASM Press; 1996 [cited 2021 Sep 21];1325–43. Available from: http://ci.nii.ac.jp/naid/10005857743/en/
21. Vanyan L, Trchounian K. HyfF subunit of hydrogenase 4 is crucial for regulating FOF1 dependent proton/potassium fluxes during fermentation of various concentrations of glucose. J Bioenerg Biomembr. 2022;54:69–79.
22. Hempfling WP, Mainzer SE. Effects of varying the carbon source limiting growth on yield and maintenance characteristics of *Escherichia coli* in continuous culture. J Bacteriol. 1975. https://doi.org/10.1128/jb.123.3.1076-1087.1975.
23. Vital M, Chai B, Østman B, Cole J, Konstantinidis KT, Tiedje JM. Gene expression analysis of *E coli* strains provides insights into the role of gene regulation in diversification. ISME J. 2015;9:1130–40. https://doi.org/10.1038/ismej.2014.204
24. Death A, Ferenci T. Between feast and famine: endogenous inducer synthesis in the adaptation of *Escherichia coli* to growth with limiting carbohydrates. J Bacteriol. 1994. https://doi.org/10.1128/jb.176.16.5101-5107.1994.
25. Hewitt CJ, Nebe-Von Caron G, Nienow AW, McFarlane CM. The use of multi-parameter flow cytometry to compare the physiological response of *Escherichia coli* W3110 to glucose limitation during batch, fed—batch and continuous culture cultivations. J Biotechnol. 1999;75:251–64.
26. Yao R, Hirose Y, Sarkar D, Nakahigashi K, Ye Q, Shimizu K. Catabolic regulation analysis of *Escherichia coli* and its crp, mlc, mgsA, pgi and ptsG mutants. Microb Cell Fact. 2011;10:67.
27. Borirak O, Rolfe MD, De Koning LJ, Hoefsloot HCJ, Bekker M, Dekker HL, et al. Time-series analysis of the transcriptome and proteome of *Escherichia coli* upon glucose repression. Biochim Biophys Acta Proteins Proteomics. 2015;1854:1269–79.
28. Castaño-Cerezo S, Bernal V, Post H, Fuhrer T, Cappadona S, Sánchez-Díaz NC, et al. Protein acetylation affects acetate metabolism, motility and acid stress response in *Escherichia coli*. Mol Syst Biol. 2014. https://doi.org/10.15252/msb.20145227.
29. Gosset G, Zhang Z, Nayyar S, Cuevas WA, Saier MH. Transcriptome analysis of Crp-dependent catabolite control of gene expression in *Escherichia coli*. J Bacteriol. 2004;186:3516–24. https://doi.org/10.1128/JB.186.11.3516-3524.2004.
30. Klumpp S, Hwa T. Bacterial growth: global effects on gene expression, growth feedback and proteome partition. Curr Opin Biotechnol. 2014;28:96–102.
31. Bäcklund E, Markland K, Larsson G. Cell engineering of Escherichia coli allows high cell density accumulation without fed-batch process control. Bioprocess Biosyst Eng. 2008;31:11–20.
32. Bäcklund E, Ignatushchenko M, Larsson G. Suppressing glucose uptake and acetic acid production increases membrane protein overexpression in *Escherichia coli*. Microb Cell Fact. 2011. https://doi.org/10.1186/1475-2859-10-35.
33. Bachmann BJ. Pedigrees of some mutant strains of *Escherichia coli* K-12. Bacteriol Rev. 1972;36:525–57.
34. Patro R, Duggal G, Kingsford C. Salmon: Accurate, versatile and ultrafast quantification from RNA-seq Data using Lightweight-Alignment. bioRxiv. 2015;021592. Available from: http://biorxiv.org/content/early/2015/06/27/021592.abstract
35. Robinson MD, Mccarthy DJ, Smyth GK. edgeR: a Bioconductor package for differential expression analysis of digital gene expression data. Bioinforma Appl. 2010;26:139–40.
36. Benjamini Y, Hochberg Y. Controlling the false discovery rate: a practical and powerful approach to multiple testing. Source J R Stat Soc Ser B. 1995;57:289–300.
37. Veit A, Polen T, Wendisch VF. Global gene expression analysis of glucose overflow metabolism in *Escherichia coli* and reduction of aerobic acetate formation. Appl Microbiol Biotechnol. 2007;74:406–21.
38. Aguilar C, Escalante A, Flores N, de Anda R, Riveros-McKay F, Gosset G, et al. Genetic changes during a laboratory adaptive evolution process that allowed fast growth in glucose to an *Escherichia coli* strain lacking the major glucose transport system. BMC Genomics. 2012;13:385.
39. Gosset G. Improvement of *Escherichia coli* production strains by modification of the phosphoenolpyruvate:sugar phosphotransferase system. Microb Cell Fact. 2005;4:14.
40. Plumbridge J. Regulation of gene expression in the PTS in *Escherichia coli*: the role and interactions of Mlc. Curr Opin Microbiol Elsevier Ltd. 2002;5:187–93.
41. Christensen DG, Meyer JG, Baumgartner JT, D'souza AK, Payne SH, Kuhn ML, et al. Identification of novel protein lysine acetyltransferases in escherichia coli. MBio. 2018;9:1–24.
42. Notley L, Ferenci'T. Differential expression of mai genes under cAMP endogenous inducer controi in nutrient-stressed *Eschericttiia coli*. Mol Microbiol. 1995. https://doi.org/10.1111/j.1365-2958.1995.tb02397.x.
43. Boos W, Shuman H. Maltose/Maltodextrin system of *Escherichia coli*: transport, metabolism, and regulation. Microbiol Mol Biol Rev. 1998;62:204–29.
44. Notley-McRobb L, Ferenci T. Adaptive mgl-regulatory mutations and genetic diversity evolving in glucose-limited *Escherichia coli* populations. Environ Microbiol. 1999;1:33–43.
45. Wackwitz B, Bongaerts J, Goodman SD, Unden G. Growth phase-dependent regulation of nuoA-N expression in *Escherichia coli* K-12 by the Fis protein: upstream binding sites and bioenergetic significance. Mol Gen Genet. 1999;262:876–83.
46. Tramonti A, De Canio M, Delany I, Scarlato V, De Biase D. Mechanisms of transcription activation exerted by GadX and GadW at the gadA and gadBC gene promoters of the glutamate-based acid resistance system in *Escherichia coli*. J Bacteriol. 2006;188:8118–27.
47. Hernández-Montalvo V, Martínez A, Hernández-Chavez G, Bolivar F, Valle F, Gosset G. Expression of galP and glk in a Escherichia coli PTS mutant restores glucose transport and increases glycolytic flux to fermentation products. Biotechnol Bioeng. 2003;83:687–94.
48. Wada A, Yamazakit Y, Fujitat N, Ishihamatt A. Structure and probable genetic location of a "ribosome modulation factor" associated with 100S ribosomes in stationary-phase *Escherichia coli* cells (growth-dependent control/translation regulation/two-dimensional gel electrophoresis). Proc Nadl Acad Sci USA. 1990;87:2657–61.
49. Izutsu K, Wada C, Komine Y, Tomoyuki S, Ueguchi C, Nakura S, et al. *Escherichia coli* ribosome-associated protein SRA, whose copy number increases during stationary phase. J Bacteriol. 2001;183:2765–73.
50. Bougdour A, Gottesman S. ppGpp regulation of RpoS degradation via anti-adaptor protein IraP. PNAS. 2007.
51. Tremblay LW, Dunaway-Mariano D, Allen KN. Structure and activity analyses of *Escherichia coli* K-12 NagD provide insight into the evolution of biochemical function in the haloalkanoic acid dehalogenase superfamily. Biochemistry. 2006;45:1183–93. https://doi.org/10.1021/bi051842j.
52. Skretas G, Makino T, Varadarajan N, Pogson M, Georgiou G. Multi-copy genes that enhance the yield of mammalian G protein-coupled receptors in *Escherichia coli*. Metab Eng. 2012;14:591–602.
53. Semsey S, Krishna S, Sneppen K, Adhya S. Signal integration in the galactose network of *Escherichia coli*. Mol Microbiol. 2007;65:465–76.
54. Geanacopoulos M, Adhya S. Functional characterization of roles of GalR and GalS asRegulators of thegalRegulon. J Bacteriol. 1997. https://doi.org/10.1128/jb.179.1.228-234.1997.
55. Lastiri-Pancardo G, Mercado-Hernamp JS, Kim J, Jimamp I. A quantitative method for proteome reallocation using minimal regulatory interventions. Nat Chem Biol. 2020. https://doi.org/10.1038/s41589-020-0593-y.
56. Chou C, Bennett GN, Sari K. Effect of modified glucose uptake using genetic engineering techniques on high-level recombinant protein production in escherichia coli dense cultures. Biotechnol Adv. 1994;44:952–60.


## Publisher's Note

Velazquez *et al. Microbial Cell Factories* (2022) 21:183
https://doi.org/10.1186/s12934-022-01906-1

Microbial Cell Factories

RESEARCH

Open Access

# Glucose transport engineering allows mimicking fed-batch performance in batch mode and selection of superior producer strains

Daniela Velazquez[1], Juan-Carlos Sigala[1], Luz María Martínez[2], Paul Gaytán[2], Guillermo Gosset[2] and Alvaro R. Lara[1*]

## Abstract

**Background:** Fed-batch mode is the standard culture technology for industrial bioprocesses. Nevertheless, most of the early-stage cell and process development is carried out in batch cultures, which can bias the initial selection of expression systems. Cell engineering can provide an alternative to fed-batch cultures for high-throughput screening and host selection. We have previously reported a library of *Escherichia coli* strains with single and multiple deletions of genes involved in glucose transport. Compared to their wild type (W3110), the mutant strains displayed lower glucose uptake, growth and aerobic acetate production rates. Therefore, when cultured in batch mode, such mutants may perform similar to W3110 cultured in fed-batch mode. To test that hypothesis, we evaluated the constitutive expression of the green fluorescence protein (GFP) in batch cultures in microbioreactors using a semi defined medium supplemented with 10 or 20 g/L glucose + 0.4 g yeast extract/g glucose.

**Results:** The mutant strains cultured in batch mode displayed a fast-growth phase (growth rate between 0.40 and 0.60 $h^{-1}$) followed by a slow-growth phase (growth rate between 0.05 and 0.15 $h^{-1}$), similar to typical fed-batch cultures. The phase of slow growth is most probably caused by depletion of key amino acids. Three mutants attained the highest GFP fluorescence. Particularly, a mutant named WHIC (Δ*ptsHIcrr*, Δ*mglABC*), reached a GFP fluorescence up to 14-fold greater than that of W3110. Strain WHIC was cultured in 2 L bioreactors in batch mode with 100 g/L glucose + 50 g/L yeast extract. These cultures were compared with exponentially fed-batch cultures of W3110 maintaining the same slow-growth of WHIC (0.05 $h^{-1}$) and using the same total amount of glucose and yeast extract than in WHIC cultures. The WHIC strain produced approx. 450 mg/L GFP, while W3110 only 220 mg/L.

**Conclusion:** The combination of cell engineering and high throughput screening allowed the selection of a particular mutant that mimics fed-batch behavior in batch cultures. Moreover, the amount of GFP produced by the strain WHIC was substantially higher than that of W3110 under both, batch and fed-batch schemes. Therefore, our results represent a valuable technology for accelerated bioprocess development.

**Keywords:** Overflow metabolism, Fed-batch, High cell-density, Glucose transport, Cell engineering

## Background

Production of recombinant proteins using *Escherichia coli* (*E. coli*) is a technology well established at industrial level. To attain high biomass yields and recombinant protein productivities, high cell-density cultures are used. These cultures require large amounts of glucose, which is the preferred carbon and energy source for this

*Correspondence: alara@cua.uam.mx

[1] Departamento de Procesos y Tecnología, Universidad Autónoma Metropolitana, Vasco de Quiroga 4871, 05348 Mexico City, Mexico
Full list of author information is available at the end of the article

bacterium. In batch cultures, the glucose uptake rate ($q_S$) reaches its maximum value, which in turn triggers the synthesis of acetate, even if oxygen is present in sufficient amounts, a phenomenon known as overflow metabolism [1, 2]. Acetate accumulation is undesired, because it negatively affects bioprocess performance. Therefore, controlling the $q_S$ below a certain threshold value to avoid overflow metabolism while keeping the maximum growth rate is highly desirable. Maintaining the $q_S$ below the threshold value is normally achieved by controlling the glucose supply in the so-called fed-batch scheme [3]. In the case of exponential feeding, the rate of nutrient addition increases in proportion to cell growth, in such a way that a certain specific growth rate ($\mu_{set} < \mu_{max}$) can be maintained and the substrate concentration in the medium is close to zero [3]. Because maximum productivities and yields can be obtained at lower growth rates than those displayed in batch cultures [4, 5], exponentially fed-batch cultures can be operated to maintain the growth rate that maximizes productivity, while overflow metabolism is avoided, and the specific oxygen uptake rate is reduced. However, fed-batch cultures have certain disadvantages, such as the requirement of additional equipment and control systems, which hinders its implementation in early-stage process development, particularly if high throughput screening of cell factories and gene circuits are sought.

Due to the importance of fed-batch cultures, several approaches have been proposed to perform this culture mode in small-scale systems [6]. For instance, diffusive glucose release from a polymeric matrix has been applied in shake flasks [7, 8] and microtiter plates [9]. Another alternative consists on the enzymatic release of glucose from a polymeric substrate that cannot be degraded by *E. coli* [10, 11]. However, in such systems the specific growth rate cannot be controlled via glucose supply. Microfluidic devices have been implemented to perform fed-batch schemes in microtiter plates [12]. Other devices have been proposed to feed glucose solutions to shake flasks [13, 14]. The specific growth rate can be efficiently controlled in mini bioreactors using mathematical models coupled to feeding strategies [15]. Nevertheless, the latter systems are expensive and require additional equipment.

An alternative to the fed-batch mode to avoid overflow metabolism is the use of mutant strains with reduced glucose import capacity. Glucose is first transported from the extracellular medium to the periplasmic space of *E. coli* by porins and then internalized into the cytoplasm by the phosphoenolpyruvate-dependent phosphotransferase system (PTS) [16]. When the external glucose concentration is lower than 1 μM, or when the PTS is inactive, proteins normally involved in the transport of other carbohydrates such as the galactose: $H^+$ symporter GalP and the high-affinity ABC transporter Mgl system are induced in *E. coli* [17]. Therefore, eliminating or reducing the activity of the PTS has been applied to decrease acetate formation. This strategy has been implemented by deleting genes encoding components of the PTS [18, 19] or by repressing their expression by means of non-coding mRNA [20]. We have previously reported that the inactivation of PTS and overexpression of the galactose transporter GalP efficiently reduced overflow metabolism and allows attaining high cell-densities in batch mode using up to 120 g/L glucose [21–25]. Fuentes and co-workers developed a library of mutant strains with single or combinatory deletions in genes encoding the PTS permeases and common components (*manX*, *malX*, *nagE*, *bglF*, *ptsG*, *ptsHIcrr*), as well as non-PTS transporters (*galP* and *mglABC*). Such mutations resulted in slower rates of glucose import and consequently, a strong reduction of acetate production and growth rate [26]. Compared to their wild type, some of these strains have the capacity to produce higher amounts of plasmid DNA [26] or recombinant protein [27]. However, their slow growth rate (from 21 to 72% lower than the wild type [26]) in mineral medium is a disadvantage for developing high cell-density cultures in batch mode. Therefore, modification of the culture media is key to increase the growth rate of the engineered strains while keeping their low aerobic acetate synthesis.

In the present work, we propose a simple strategy to mimic fed-batch mode using the strains library of Fuentes and co-workers when cultured in batch mode. Fast growth rate in these strains was promoted by adding extra nutrients to a chemically defined medium. Upon the exhaustion of key nutrients, the cells shifted to slow growth, similar to a fed-batch. The strains were characterized for constitutive GFP expression in microtiter plates using 10 or 20 g $L^{-1}$ glucose. The best GFP producer strain was then cultured in 2 L bioreactors with 100 g $L^{-1}$ glucose in batch mode. The wild type strain W3110 was cultured in an exponentially fed-batch culture at the same growth rate than the mutant strain WHIC using the same total amount of glucose. The mutant strain displayed the biphasic growth and produced only small amounts of acetate, while doubling the amount of GFP produced in fed-batch cultures when compared to the wild-type and reaching more than 50 g $L^{-1}$ of biomass. Therefore, the library of mutants can be used to mimic fed-batch cultures in batch mode, which are useful to accelerate early bioprocess development.

## Results and discussion

### High throughput screening of *E. coli* strains with reduced glucose import capacity

The strains employed in this study were taken from the library of mutants developed by Fuentes and coworkers [25]. The genotype of the strains is shown in Table 1. All strains were transformed with plasmid pWF14, which carries a gene encoding *gfp* under transcriptional control of a constitutive promoter, as detailed in "Methods" section. Aerobic cultures were performed in mineral medium with yeast extract and glucose. Two different glucose concentrations were used: 10 and 20 g $L^{-1}$, supplemented with 4 or 8 g $L^{-1}$ of yeast extract, respectively. Cultures were performed in baffled microtiter plates where the oxygen transfer rate can be higher than 100 mmol $L^{-1}$ $h^{-1}$ [28].

Figure 1 shows the biomass and GFP fluorescence profiles in cultures with 10 g $L^{-1}$ glucose. The levels of GFP fluorescence exhibited important differences between strains. Therefore, the results are grouped depending on the GFP fluorescence obtained. The strains WGP, W3110, WGMX and WHIC presented *lag* phases ranging from 1 to 5 h (Fig. 1, left panel). All the strains had a fast growth rate phase, followed by a slow growth rate phase, which may occur due to depletion of glucose and yeast extract nutrients, as discussed below. The growth rates of both phases are reported in Table 2. The maximum scattered light intensity (ScL) reached ranged from 56 to 174 (Fig. 1). The mutant strains displayed GFP fluorescence lower than that of the wild type (Fig. 1, right panel), with the exception of WHIC, that reached a GFP fluorescence 2.7-fold greater than W3110. Although the extracellular glucose was not monitored, it was considered that the cultures had a very low metabolic activity after little DOT changes (Fig. 2) and relatively stable GFP fluorescence signal. At this point, cultures were finalized.

**Table 1** Genes inactivated in each of the strains used in this study

| Strain | Inactivated genes |
|---|---|
| W3110 | Wild type |
| WG | *ptsG* |
| WGX | *ptsG*, *malX* |
| WGB | *ptsG*, *bglF* |
| WGE | *ptsG*, *nagE* |
| WGM | *ptsG*, *manX* |
| WGMX | *ptsG*, *manX*, *malX* |
| WGMB | *ptsG*, *manX*, *bglF* |
| WGME | *ptsG*, *manX*, *nagE* |
| WGP | *ptsG*, *galP* |
| WGC | *ptsG*, *mglABC* |
| WGMP | *ptsG*, *manX*, *galP* |
| WGMC | *ptsG*, *manX*, *mglABC* |
| WHI | *ptsHlcrr* |
| WHIP | *ptsHlcrr*, *galP* |
| WHIC | *ptsHlcrr*, *mglABC* |

The microtiter plates included optodes for dissolved oxygen (DOT) and pH monitoring online. As shown in Fig. 2, DOT remained above 20%, and between 6.9 and 7.9 in all cultures. Therefore, it can be assumed that the cultures were not oxygen limited and that pH was not a stress factor.

The strains were also evaluated using 20 g $L^{-1}$ glucose with the aim of increasing the amount of biomass achievable in batch mode. The culture profiles are shown in Fig. 3, grouped as in Fig. 1, while DOT and pH profiles are shown in Fig. 4. Similar to cultures with 10 g $L^{-1}$ glucose, the cells displayed two growth phases. The maximum ScL reached ranged from 89 to 323, nearly doubling the ScL signal of the previous cultures for each strain. Contrary to what was observed in cultures with a lower amount of glucose, three mutant strains reached GFP fluorescence values higher than that of the wild type. Namely, the GFP fluorescence in cultures of strains WGMB and WGM were 19 and 74% higher than that of W3110 (Fig. 3F). The better performance of these strains, which was not observed in cultures using 10 g $L^{-1}$ glucose, could be attributed to their very low acetate production [26], which is more advantageous when a higher amount of glucose is used. Notably, the GFP fluoresce in cultures of strain WHIC was 4.5-fold greater when compared to W3110 (Fig. 3H). Fragoso et al. [27], reported cultures of strains WG, WGM, WGX, WGMC, WHI and WHIC in M9 medium expressing GFP. They found that all the mutant strains produced more GFP than W3110 in M9 medium supplemented with 20 g $L^{-1}$ glucose, being WGM the best producer. In addition to the differences in medium composition, there are other factors possibly causing these contrasting results. Fragoso and coworkers [27] employed an IPTG to express GFP. The use of IPTG combined with the altered cAMP intracellular amount in the mutant

(See figure on next page.)

**Fig. 1** Cultures of *E. coli* strains constitutively expressing the GFP in semi-defined medium supplemented with 10 g $L^{-1}$ glucose and 4 g $L^{-1}$ yeast extract. The left panel shows scattered light intensities, and the right panel shows GFP fluorescence intensities. **A**, **B** Cultures of strains WG, WGE, WEP and WHI; **C**, **D** cultures of strains WGB, WGME, WGMX, and WGMP; **E**, **F** cultures of W3110, WGM, WGX and WGMB; **G**, **H** cultures of strain WHIC. Culture conditions: 48 well FlowerPlates®, $V_L$ = 800 µL, $n$ = 1500 rpm, $d_0$ = 3 mm. Note that the scales are not identical. Shaded bands indicate the standard deviation between triplicate experiments

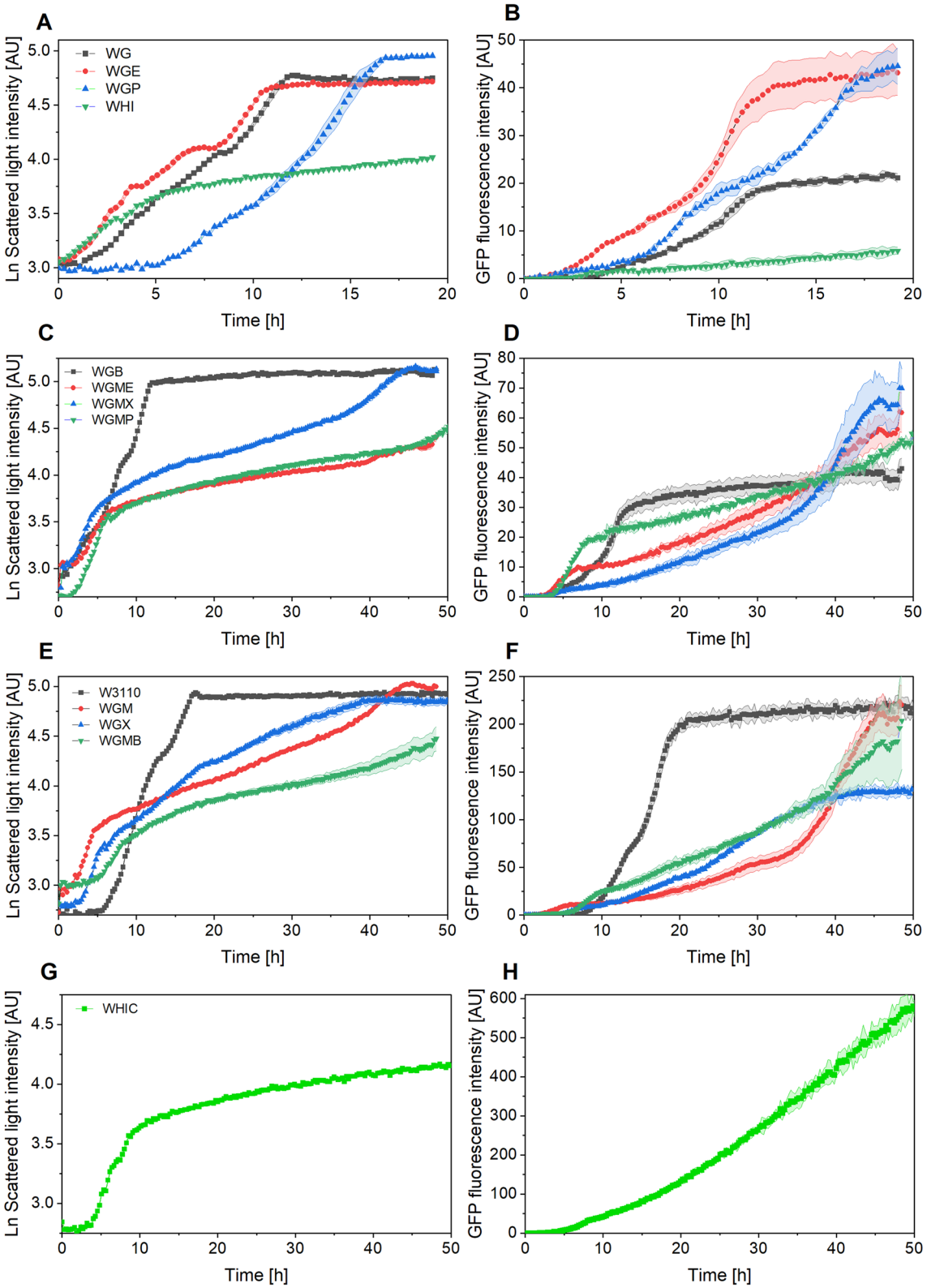


**Fig. 1** (See legend on previous page.)

**Table 2** Specific growth rates of the strains ($\mu$) in batch cultures with 10 g $L^{-1}$ glucose. Subscripts 1 and 2 refer to the first and second growth phase, respectively

| Strain | $\mu_1$ [$h^{-1}$] | $\mu_2$ [$h^{-1}$] |
|---|---|---|
| W3110 | 0.67 ± 0.03 | 0.22 ± 0.01 |
| WG | 0.54 ± 0.03 | 0.34 ± 0.02 |
| WGB | 0.42 ± 0.03 | 0.30 ± 0.01 |
| WGE | 0.52 ± 0.06 | 0.30 ± 0.01 |
| WGM | 0.56 ± 0.05 | 0.05 ± 0.01 |
| WGMB | 0.61 ± 0.27 | 0.06 ± 0.01 |
| WGME | 0.38 ± 0.06 | 0.03 ± 0.00 |
| WGMP | 0.62 ± 0.03 | 0.04 ± 0.01 |
| WGMX | 0.47 ± 0.02 | 0.05 ± 0.00 |
| WGP | 0.71 ± 0.03 | 0.35 ± 0.05 |
| WGX | 0.64 ± 0.02 | 0.07 ± 0.01 |
| WHI | 0.53 ± 0.07 | 0.11 ± 0.01 |
| WHIC | 0.46 ± 0.01 | 0.04 ± 0.01 |

strains, as result of the lower glucose uptake rate, could enhance the activation of the *lac* promoter [27].

This bias may be dependent on the specific strain, due to their particular characteristic of the glucose transport. Such effects are not expected in the constitutive system used here, although the strength of the used promoter has not been compared with that of the inducible promoter used by Fragoso and coworkers [27]. Figure 5 contains the maximum GFP fluorescence and the specific GFP fluorescence (SGF) reached in all cultures. Even though strains WGM and WGMB did not reach a GFP fluorescence level higher than that of W3110 in cultures with 10 g $L^{-1}$ glucose, their SGF was greater than that of the wild type (Fig. 5A, C). Therefore, when higher cell densities are attained (presumably due to low acetate production), the GFP fluorescence in cultures of WGM and WGMB was higher than for W3110 (Fig. 5B, D). Interestingly, strain WHIC displayed considerably higher GFP fluorescence and SGF than all the other strains, but its SGF decreased when the glucose concentration was increased from 10 to 20 g $L^{-1}$ (Fig. 5B, D).

Samples were taken at the end of the cultures with 20 g $L^{-1}$ glucose to measure the amount of GFP produced. Table 3 shows the specific growth rates and GFP fluorescence during the two growth phases, and the final GFP concentration in each culture. With the exception of WGB, WGE and WGP, the mutant strains reached specific growth rates similar to those of W3110 during the first growth phase ($\mu_1$).

The growth rate during the second growth phase ($\mu_2$) was considerably lower for the mutant strains, compared to $\mu_1$. Namely, $\mu_2$ was reduced around 90% with respect to $\mu_1$ in strains WGM, WGMB, WGME, WGMX, WGMP, WGX. While these strains are derivatives of WG (Δ*ptsG*), the growth rate of WG during the second growth phase was less affected than in the double or triple mutants. The *manX* gene has been deleted in strains WGM, WGMB, WGME, WGMX and WGMP. Such gene codes for the mannose transporter and it can also import glucose [27]. The observed decrease in growth rate could be attributed to this deletion, since strains with deletions of genes *bglF* and *nagE* but with intact *manX* (WGB and WGE, respectively) the growth rate decrease was around 4% (Table 2). In strains WHI and WHIC, the *ptsHIcrr* operon has been inactivated. These strains also exhibited a reduction in growth rate of more than 9%, when compared to the first growth phase (Table 3). With the exception of WGP, the SGF of the second growth phase increased, compared to the first phase (Table 3). In general, this is similar to what is observed in fed-batch cultures, where a decrease in growth rate due to glucose limitation leads to increased recombinant protein yields [4, 5]. The amount of GFP quantified in the cultures agreed with the GFP fluorescence, but GFP was not detected by the method used in the case of the lowest GFP fluorescence (Table 3). Figure 6 shows the relationship between growth rate and SGF in all cultures. As can be seen, there seems to be a maximum SGF at a low growth rate, but then it decreases at the lowest growth rates. This agrees with previous studies, which suggest that the optimum growth rate depends on the specific produced protein [29, 30].

The modification of glucose transport can also have metabolic consequences beyond reduction of growth rate. For instance, Fig. 7 shows the specific NADH fluorescence in cultures of W3110 and WHIC with 10 g $L^{-1}$ glucose. The specific NADH fluorescence was similar for both strains at the beginning of the cultures, decreasing as time progressed, but at a lower rate for WHIC than for W3110. The NADH specific fluorescence decreased more slowly after a time that is coincident with the shift to a low growth rate (Fig. 3). It is possible that at this point, the energy demand to synthesize the depleted nutrients could increase the respiratory activity and thus the NADH consumption. Interestingly, the NADH specific fluorescence remained higher for WHIC than for W3110 since 10 h of culture (Fig. 7). It may occur due to the higher acetate production of strain W3110, since acetate is synthesized to supply $NAD^+$ to glycolysis [1]. Moreover, during the acetate excretion, the pH gradient of the cell is uncoupled [1], and thus extra energy will be required to maintain the homeostasis. Furthermore, during the second growth phase, the respiratory activity of WHIC is expected to be lower than that of W3110 [18]. Taken together, these factors may explain the higher NADH fluorescence.

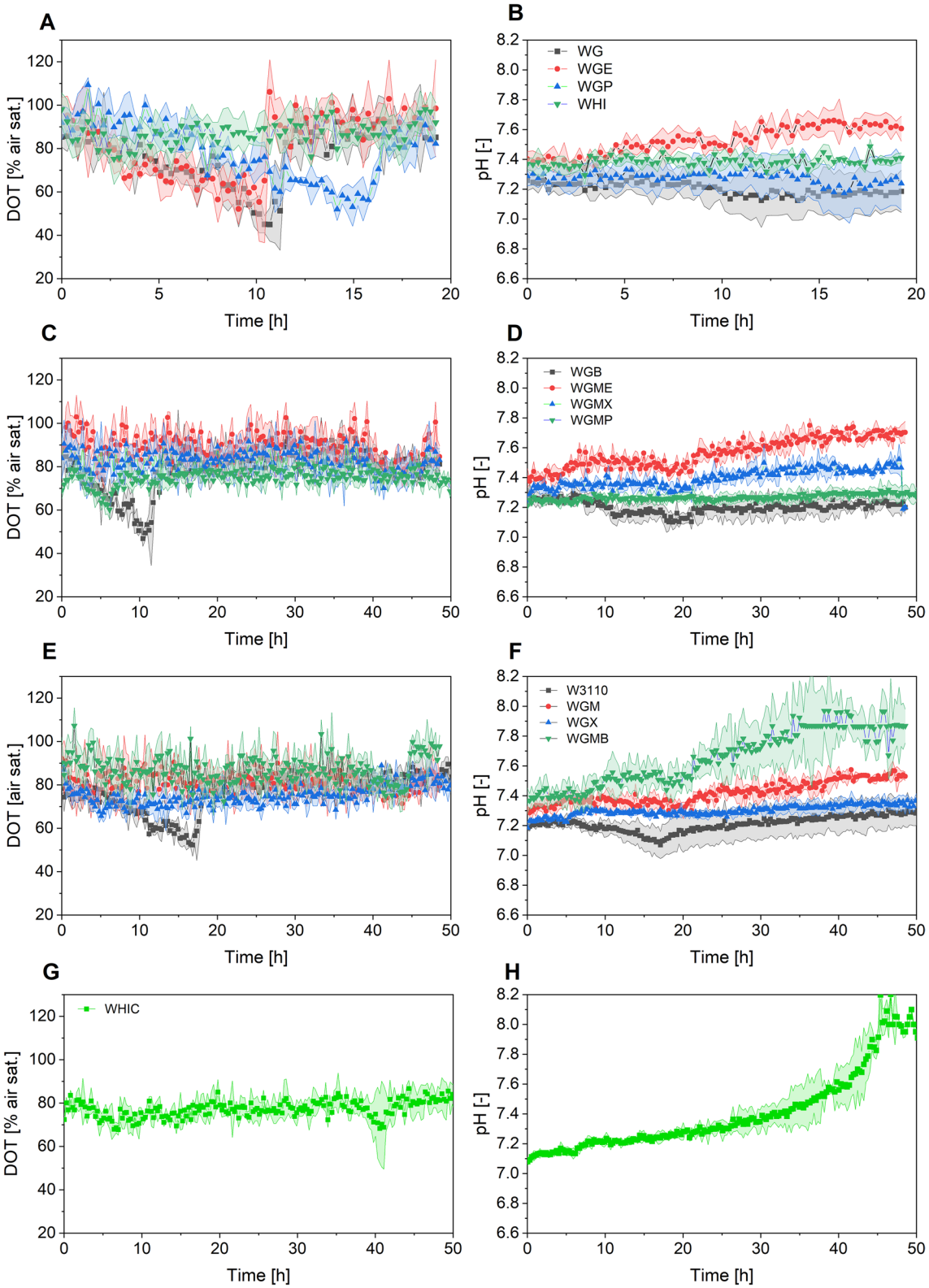


**Fig. 2** Cultures of *E. coli* strains constitutively expressing the GFP in semi-defined medium supplemented with 10 g $L^{-1}$ glucose and 4 g $L^{-1}$ yeast extract. The left panel shows the Dissolved oxygen tension (DOT), and the right panel shows pH values. **A**, **B** Cultures of strains WG, WGE, WEP and WHI; **C**, **D** cultures of strains WGB, WGME, WGMX, and WGMP; **E**, **F** cultures of W3110, WGM, WGX and WGMB; **G**, **H** cultures of strain WHIC. Culture conditions: 48 well FlowerPlates®, $V_L = 800$ µL, $n = 1500$ rpm, $d_0 = 3$ mm

Based on the discussed results, strain WHIC was selected for high cell-density cultures in batch mode.

## WHIC batch cultures vs. W3110 fed-batch cultures

To further assess the potential of the WHIC strain for high cell-density cultures with reduced acetate accumulation and improved recombinant protein production, batch cultures were performed and compared to W3110 fed-batch cultures. To better compare the performance of these strains, W3110 was cultured in exponentially fed-batch mode the attain an specific growth rate of 0.05 $h^{-1}$, to match the growth rate of WHIC during the second growth phase. Strain WHIC was cultured using 100 g $L^{-1}$ glucose. The amount of yeast extract and total amount of glucose were the same for both cultures. The culture profiles are shown in Fig. 8. Cultures of W3110 showed the typical profile of a fed-batch culture (Fig. 8A). W3110 grew at $\mu$ of $0.46 \pm 0.02$ $h^{-1}$ during the batch phase, and acetate was accumulated. This phase of acetate production occurred during the first 3 h of culture (Fig. 8A), which was consumed during the first hours of the glucose-limited phase (acetate consuming phase, from 3 to 8 h). Acetate was the only by-product detected for both strains. The acetate concentration remained below detectable levels after this and no glucose accumulation was observed, as expected for an exponentially fed-batch scheme. Mutant WHIC showed again two growth phases (Fig. 8B). The first phase lasted 6 h with a $\mu$ of $0.33 \pm 0.04$ $h^{-1}$, while the second phase lasted 26 h with a $\mu$ of $0.04 \pm 0.01$ $h^{-1}$. The growth rate during the first phase was approx. 30% lower for both strains, compared to cultures using 20 g $L^{-1}$ glucose (Table 3), which could be attributed to the osmotic stress caused by the concentrated medium [24]. At the point of growth rate decrease, the biomass concentration of WHIC was 14.4 g $L^{-1}$. Based on the typical protein content in *E. coli* [31], and the amino acid content in the proteins of *E. coli* [32], we estimated the amount of *E. coli* biomass that could be synthesized exclusively using the amino acids from the yeast extract. Based on the yeast extract composition reported by Popdora and coworkers [33], it was estimated that proline and glycine could limit the formation of biomass, since their availability could sustain the synthesis of only 10.4 and 7.52 g $L^{-1}$ of biomass, respectively. Despite the variations in composition of the yeast extract and exact amino acids composition of strain WHIC, this rough estimation illustrates that the assumption that growth rate decrease occurs due to amino acids depletion is reasonable.

Bäcklund et al. [18] also compared the performance of W3110 and a PTS mutant for recombinant protein production. They showed that the specific production rate of beta-galactosidase was similar for W3110 in fed-batch and the mutant strain in batch cultures. However, the growth profiles were very different in both cultures, and cell densities were approx. 10 g $L^{-1}$ for W3110 and less than 5 g $L^{-1}$ for the mutant strain. In contrast, as shown in Fig. 8, no important differences were observed in the final biomass concentration between W3110 and WHIC, reaching 48 and 53.5 g $L^{-1}$ of biomass, respectively in our experiments. Remarkably, there were significant differences in the amounts of acetate accumulation, GFP titer, and $Y_{GFP/X}$. Acetate concentration in cultures of W3110 reached a maximum of 3.3 g $L^{-1}$, whereas acetate production was 64% lower for WHIC strain, reaching only 1.2 g $L^{-1}$. GFP final concentration was twofold higher in WHIC than in W3110, while $Y_{GFP/X}$ and specific rate of GFP production ($q_{GFP}$) were 77 and 14.5% higher in WHIC compared to W3110 during the phase of no acetate production (8–20 h for W3110 and 23–35 h for WHIC). The fact that more GFP is produced by WHIC, despite the fact that acetate was not produced by any strain in this phase, can be explained by the metabolic differences of the mutant strain. When glucose is transported by the PTS (like in W3110), one ATP mol is consumed per mol of glucose that is internalized, and glucose 6-phosphate is formed during the transport of glucose inside the cell. In this case, the phosphate group is transferred from phosphoenolpyruvate. In the mutant strain, glucose is phosphorylated by the glucokinase. Thus more PEP is available for energy generation and biosynthesis. Such differences have in general, positive effects from a bioprocessing perspective [17], which can explain the results from Fig. 8. The overall volumetric GFP productivity was $11.0 \pm 1.0$ mg $L^{-1}$ $h^{-1}$ in cultures of W3110, while reached $12.9 \pm 1.1$ mg $L^{-1}$ $h^{-1}$ in cultures of WHIC. Therefore, despite the longer cultivation time required, the engineered strain performed better than its wild type.

## Conclusion

The presented results demonstrate that, in general, a typical fed-batch performance can be mimicked using engineered strains cultured in batch mode. This is valid

(See figure on next page.)

**Fig. 3** Cultures of *E. coli* strains constitutively expressing the GFP in semi-defined medium supplemented with 20 g $L^{-1}$ glucose and 8 g $L^{-1}$ yeast extract. The left panel shows scattered light intensities, and the right panel shows GFP fluorescence intensities. **A**, **B** Cultures of strains WG, WGE, WEP and WHI; **C**, **D** cultures of strains WGB, WGME, WGMX, and WGMP; **E**, **F** cultures of W3110, WGM, WGX and WGMB; **G**, **H** cultures of strain WHIC. Culture conditions: 48 well FlowerPlates®, $V_L$ = 800 µL, $n$ = 1500 rpm, $d_0$ = 3 mm. Note that the scales are not identical. Shaded bands indicate the standard deviation between triplicate experiments

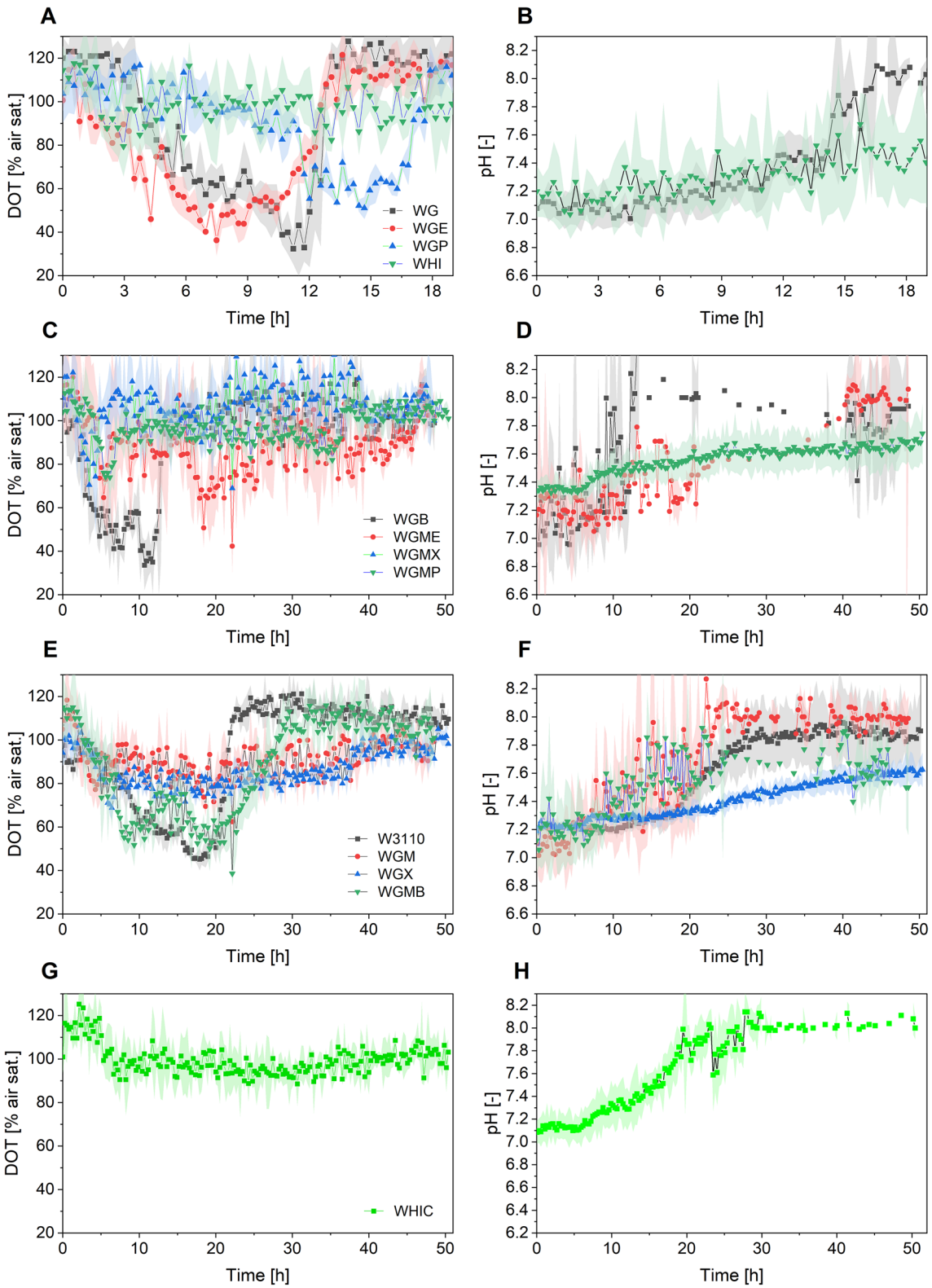


**Fig. 3** (See legend on previous page.)

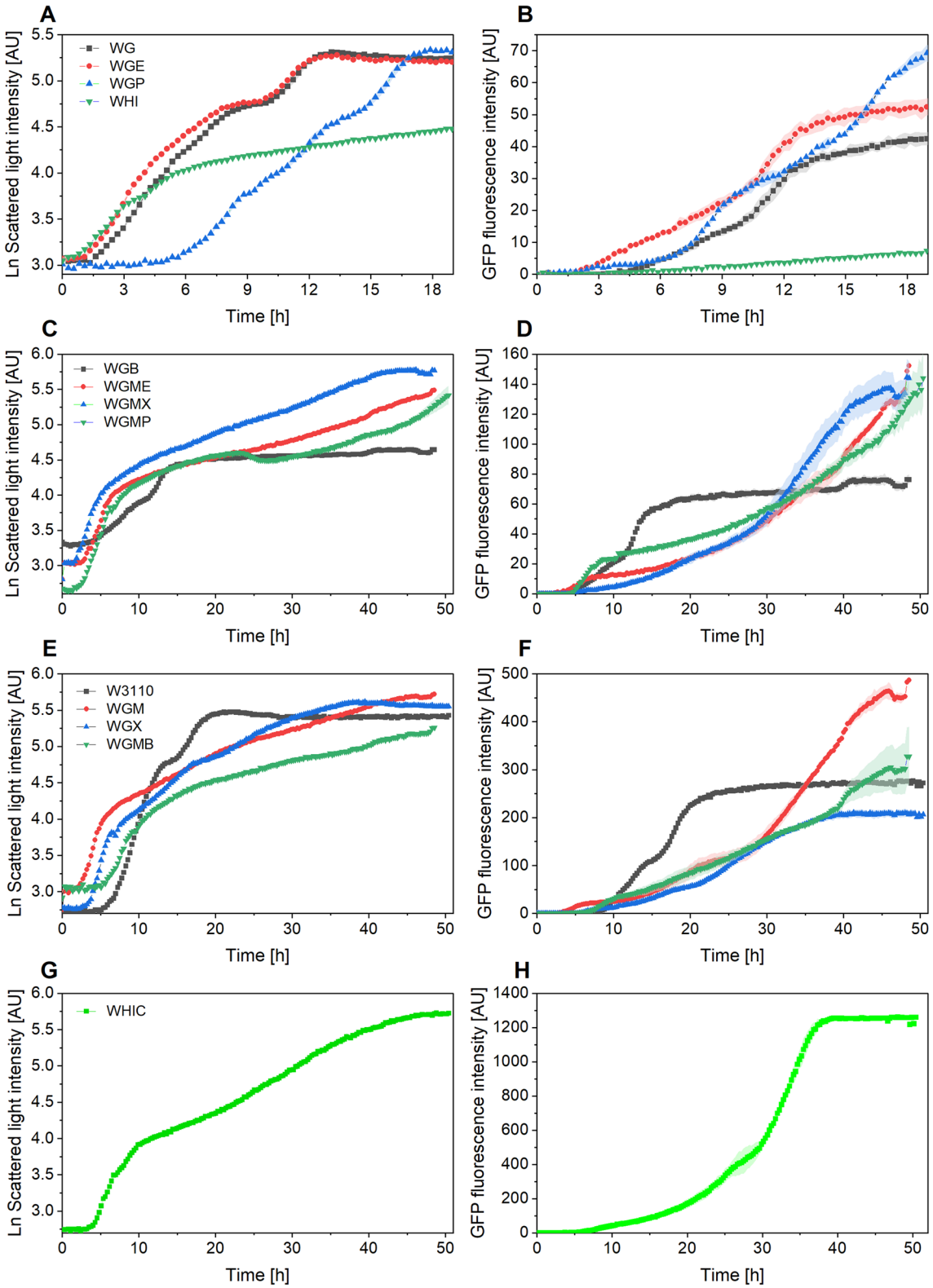


**Fig. 4** Cultures of *E. coli* strains constitutively expressing the GFP in semi-defined medium supplemented with 20 g $L^{-1}$ glucose and 8 g $L^{-1}$ yeast extract. The left panel shows the dissolved oxygen tension (DOT), and the right panel shows pH values. **A**, **B** Cultures of strains WG, WGE, WEP and WHI; **C**, **D** cultures of strains WGB, WGME, WGMX, and WGMP; **E**, **F** cultures of W3110, WGM, WGX and WGMB; **G**, **H** cultures of strain WHIC. Culture conditions: 48 well FlowerPlates®, $V_L = 800$ µL, $n = 1500$ rpm, $d_0 = 3$ mm. pH data from WGE and WGP are not included due to failure of the readings

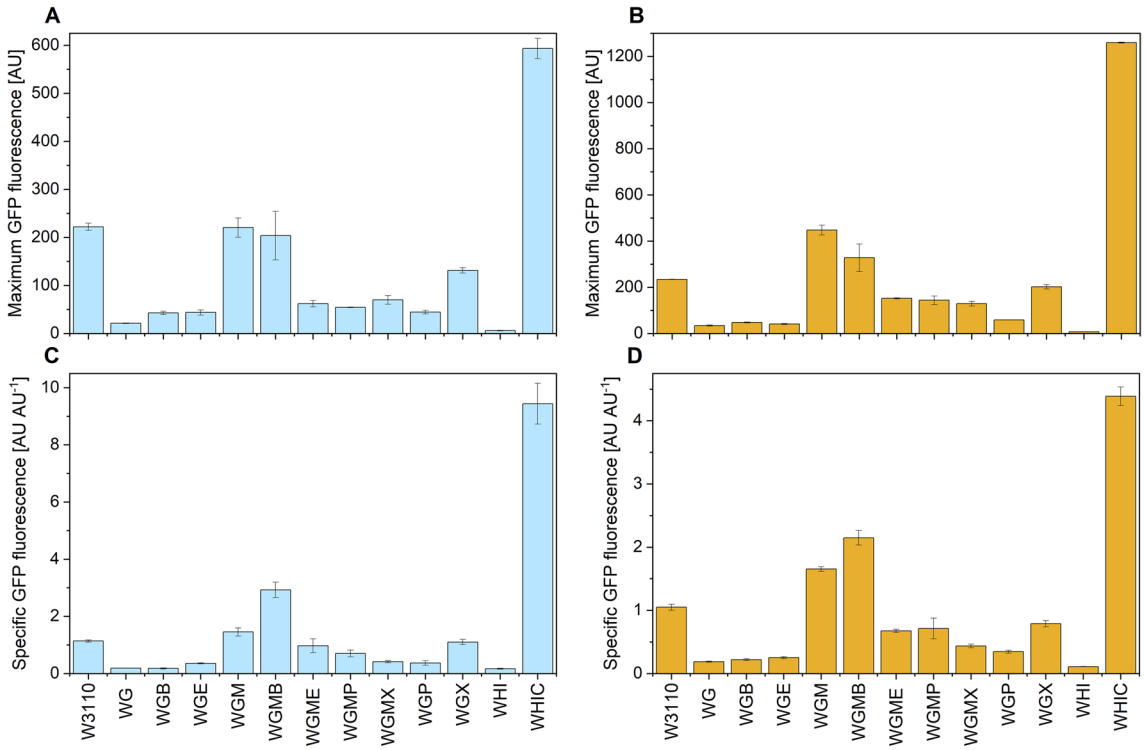


**Fig. 5** GFP expression performance of the wild type and mutant strains cultures in semi-defined medium supplemented with 10 g/L glucose and 4 g $L^{-1}$ yeast extract (**A**, **B**) or 20 g $L^{-1}$ glucose and 8 g $L^{-1}$ yeast extract (**C**, **D**). Top panel: maximum GFP fluorescence; bottom panel: specific GFP fluorescence. Values were calculated over the slow-growth phase. Culture conditions: 48 well FlowerPlates. $V_L = 800$ µL, $n = 1500$ rpm, $d_0 = 3$ mm. Note that the scales are not identical. Vertical lines indicate the standard deviation between triplicate experiments

**Table 3** Specific growth rates and final GFP concentration in batch cultures with 20 g $L^{-1}$ glucose. ND: Not detected by the method used; $\mu$: specific growth rate; SGF: specific GFP fluorescence. Subscripts 1 and 2 refer to the first and second growth phase, respectively

| Strain | $\mu_1$ [$h^{-1}$] | $SGF_1$ [–] | $\mu_2$ [$h^{-1}$] | $SGF_2$ [–] | Final GFP conc. [mg $L^{-1}$] |
|---|---|---|---|---|---|
| W3110 | 0.70 ± 0.03 | 1.00 ± 0.08 | 0.12 ± 0.01 | 1.24 ± 0.09 | 1.5 ± 0.0 |
| WG | 0.52 ± 0.03 | 0.20 ± 0.01 | 0.24 ± 0.02 | 0.24 ± 0.01 | ND |
| WGB | 0.43 ± 0.03 | 0.20 ± 0.00 | 0.26 ± 0.01 | 0.29 ± 0.01 | ND |
| WGE | 0.42 ± 0.02 | 0.21 ± 0.01 | 0.23 ± 0.01 | 0.31 ± 0.01 | ND |
| WGM | 0.66 ± 0.04 | 0.53 ± 0.02 | 0.04 ± 0.00 | 1.28 ± 0.08 | 1.91 ± 0.40 |
| WGMB | 0.61 ± 0.27 | 1.00 ± 0.05 | 0.03 ± 0.00 | 2.73 ± 0.23 | 1.35 ± 0.80 |
| WGME | 0.59 ± 0.06 | 0.28 ± 0.01 | 0.04 ± 0.00 | 0.90 ± 0.01 | 0.82 ± 0.21 |
| WGMP | 0.46 ± 0.03 | 0.66 ± 0.03 | 0.03 ± 0.01 | 0.95 ± 0.10 | 0.53 ± 0.04 |
| WGMX | 0.66 ± 0.02 | 0.13 ± 0.01 | 0.05 ± 0.00 | 0.63 ± 0.05 | 0.48 ± 0.04 |
| WGP | 0.43 ± 0.03 | 0.77 ± 0.06 | 0.31 ± 0.01 | 0.35 ± 0.01 | ND |
| WGX | 0.94 ± 0.02 | 0.57 ± 0.05 | 0.07 ± 0.01 | 1.07 ± 0.09 | 0.82 ± 0.04 |
| WHI | 0.51 ± 0.07 | 0.05 ± 0.01 | 0.04 ± 0.00 | 0.22 ± 0.01 | ND |
| WHIC | 0.46 ± 0.01 | 1.73 ± 0.01 | 0.06 ± 0.00 | 6.05 ± 0.02 | 5.15 ± 0.76 |

at least for the specific expression system and protein produced, but in principle could be extended to other recombinant proteins, where the initial screening could

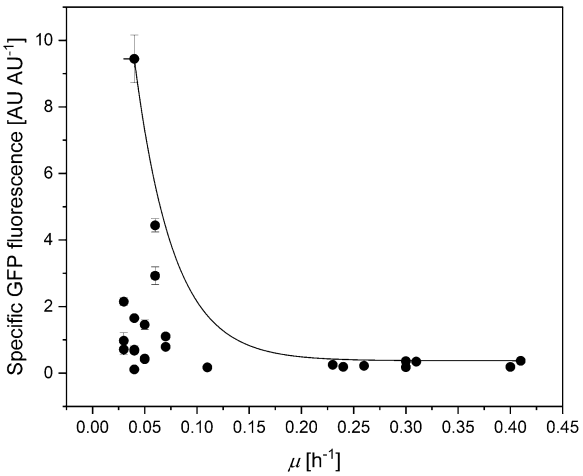


**Fig. 6** Specific GFP fluorescence vs. specific growth rate ($\mu$) of the different mutant strains and culture conditions in microbioreactors. Vertical lines indicate the standard deviation between triplicate experiments

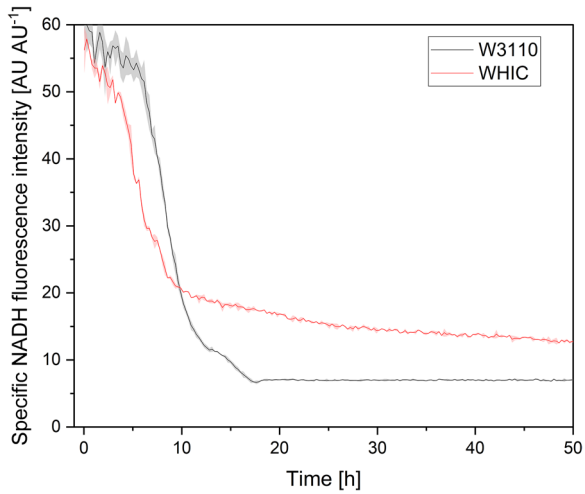


**Fig. 7** Specific NADH fluorescence of strains W3110 and WHIC in cultures in semi-defined medium supplemented with 10 g $L^{-1}$ glucose and 4 g $L^{-1}$ yeast extract. Culture conditions: 48 well FlowerPlates, $V_L = 800$ µL, $n = 1500$ rpm, $d_0 = 3$ mm. Shaded bands indicate the standard deviation between triplicate experiments

result in a different optimum growth rate/specific mutant for culture scale-up. Moreover, it was demonstrated that batch cultures of the engineered strain with high glucose concentration can perform better than fed-batch cultures of the wild type strain at the same growth rate. Batch operations are easier to perform than fed-batch, which make attractive the use of the mutant strains presented. Furthermore, a glucose-feeding pump will not be necessary for cultures of the mutant strains, which would reduce the energy consumption during the process. Therefore, we consider that this approach is a valuable alternative for accelerated high-throughput screening and culture scale-up.

## Methods

### Plasmid

Plasmid pWF14 (3824 bp) expresses the supergloGFP (sgGFP) green fluorescent protein from a constitutive promoter. This plasmid contains genes conferring resistance to kanamycin and chloramphenicol and the pUC origin of replication. Protein sgGFP contains four amino acid changes (F64L, S65C, I167T y K238N) when compared to the sequence from the GFP from *Aequorea victoria* (avGFP) [34]. At 37 °C, sgGFP displays better folding and fluorescence when compared to avGFP. The synthetic constitutive promoter in pWF14 was generated from a design based on a consensus sequenced derived from 46 promoters [34].

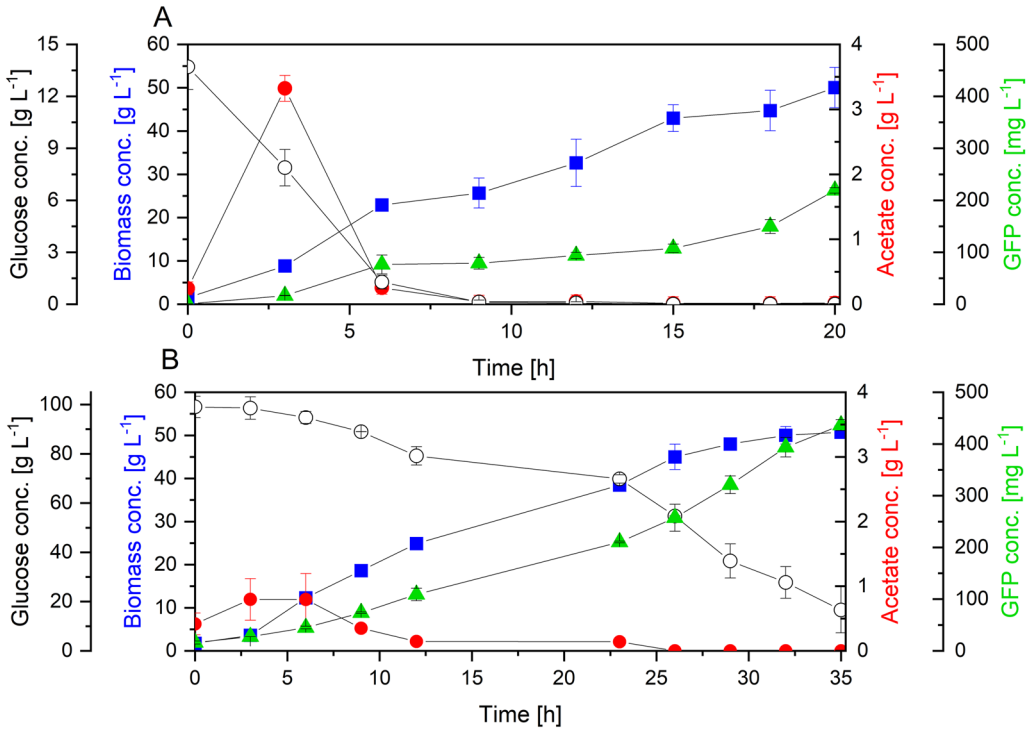


**Fig. 8** High cell-density cultures of W3110 (**A**) and WHIC (**B**). Strain W3110 was cultured in fed-batch mode with an exponentially increasing feeding rate of 0.05 $h^{-1}$, and WHIC in batch mode. The total amount of glucose used in both cultures was 100 g $L^{-1}$. Empty circles: glucose; filled circles: acetate; squares: biomass; triangles: GFP concentrations. Vertical lines show the experimental error in duplicate cultures

The 42 bp promoter sequence was further modified by random insertion mutagenesis of each of the four DNA bases dA, dC, dG or dT. The promoter library was generated by conventional oligonucleotide chemical synthesis. The random insertional mutagenesis was performed by employing a diluted equimolar mixture of the four bases and a synthesis cycle lacking the capping step. A library was generated by ligating the mutant promoters to a plasmid vector. Selection of clones from the random library was based on detecting the transformed bacterial colonies with the highest fluorescent level. Plasmid pWF14 was selected as it displayed the highest fluorescence level in the library. The sequencing of the promoter region in pWF14 showed the insertion of an A (adenine) in the spacer region. The complete sequence and features of pWF14 is provided in Additional file 1.

## Bacterial strains and culture media

The *E. coli* strains used in this work are described in Table 1. The wild type strain W3110 is a derivative of K-12. All the mutants are derivatives of W3110. Strains were transformed with pWF14 and preserved in 40% glycerol stocks at −70 °C. All cultures were performed in a semi defined mineral medium containing glucose and yeast extract. The composition of the mineral medium (in g $L^{-1}$) was: $K_2HPO_4$, 17; $KH_2PO_4$, 5.3; $(NH_4)_2SO_4$, 2.5; $NH_4Cl$, 1.0; Citrate-$Na_3{\cdot}2H_2O$, 2; $MgSO_4{\cdot}7H_2O$, 1.0; Thiamine-HCl, 0.01. The medium was supplemented with 2 mL $L^{-1}$ trace element solution and either 0.05 g $L^{-1}$ kanamycin sulfate or 0.03 g $L^{-1}$ chloramphenicol. The trace element solution composition (in g $L^{-1}$) was: $ZnCl_2$, 10.5; Na·EDTA, 5.5; $CoSO_4{\cdot}7H_2O$, 1.5; $MnSO_4{\cdot}H_2O$, 6.4; $CuSO_4{\cdot}5H_2O$, 1.1; $H_3BO_3$, 1.5; $Na_2MoO_4{\cdot}2H_2O$, 1; $FeCl_3{\cdot}6H_2O$, 51.4; and Fe(III)Cit-H·$H_2O$, 39.9. Glucose, trace elements solutions and salt solutions were sterilized separately. Kanamycin, chloramphenicol, and thiamine solutions were sterilized by filtration and kept frozen at −20 °C. The pH of the medium was adjusted to 7.4 before sterilization. The strains were precultured overnight in shake flasks with mineral medium containing 5 g $L^{-1}$ glucose and 2 g $L^{-1}$ yeast extract. Aliquots were taken to inoculate the main cultures at an initial optical density ($OD_{600nm}$) of approx. 0.1. All the chemicals were purchased to Sigma Aldrich (MO, USA).

## Microbioreactor cultures

Microtiter plates cultures were performed in a Multiparameter FlowerPlate (m2p-labs GmBH, Bäsweiler, Germany) using the semi defined medium containing 10 or 20 g $L^{-1}$ glucose, plus 0.4 g of yeast extract per g of glucose. The microtiter plates were incubated at 37 °C in a BioLector (m2p-labs GmBH, Bäsweiler, Germany) with filling volume of 800 µL and a constant orbital shaking of 1500 rpm, shaking diameter 3 mm. Biomass was measured by scattered light (ScL) at 620 nm, using a gain of 15. NADH fluorescence was measured with excitation and emission wavelengths of 365 and 450 nm, respectively with a gain of 90. GFP production was followed at 488 nm for excitation and 520 nm for emission and a gain of 85. Specific GFP fluorescence intensity (SGF) was calculated as the slope of the curve of ScL intensity vs. GFP fluorescence intensity over the time involved. All cultures were carried out in triplicate. The total volume of each well was taken at the end of the cultures and stored at −20 ° C until further analysis.

## 2 L stirred tank bioreactor cultures

Fed-batch cultures were carried out in a 2 L Biostat B Plus stirred tank bioreactor (Sartorius, Göttingen, Germany) equipped with controls for pH, temperature, agitation, and dissolved oxygen. $NH_4OH$ and $H_2PO_4$ solutions were automatically added to control pH at 7.0. Temperature was maintained at 37 °C, DOT was maintained above 30% by increasing the stirrer speed and airflow. The batch phase started with 15 g $L^{-1}$ glucose and 50 g $L^{-1}$ yeast extract in 0.5 L mineral medium supplemented with 0.05 g $L^{-1}$ kanamycin sulfate. The fed-batch phase was started after 9 h, when initial glucose depletion was evidenced by a sudden increase of the DOT and pH signals. A concentrated 500 g $L^{-1}$ glucose solution supplemented with 0.05 g $L^{-1}$ kanamycin was added to the medium using a Watson–Marlow 101U/R programmable peristaltic pump. The feeding rate was programmed to maintain a specific growth rate of 0.05 $h^{-1}$ using the following equation:

$$\mathrm{F} = \left(\frac{\mu_{\mathrm{set}}}{Y_{x/s}} + m_s\right)\frac{xVe^{\mu_{set}(t)}}{S_i} \quad (1)$$

where $F$ is the glucose feeding rate (L $h^{-1}$), $Y_{x/s}$ is the biomass yield on glucose, $m_s$ is the specific consumption rate of glucose associated with maintenance (0.059 g $g^{-1}$ $h^{-1}$), $V$ is the actual volume (L), $x$ is the biomass concentration (g $L^{-1}$), $\mu_{set}$ is the desired specific growth rate, $t$ is the feeding elapsed time (h) and $S_i$ is the glucose concentration in the feeding solution. Biomass concentration was determined as the dry cell weight. Samples were taken periodically for offline analyses. Fed-batch cultures were performed in duplicate.

High cell-density cultures of strain WHIC in batch mode were performed a 2 L Biostat B Plus stirred tank bioreactor (Sartorius, Göttingen, Germany) with 0.6 L of

mineral medium containing 100 g $L^{-1}$ glucose, 50 g $L^{-1}$ yeast extract and 0.05 g $L^{-1}$ kanamycin. DOT and pH were controlled as described above. Biomass concentration was determined as the dry cell weight. Samples were taken periodically for offline analyses. Batch cultures were performed in triplicate. For the stirred tank bioreactor cultures, GFP production was monitored by fluorescence readings in a ChronosBH Fluorometer (ISS Inc., Champaing, EUA). Wavelengths of 480 and 510 nm were used for excitation and emission, respectively. GFP was quantified as explained below.

## Metabolite analysis

Glucose and acetate were quantified by a chromatographic method in a Varian ProStar 210 (Varian Inc., California, EUA) HPLC system equipped with an Aminex HPX-87 H column (Bio-Rad Laboratories, California, EUA). The separation was carried out at 0.5 mL $min^{-1}$ at 60 °C, and metabolites were detected in a spectrophotometric detector UV-Vis Varian PS-235 (Varian Inc., California, EUA) at 210 nm.

## GFP quantification

Cells recovered from the cultures were used to quantify GFP production. For cell lysis, a 10 g $L^{-1}$ lysozyme solution was added to the sample and then incubated at 37 °C for 15 min. Later, the cells were frozen at −70 ° C for 30 min and thawed at room temperature. After centrifugation at 13,000 rpm for 2 min, the supernatant was recovered. GFP quantification was performed by microfluidics electrophoresis using the commercial Agilent Protein 80 Kit package (Agilent Technologies, California, USA) according to the manufacturer's recommendations. For both quantifications, a standard curve of GFP concentration (rGFP, Sigma-Aldrich, MO, USA) was used against the area under the curve provided by the Agilent Expert software (Agilent Technologies, California, USA) or the emitted fluorescence units.

## Supplementary Information

The online version contains supplementary material available at https://doi.org/10.1186/s12934-022-01906-1.

**Additional file 1.** Plasmid pWF14 sequence.

**Acknowledgements**
Not applicable.

**Author contributions**
DV, JCS, GG, and ARL were involved in the conception, design and writing of the manuscript. LMM and PG designed plasmid pWF14. Experiments were designed by ARL and performed by DV. ARL and DV performed the data analysis and interpretation of the results. All authors read and approved the final manuscript.

**Funding**
This work was supported by CONACyT grant A1-S-8646. DV was supported by a fellowship from CONACyT.

**Availability of data and materials**
All data generated or analysed during this study are included in this published article and its Additional file 1.

## Declarations

**Ethics approval and consent to participate**
Not applicable.

**Consent for publication**
Not applicable.

**Competing interests**
The authors declare that they have no competing interests.

**Author details**
[1]Departamento de Procesos y Tecnología, Universidad Autónoma Metropolitana, Vasco de Quiroga 4871, 05348 Mexico City, Mexico. [2]Departamento de Ingeniería Celular y Biocatálisis, Instituto de Biotecnología, Universidad Nacional Autónoma de México, Avenida Universidad 2001, Col. Chamilpa, 62210 Cuernavaca, MOR, Mexico.

Received: 13 June 2022 Accepted: 9 August 2022
Published online: 07 September 2022

**References**

1. Wolfe AJ. The acetate switch. Microbiol Mol Biol Rev. 2005;69(1):12–50.
2. Taymaz-Nikerel H, Lara AR. *Vitreoscilla* haemoglobin: a tool to reduce overflow metabolism. Microorganisms. 2022;10: 43.
3. Eiteman MA, Altman E. Overcoming acetate in *Escherichia coli* recombinant protein fermentations. Trends Biotechnol. 2006;24: 530–536.
4. Peebo K, Neubauer P. Application of continuous culture methods to recombinant protein production in microorganisms. Microorganisms. 2018;6(3):56.
5. Shiloach J, Kaufman J, Guillard AS, Fass R. Effect of glucose supply strategy on acetate accumulation, growth, and recombinant protein production by *Escherichia coli* BL21 (lambdaDE3) and *Escherichia coli* JM109. Biotechnol Bioeng. 1996;49(4):421–428.
6. Teworte S, Malcı K, Walls LE, Halim M, Rios-Solis L. Recent advances in fed-batch microscale bioreactor design. Biotechnol Adv. 2022;55:107888.
7. Bähr C, Leuchtle B, Lehmann C, Becker J, Jeude M, Peinemann F, Arbter R, Büchs J. Dialysis shake flask for effective screening in fed-batch mode. Biochem Eng J. 2012;69:182–195.
8. Philip P, Kern D, Goldmanns J, Seiler F, Schulte A, Habicher T, Büchs J. Parallel substrate supply and pH stabilization for optimal screening of *E. coli* with the membrane-based fed-batch shake flask. Microb Cell Fact. 2018;17:1–17.
9. Keil T, Dittrich B, Lattermann C, et al. Polymer-based controlled-release fed-batch microtiter plate—diminishing the gap between early process development and production conditions. J Biol Eng. 2019;13:18.
10. Ukkonen AVK, Neubauer A, Pereira VJ. High yield of recombinant protein in shaken *E. coli* cultures with enzymatic glucose release medium EnPresso B. In: Burgess-Brown NA, editor. Heterologous gene expression in *E. coli*: methods and protocols, methods in molecular biology. New York: Springer Science + Business Media LLC; 2017. p. 33–43.
11. Panula-Perälä J, Šiurkus J, Vasala A, Wilmanowski R, Casteleijn MG, Neubauer P. Enzyme controlled glucose auto-delivery for high cell density cultivations in microplates and shake flasks. Microb Cell Fact. 2008;7:1–12.
12. Morschett H, Jansen R, Neuendorf C, Moch M, Wiechert W, Oldiges M. Parallelized microscale fed-batch cultivation in online-monitored microtiter plates: implications of media composition and feed strategies

for process design and performance. J Ind Microbiol Biotechnol. 2020;47(1):35–47.
13. Ganjave SD, Dodia H, Sunder AV, Madhu S, Wangikar PP. High cell density cultivation of *E. coli* in shake flasks for the production of recombinant proteins. Biotechnol Rep (Amst). 2021;33:e00694.
14. Weuster-Botz D, Altenbach-Rehm J, Arnold M. Parallel substrate feeding and pH-control in shaking-flasks. Biochem Eng J. 2001;7:163–170.
15. Hans S, Haby B, Krausch N, Barz T, Neubauer P, Cruz-Bournazou MN. Automated conditional screening of multiple *Escherichia coli* strains in parallel adaptive fed-batch cultivations. Bioengineering (Basel). 2020;7(4):145.
16. Tchieu JH, Norris V, Edwards JS, Saier MH Jr. The complete phosphotransferase system in *Escherichia coli*. J Mol Microbiol Biotechnol. 2001;3(3):329–46.
17. Gosset G. Improvement of *Escherichia coli* production strains by modification of the phosphoenolpyruvate:sugar phosphotransferase system. Microb Cell Fact. 2005;4:14.
18. Bäcklund E, Markland K, Larsson G. Cell engineering of *Escherichia coli* allows high cell density accumulation without fed-batch process control. Bioprocess Biosyst Eng. 2008;31(1):11–20.
19. Picon A, Teixeira de Mattos MJ, Postma PW. Reducing the glucose uptake rate in *Escherichia coli* affects growth rate but not protein production. Biotechnol Bioeng. 2005;90(2):191–200.
20. Negrete A, Shiloach J. Improving *E. coli* growth performance by manipulating small RNA expression. Microb Cell Fact. 2017;6:198.
21. Borja GM, Meza Mora E, Barrón B, Gosset G, Ramírez OT, Lara AR. Engineering *Escherichia coli* to increase plasmid DNA production in high cell-density cultivations in batch mode. Microb Cell Fact. 2012;11:132.
22. Soto R, Caspeta L, Barrón BL, Gosset G, Ramírez OT, Lara AR. High cell-density cultivation in batch mode for plasmid DNA vaccine production by a metabolically engineered *E. coli* strain with minimized overflow metabolism. Biochem Eng J. 2011;56(3):165–71.
23. Knabben I, Regestein L, Marquering F, Steinbusch S, Lara AR, Büchs J. High cell-density processes in batch mode of a genetically engineered *Escherichia coli* strain with minimized overflow metabolism using a pressurized bioreactor. J Biotechnol. 2010;150: 73–79.
24. Lara AR, Caspeta L, Gosset G, Bolívar F, Ramírez OT. Utility of an *Escherichia coli* strain engineered in the substrate uptake system for improved culture performance at high glucose and cell concentrations: an alternative to fed-batch cultures. Biotechnol Bioeng. 2008;99:893–901.
25. Pablos TE, Mora EM, Le Borgne S, Ramírez OT, Gosset G, Lara AR. *Vitreoscilla* hemoglobin expression in engineered *Escherichia coli*: improved performance in high cell-density batch cultivations. Biotechnol J. 2011;6:993–1002.
26. Fuentes LG, Lara AR, Martínez LM, Ramírez OT, Martínez A, Bolívar F, Gosset G. Modification of glucose import capacity in *Escherichia coli*: physiologic consequences and utility for improving DNA vaccine production. Microb Cell Fact. 2013;12:42.
27. Fragoso-Jiménez JC, Baert J, Nguyen TM, Liu W, Sassi H, Goormaghtigh F, Van Melderen L, Gaytán P, Hernández-Chávez G, Martinez A, Delvigne F, Gosset G. Growth-dependent recombinant product formation kinetics can be reproduced through engineering of glucose transport and is prone to phenotypic heterogeneity. Microb Cell Fact. 2019;18(1):26.
28. Funke M, Diederichs S, Kensy F, Müller C, Büchs J. The baffled microtiter plate: increased oxygen transfer and improved online monitoring in small scale fermentations. Biotechnol Bioeng. 2009;103(6):1118–1128.
29. Turner C, Gregory ME, Turner MK. A study of the effect of specific growth rate and acetate on recombinant protein production of *Escherichia coli* JM107. Biotechnol Lett.1994;16:891–896.
30. Kumar J, Bhat SU, Rathore AS. Slow post-induction specific growth rate enhances recombinant protein expression in *Escherichia coli*: pramlintide multimer and ranibizumab production as case studies. Proc Biochem. 2022;114:21–7.
31. Neidhardt FC, Ingraham JL, Schaechter. Physiology of the bacterial cell: a molecular approach. Sunderland: Sinauer Associates Inc.; 1990. p. 507.
32. Okayasu T, Ikeda M, Akimoto K, Sorimachi K. The amino acid composition of mammalian and bacterial cells. Amino Acids. 2005;13;379–391.
33. Podpora B, Świderski F, Sadowska A, Rakowska R, Wasiak-Zys G. Spent Brewer's yeast extracts as a new component of functional food. Czech J Food Sci. 2016;34:554–63.
34. Palm GJ, Zdanov A, Gaitanaris GA, Stauber R, Pavlakis GN, Wlodawer A. The structural basis for spectral variations in green fluorescent protein. Nat Struct Biol. 1997;4(5): 361–365.

## Publisher's Note